Dissertation

submitted to the

Combined Faculties for the Natural Sciences and for Mathematics

of the Ruperto-Carola University of Heidelberg, Germany

for the degree of

Doctor of Natural Sciences

presented by

Rajesh Kumar, M.Sc.- Biotechnology

born in Alwar, India

Oral-examination: **.....**

Recognition and Targeting of Prion Aggregates to the Insoluble Protein Deposit (IPOD) in *Saccharomyces cerevisiae*

Referees:

Prof. Dr. Bernd Bukau

Dr. Brian Luke

I hereby declare that I have written the submitted dissertation myself and in this process have used no other sources or materials than those explicitly indicated. The work was carried out at the Department of Medicine I and Clinical Chemistry, University of Heidelberg, Heidelberg in the group of Dr. Jens Tyedmers.

Heidelberg, October 2016 Rajesh Kumar

Abstract

Protein quality control is a well-organized cellular process in which potentially toxic misfolded proteins are either refolded back to their native state, degraded or deposited into special deposition sites. Sequestration of misfolded protein species into specific deposition sites occurs in all kingdoms of life and serves as a second line of defense when refolding or degradation machineries that normally deal with these misfolded proteins are overwhelmed. In *Saccharomyces cerevisae,* three major subcellular sequestration sites have been described for deposition of different protein aggregates: INQ (*i*ntra*n*uclear *q*uality control compartment)/JUNQ (*ju*xta*n*uclear *q*uality control compartment), IPOD (*i*nsoluble *pro*tein *d*eposit) and CytoQ. Amorphously aggregating proteins are targeted either to the INQ/JUNQ by the nuclear sorting factor Btn2, or they are targeted to a peripheral deposition site termed as Cyto Q with the aid of the cytosolic small heat shock protein Hsp42.

Amyloidogenic aggregates including yeast prions are predominantly sequestered at the IPOD, a perivacuolar deposition site. The perivacuolar IPOD is located in close proximity to the PAS (Phagophore Assembly Site) where the cells initiate formation of autophagosomes and CVT (Cytoplasm-to-Vacuole Targeting) vesicles. The cellular machinery, however, by which amyloid aggregates are recognized and deposited at the IPOD is still unknown.

Using a fishing approach with immobilized prion fibers formed by the prion domain of Sup35 (PrD), I identified components of actin cable-based and SNARE-mediated vesicular transport machinery to bind to PrD fibers. Using an auxin-based depletion system, I show that proper recruitment of the model prion amyloid PrD-GFP to the IPOD and the CVT substrate preApe1 to the PAS is disrupted upon depletion of essential components of the actin-based transport machinery, Myo2, Cmd1 and Tpm1/2, as well as Sec18-mediated SNARE function. Interestingly, the IPOD substrate PrD-GFP and the two PAS markers preApe1 and Atg8 accumulate reversibly in the cytosol in these mutants. Using fluorescence microscopy, I observed that PrD-GFP aggregates are associated with Atg9 transport vesicles similar to preApe1 and are targeted to the IPOD through these vesicles along actin cables. In addition, these PrD-GFP aggregates are shown to interact with Myo2 *in vivo* upon disruption of Sec18 SNARE function.

In a next approach, I investigated the possible fate of PrD-GFP aggregates deposited at the IPOD, that is located adjacent to the site in the cell where autophagosomes/CVT vesicles are formed. I demonstrate that PrD-GFP aggregates are not turned over in bulk via autophagy, but can be degraded by proteasomal and other unknown cellular degradation pathway(s) only after their slow and progressive extraction by the disaggregase Hsp104 from the IPOD. Thus accumulation of PrD-GFP amyloids at the IPOD might serve a temporary storage function when downstream cellular degradation systems are overwhelmed. Based on the above findings, a model was proposed where PrD-GFP and preApe1 use an Atg9-vesicular transport machinery and Myo2 as a linking factor to be deposited at their recruitment sites IPOD and PAS, respectively, along tropomyosin-coated actin cables.

Zusammenfassung

Proteinqualitätskontrolle ist ein gut organisierter zellulärer Prozess, bei dem potentiell toxische, fehlgefaltete Proteine entweder rückgefaltet oder abgebaut werden oder zu speziellen Ablagerungsstellen transportiert werden. Die Ablagerung falsch gefalteter Proteine an spezifische intrazelluläre Ablagerungsstellen kommt in allen Lebewesen vor und dient als alternativer Mechanismus, falls Rückfaltungs- und Abbauprozesse ausgelastet sind. In *Saccharomyces cerevisiae* wurden bislang drei unterschiedliche subzelluläre Strukturen identifiziert, an denen verschiedene Proteinaggregate abgelagert werden: INQ (*i*ntra*n*uclear *q*uality control compartment)/JUNQ (*ju*xta*n*uclear *q*uality control compartment), IPOD (*i*nsoluble *p*rotein *d*eposit) und CytoQ. Fehlgefaltete Proteine werden entweder mittels dem nuclear sorting factor Btn2 an das INQ/JUNQ Kompartiment transportiert oder mit Hilfe des zytosolischen kleinen Hitzeschockproteins Hsp42 an das peripher lokalisierte CytoQ geleitet. Amyloidartige Aggregate einschließlich Prionen werden in der Hefe hauptsächlich zum IPOD transportiert, welches perivakuolär lokalisiert ist. Bislang ist unklar, wie genau die Amyloid-Aggregate erkannt und dann an das IPOD gebracht werden. Das IPOD liegt in unmittelbarer Nähe des PAS (Phagophore Assembly Site), wo die Zelle die Bildung von Autophagosomen und CVT (Cytoplasm-to-Vacuole Targeting) Vesikeln initiiert.

Mit Hilfe eines sogenannten „Fishing Approaches“ durch immobilisierte Sup35-PrD Fibrillen konnte ich Komponenten der Aktin- und SNARE-vermittelten vesikulären Transportmaschinerie identifizieren, welche das IPOD ansteuern. Ein Auxin-basiertes Depletionssystem wurde benutzt um zu zeigen, dass die Rekrutierung des Modell-Prions PrD-GFP an das IPOD und des CVT-Substrats preAPE-1 an das PAS durch den Verlust essentieller Komponenten des Aktin-basierenden Transports gestört ist. Zu diesen Komponenten zählen Myo2, Cmd1 und Tpm1/2 sowie Sec18, welches SNARE-Funktionen reguliert. Interessanterweise akkumulierten die IPOD-Substrate PrD-GFP und die PAS-Marker pre-Ape1 und Atg8 reversibel im Zytosol dieser Mutanten. Mittels Fluoreszenzmikroskopie konnte ich nachweisen, dass die PrD-GFP Aggregate ähnlich wie preApe1 mit Atg9 Transportvesikeln assoziiert sind und so entlang von Aktinkabeln zum IPOD gebracht werden. Darüber hinaus interagierten diese PrD-GFP Aggregate bei Verlust der SNARE-Funktion durch Depletion von Sec18 mit Myo2 *in vivo*.

Im nächsten Schritt untersuchte ich das weitere Schicksal der PrD-GFP Aggregate, die am IPOD abgelgert wurden. Das IPOD liegt in unmittelbarer Nachbarschaft zur Phagophore-Assemby Site (PAS). Ich konnte zeigen, dass PrD-GFP Aggregate nicht als Ganzes durch Autophagie abgebaut werden, sondern dass diese erst nach langsamer und progressiver Extraktion durch Hsp104 vom IPOD durch das Proteasom und andere unbekannte Abbausysteme degradiert werden. Demnach könnte die Akkumulierung von PrD-GFP Amyloiden am IPOD eine befristete Lagerfunktion haben, wenn zelluläre Abbausystem überlastet sind. Basierend auf den oben genannten Ergebnissen wurde ein Model vorgeschlagen, in dem PrD-GFP und preApe1 die Machinerie der Atg9-Transportvesikel und Myo2 als Bindungsfaktor nutzen, um entlang von Tropomyosin-gebundenen Aktinkabeln an das IPOD bzw. PAS zu gelangen.

Contents

1

Introduction

Proteins perform the vast majority of cellular processes in all kingdoms of life such as enzymatic activity, regulatory function, transport of biomolecules, and structural component of subcellular organelles. For proper function of proteins, they have to fold into the correct three-dimensional structure and may additionally require other co-factors for proper folding. Inside the crowded cellular environment, protein folding to the native state is not an easy task to accomplish. Only one out of the many possible conformations that each protein can adopt, is the functional 3-D native fold [1]. In addition to the crowded cellular environment, endogenous errors (mutations, translational errors) or environmental stress (heat/metabolic/oxidative stress) can cause protein misfolding during and after synthesis. To cope with these challenges, cells evolved a complex protein quality control machinery to ensure either proper *de novo* folding, refolding of misfolded proteins to the native state or their degradation by different cellular proteolysis systems to prevent the accumulation of misfolded proteins.
Increased protein misfolding and failure of removal of these potentially toxic protein species leads to coalescence of excess misfolded species into aggregates and is associated with several pathological conditions. Furthermore, a decline/failure in the capacity of the protein quality control machinery is associated with aging. Thus understanding the underlying molecular and cellular mechanism of protein homeostasis or proteostasis is of great interest for basic and applied research [2].

In general, mechanisms and principles that govern protein aggregation have gained attention at the foreground of research. Several age-related neurodegenerative diseases, including Alzheimer's disease (AD), Parkinson's disease (PD) and polyglutamine expansion diseases are associated with the accumulation of misfolded proteins into aggregates in the brain. However, mounting evidence suggests that protein aggregation is not only the result of a failure of the protein quality control network, but it is also a well-controlled, non-random process serving as another line of defense to deal with protein folding stress and to protect the cellular environment from potentially toxic misfolded species.

1.1. Protein aggregation

1.1.1. Protein misfolding and aggregation

During *in vivo* protein folding of a polypeptide chain, there is a kinetic competition between aggregation and the productive folding process due to non-native interactions. Several local energy minima exist within the funnel-shaped energy landscape of a folding polypeptide chain. Therefore, no specific folding route is pre-determined, but many different routes are possible [3]. Along these protein folding routes, polypeptide chains are often at continuous risk to be trapped in nonnative, aggregation-prone conformers which subsequently assemble into protein aggregates. Even if the protein has reached its native state, it is still at continuous risk of misfolding due to several stresses. Partially unfolded or misfolded polypeptide chains are more prone to aggregation due to non-polar interactions of exposed hydrophobic residues that would normally be buried in the interior of the native protein [4].

During the aggregation process, “sticky” hydrophobic patches of the polypeptide chains, which are usually buried inside the core of the protein, undergo a hydrophobic collapse into unstructured/ disordered amorphous aggregates [5]. In addition to that, a small subset of proteins termed amyloidogenic proteins can undergo conformational changes to form stable, insoluble and highly ordered β-sheet-rich amyloid aggregates [6] (Fig 1). The protein quality control network has evolved such that under normal growth conditions, protein aggregation is prevented or rapidly reversed in the cytoplasm. Within the protein quality control network, molecular chaperones work in both co- and post-translational quality control systems to reverse erroneous conformations as well as to resolubilize protein aggregates to allow folding of single polypeptide chains back to the native state [7]. Instead of recognizing a specific amino-acid sequence, molecular chaperones bind to exposed hydrophobic stretches of client unfolded/misfolded proteins and can handle a large number of different protein substrates [8]. In case disordered aggregates and misfolded intermediates are unable to refold into their native conformation, chaperone activity guides them for degradation by ubiquitin-proteasome system (UPS) and autophagy to keep the cytoplasm free from potentially toxic misfolded/aggregated species [2]. Many components of the protein quality control network are under control of stress response pathways, and their expression is upregulated during several proteotoxic stresses. The basic principles of the protein quality control network are well conserved throughout evolution. However, the complexity of this network increases with the complexity of multicellular organisms and organismal stress signaling [9]. In eukaryotic cells, each cellular compartment, for example the cytosol, the endoplasmic reticulum and mitochondria have a unique protein-folding environment to cope with different stresses. Therefore specific stress

response pathways are linked with these subcellular compartments. The main objective of this thesis is to investigate the recruitment machinery for amyloid aggregates to a specific deposition site termed “Insoluble Protein Deposition (IPOD)” (see section 1.4.3) localized in a perivacuolar site in the cytoplasm. Therefore, the focus of this thesis is on cytosolic processes.

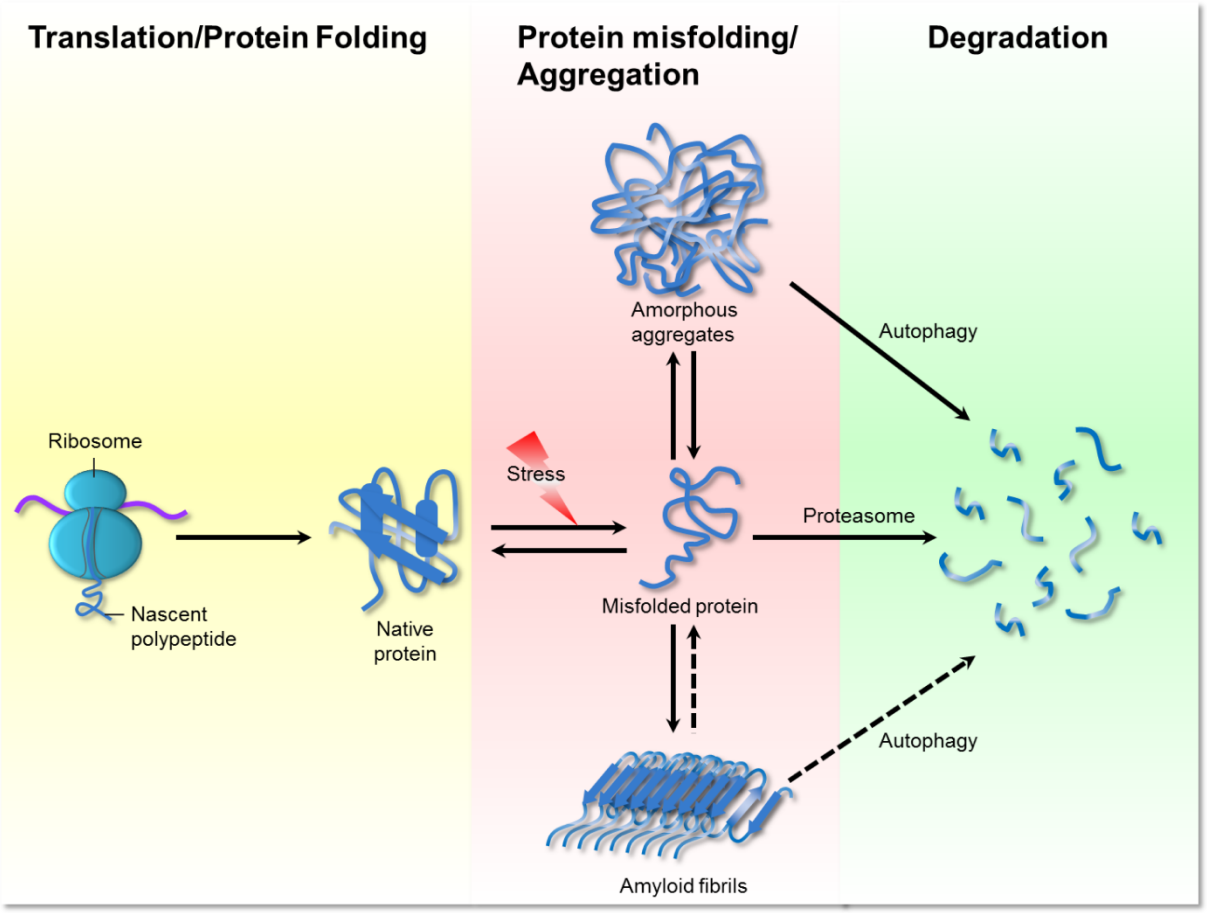

FIGURE 1: Protein misfolding and aggregation – Nascent polypeptide chains, after being translated on ribosomes, have to adopt their functional 3-D native state to exert their specific cellular functions. This complex folding process is threatened by multiple stresses such as mutations, translational errors or environmental stress conditions that lead to the formation of misfolded protein species. These misfolded proteins are either refolded back to their native states with the action of chaperones, are directly degraded by the ubiquitin-proteasome system (UPS) or accumulate into amorphous aggregate structures. A subset of amyloidogenic proteins undergoes conformational changes under physiological conditions and forms stable and insoluble amyloid fibers. Amorphous aggregates are refolded efficiently by disaggregation machinery. In eukaryotes, aggregates can be degraded directly through autophagic pathways. Arrows indicate a process of major significance; dashed arrows indicate a process where the physiological significance is unclear.

1.1.2. Conditions causing protein misfolding and aggregation

Protein aggregation is driven by hydrophobic interactions, by which exposed hydrophobic portions of one polypeptide chain interact non-covalently with the exposed hydrophobic regions of other polypeptides that are normally buried inside the protein core in the native state [10]. Partially folded intermediates during the folding process are often prone to form amorphous aggregates [11, 12]. Different internal and external/environmental factors influence protein folding and can cause aggregation by either destabilizing the native fold or preventing the proper folding. Usually, the protein quality control system effectively handles these erroneous, misfolded or unfolded species by supporting either their proper refolding or degradation. However, the capacity of this system is restricted, and formation of aggregates is a result of the overwhelmed protein quality control network. Remarkably, not only very harsh condition can cause protein aggregation, but also a combination of multiple harmless conditions which act at once, can cause aggregation [13].

Genetic factors

Genetic mutations can cause an altered amino acid sequence, thereby changing the biophysical properties of a protein and consequently influencing its intrinsic aggregation propensity. For instance, trinucleotide repeat expansions such as repetitive $[CAG]_n$ result in polyglutamine (polyQ) stretches that cause aggregation of the protein carrying it [14, 15]. These variations for example in the huntingtin gene are associated with neurodegenerative disease such as Huntington's disease. The length of the CAG repeat (polyQ-stretch) correlates with the aggregation propensity of the translated poly(Gln) chain [16] and age of disease onset [17].

Small point mutations at critical positions/domains also can cause protein aggregation by altering the protein conformation. It was for example shown that a mutant of superoxide dismutase 1 (SOD1) is associated with familial amyotrophic lateral sclerosis (FALS) and forms protein inclusions [18]. These mutations not only affect the stability and aggregation propensity of native proteins but also affect assembly of oligomers into large complexes by promoting hydrophobic interactions. In addition, point mutations in components of the protein quality-control system can also initiate protein aggregation. For example, a point mutation in a gene encoding the small HSP (sHSP) α-crystallin causes congenital cataract [19] and mutation in the PARKIN/PARK2 gene that encodes E3 ubiquitin ligase Parkin results in young-onset Parkinson's disease (YOPD) [20].

Translational errors

Alterations in the polypeptide sequence are not only caused by genetic mutations but can also result from the error-prone translation of mRNAs at the ribosome, amino acid misincorporation, frameshift mutation or stop codon readthrough [21]. Translation errors are also caused by misassembly of ribosomal subunits, tRNA synthesis errors and mRNA sequence modifications. Nascent polypeptide chains are particularly prone to misfolding and aggregation in a crowded cellular environment [22]. Therefore, they are prevented from aggregation by the action of ribosome-associated chaperones which specially promote the native conformation and avoid non-native interactions even in non-stressed situations [22].

In addition, in eukaryotes, truncated mRNAs cause ribosome stalling in which the stalled/aberrant nascent chain is ubiquitinated by the E3 ubiquitin ligase, Listerin/Ltn1 and co-translationally degraded by proteasomes. These processes are termed ribosome quality control (RQC). In line with this, it was shown that mutations in the E3 ligase Listerin cause protein aggregation and neurodegeneration in mice [23]. In the cell, translation errors are avoided by several ways. Firstly, monitoring ribosome biosynthesis and assembly faithfully, proof reading of tRNA amino acetylation for correct amino acid incorporation into the growing polypeptide chain and degradation of defective mRNAs to prevent aberrant protein synthesis [24]. Secondly, a sophisticated ribosome-associated chaperone network facilitates correct folding of nascent polypeptides upon emerging from the ribosomal exit tunnel [25, 26]. In human cells, 12-15% of nascent polypeptides are ubiquitinated co-translationally for their degradation to prevent the formation of defective ribosomal products [27]. In yeast, 2%–5% of nascent polypeptides are co-translationally ubiquitinated for degradation [28].

Environmental stresses

Besides genetic mutations and translational errors, various environmental stress conditions such as heat and oxidative stress can cause proteins to lose their native structures and promote the formation of protein aggregates by influencing directly the protein folding landscape. An increase in ambient temperature than normal growth temperature leads to massive unfolding of cellular proteins and can overwhelm the capacity of the cellular protein quality control system. This leads to protein aggregation. Yet, this heat-induced unfolding/ aggregation is a reversible process [29]. Oxidative stress can generate reactive oxygen species (ROS), which can modify proteins irreversibly through either direct fragmentation of the polypeptide chain or irreversible modification of specific amino acids. These irreversible chemical modifications can cause proteins to misfold and aggregate. Since oxidative modifications often alter the primary amino acid sequence, those proteins can usually not fold back to the native state, but have to be removed from the system [30-32].

Ageing

During ageing, the cellular protein quality control (proteostasis) capacity is declined. This increases accumulation of misfolded/damaged proteins and protein aggregation in different organisms. For example, a misfolding-prone mutant of human superoxide dismutase 1 (SOD1) in mice and an extension of polyQ protein in *C. elegans* accumulates in aggregates only during ageing [33, 34]. Oxidatively damaged and carbonylated proteins also accumulate in aged yeast cells [35]. In human, ageing cells can accumulate misfolded species that lead to several age- associated neurodegenerative disease such as Parkinson's , Alzheimer's, and Huntingtin's Disease or Type II Diabetes [36, 37].

1.1.3. Structural features of protein aggregates

Protein aggregates are insoluble in aqueous solutions, and some are even detergent-insoluble. These aggregates are made up of non-native proteins and are found in the intracellular or in the extracellular space [12]. These aggregates are classified structurally into two categories as: (I) disordered aggregates (amorphous aggregates, folding aggregates and inclusion bodies) and (II) highly ordered cross- β-sheet-rich fibrils (amyloids) [12].

Amorphous aggregates are generally formed under stress conditions. Overexpression of recombinant proteins in bacteria can also cause the formation of amorphous aggregates such as inclusion bodies in *E. coli* [12]. However, compelling evidence shows that bacterial inclusion bodies can also contain highly ordered amyloid aggregates during recombinant proteins expression [38, 39]. For example, it was shown that Aβ42-GFP aggregates inside the prokaryotic inclusion bodies show amyloid-like properties [38].

Deposition of amyloid aggregates is a pathological hallmark of many neurodegenerative diseases [40]. Amyloids are protease resistant, often SDS-insoluble and form even in the absence of stress. PolyQ amyloid aggregates, formed by polyglutamine (polyQ) stretches, were shown to cause cellular toxicity, yet the source of toxicity is under debate [41]. "Prions" are self-propagating proteinaceous infectious particles that cause several prion-based neurodegenerative diseases in mammals. These prions also show characteristics of amyloid aggregates i.e. cross-β fibrillar structures [42]. Mammalian prions are infectious (amyloidogenic) proteins that spread a disease/trait via horizontal transmission without any nucleic acid. Mammalian prion proteins are denoted as Prion Protein (PrP) that exist in two conformations: (I) PrP^{C}, the normal cellular and non-toxic form and (II) PrP^{Sc}, the pathogenic form which is a conformationally altered isoform of the PrP^{c}. The PrP^{Sc} form was initially found in sheep suffering from Scrapie [43]. PrP^{Sc} generates cross-β fibrillar structures (amyloids) that accumulate in the brains of humans and animals. Prion fiber assembly is a two-step process: (I) A soluble prion protein (PrP) undergoes conformational conversion and forms small oligomers (transient

intermediates) that act as seed/nucleus (II) The seed polymerizes conformational conversion of other soluble protein of the same type into mature amyloid fibers [44]. The most common prion diseases in humans and animals are: Transmissible Spongiform Encephalopathy (TSE) or Scrapie, Bovine Spongiform Encephalopathy (BSE), Kuru and Creutzfeld-Jakob-Disease [45]. Prions are also present in yeast, where they act as protein-based epigenetic elements and are inherited via the cytoplasm in a non-Mendelian fashion [46] (see section 1.2). Yeast prions are involved in epigenetic, transcriptional and translational regulatory processes and can be beneficial [47]. For example, it was shown that prion formation is induced in variable environmental stress conditions and, depending on the yeast strain background, sometimes had a beneficial effect on cell viability under these conditions [48, 49].

1.2. Yeast Prions

Yeast prions are self-propagating amyloid-like conformations. Yeast has different proteins that can adopt a prion conformation. The first discovered yeast prions were [*PSI*$^{+}$] and [*URE*3], that are prion forms of Sup35 and Ure2 proteins, respectively [50, 51]. These prions can be formed spontaneously at low rates. During prion conversion, Ure2 or Sup35 proteins undergo conformational changes, becoming protease resistant and insoluble and form amyloid fibers [52]. Prion-states often lose the normal cellular functions of the protein that is responsible for the prion. However, the [*RNQ*$^{+}$]/[*PIN*$^{+}$] prion, caused by the Rnq1 protein can have a gain-of-function phenotype, which is to enhance the de novo formation of [*PSI*$^{+}$] prions via a prion cross-seeding mechanism [51-54]. Generally, yeast prions are not toxic to yeast cells [55, 56]. The biological significance of yeast prions is still under debate, but it was suggested that they can act as protein-based genetic elements (i.e. non-chromosomal) that are inherited to the progeny without following Mendel's laws of inheritance [57, 58]. The prion state is associated with several phenotypic changes that can be beneficial under certain environmental conditions [48, 49]. In line with this, it was shown that stress can induce prion formation [49]. It was hypothesized that this stress-induced prion formation creates a larger variety of phenotypes, some of which might help to cope better with the stress conditions such as high salt concentrations, oxidative stress (H_2O_2), and high temperature [49].

1.2.1. Formation of Yeast Prions

Yeast prions often contain a glutamine (Q) and asparagine (N) rich prion domain that is responsible for the prion-like properties of the respective protein due to its self-propagating propensity [59, 60]. These Q/N-rich domains are present either at the N-terminus (in Sup35 and Ure2) or at the C-terminus (in Rnq1) of the proteins [60]. Transient overexpression of a full-length prion protein or its prion domain can induce

the *de novo* formation of yeast prions [61]. These prion proteins can form amyloids either spontaneously on their own, or their initial appearance can be promoted by the presence of other prions. For example, the [*RNQ*$^+$] prion acts as a template for cross-seeding and enhances the *de novo* formation of the [*PSI*$^+$] prion. Hence [*RNQ*$^+$] is also termed as [*PIN*$^+$] ([*PSI*$^+$]-*in*ducible) [62, 63].

The protein-remodeling factor Hsp104 (AAA$^+$ ATPase chaperone) is involved in the faithful propagation of most known yeast prions including the [*PSI*$^+$] prion [64]. Hsp104 works in combination with Hsp70 and Hsp40 for remolding of misfolded proteins as well as for maintaining prions. Elimination of Hsp104 function, either by deletion of the HSP104 gene or by inhibition of its ATPase activity by GdnHCl (termed curing) induces a slow loss of [*PSI*$^+$] over several generations, and the cells become [*psi*$^-$] [61, 65, 66]. This process is reversible. Fragmentation of prion fibrils by Hsp104 threading activity results in the generation of smaller units (termed propagons) that are inherited to the progeny [67, 68]. These propagons also act as seeds to form long prion fibrils. Therefore, loss of Hsp104 function abolishes prion fiber fragmentation and hence, no smaller units are generated that can be passed to the progeny. This causes a loss of the prion state in the progeny over multiple generations due to failure in the formation of new propagon/seed [68].

1.2.2. The yeast [*PSI*$^+$] prion

The [*PSI*$^+$] prion is the best-characterized yeast prion. It is the amyloid isoform of the translation termination factor Sup35p [69]. The non-prion form is indicated as [*psi*$^-$] where the Sup35p protein remains in the soluble, functional conformation. Formation of the prion isoform is associated with a phenotypic switch. In case of the [*PSI*$^+$] prion, the phenotypic switch is caused by a reduction of the translation termination function of Sup35p, because the aggregated/prion form of Sup35 is unable to terminate the translation properly. The result is translational readthrough of some STOP codons in the [*PSI*$^+$] form.

This feature facilitates to differentiate these two isoforms of Sup35 based on the red/white colony assay. Both isogenic strains carry a premature stop codon (UGA) in the ADE1 gene (ade1-14) [70, 71]. In [*psi*$^-$] cells, translation of the ade1-14 allele is terminated prematurely due to the translation termination activity of soluble Sup35p. The truncated Ade1 protein is not functional in the adenine biosynthesis pathway. Consequently, the cells are auxotroph for adenine and accumulate a red adenine synthesis byproduct (Fig 2). The colonies of these [*psi*$^-$] cells appear red on YPD [70, 71]. On the contrary, in [*PSI*$^+$] cells a large portion of the Sup35p protein forms insoluble amyloid fibrils and cannot perform its normal translation termination function. Consequently, functional full-length Ade1 protein is synthesized by stop-codon readthrough, the [*PSI*$^+$] cells are prototroph for adenine and accumulate much less of the red synthesis byproduct and hence appear white to light pink on YPD plates [70, 71].

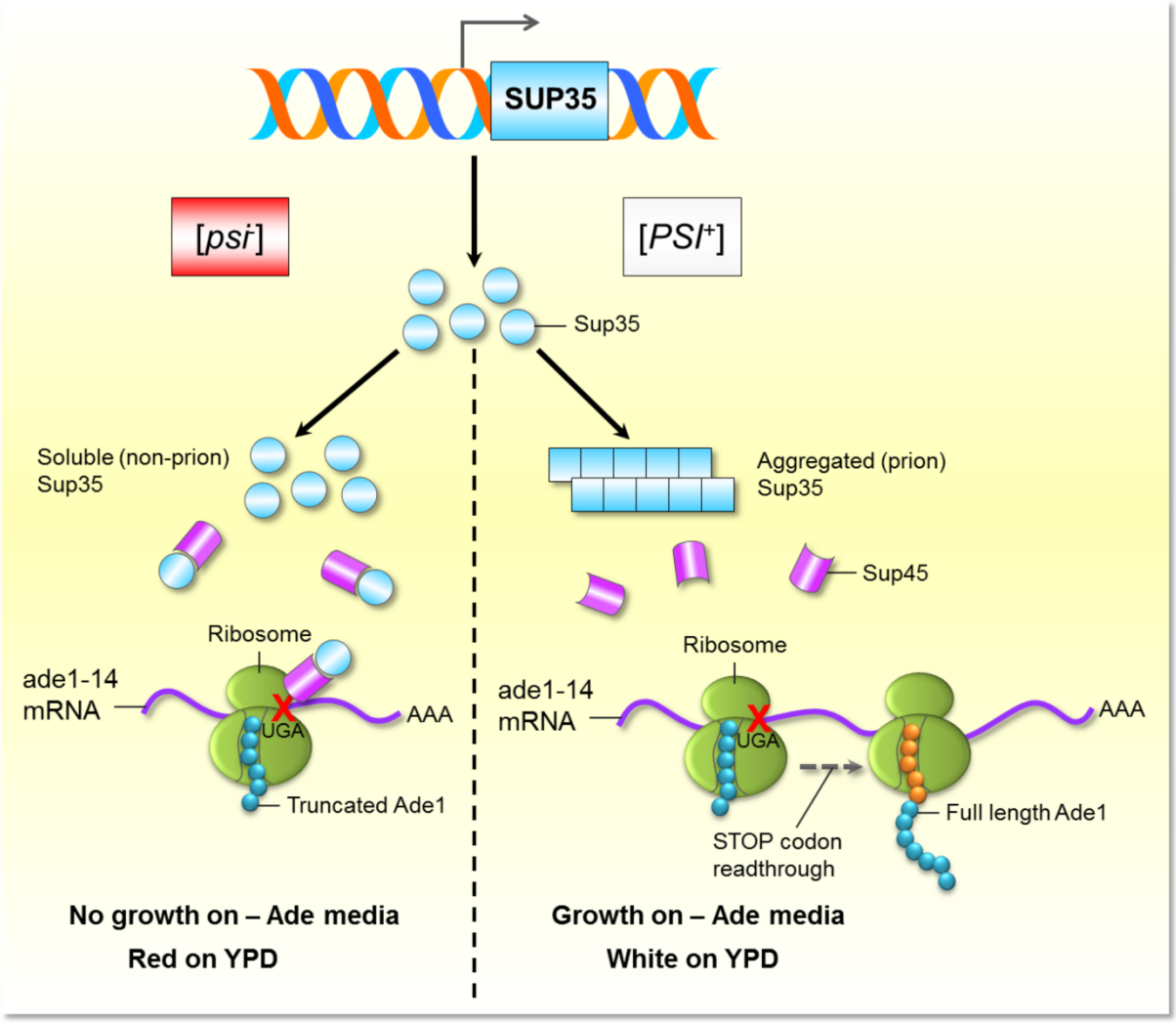

FIGURE 2: The [*PSI*$^+$] prion and [*psi*$^-$] non-prion states in *S. cerevisae* – Both isogenic strains harbor a premature UGA stop codon in their ADE1 gene (termed ade1-14 mutation). In [*psi*$^-$] cells, the Sup35p terminates the translation together with Sup45p and releases the truncated Ade1 protein, which is not functional in adenine biosynthesis. Therefore, [*psi*$^-$] cannot grow on media lacking adenine (−Ade) and corresponding colonies are red on YPD due to the accumulation of a side product of adenine biosynthesis. In [*PSI*$^+$], since most of the Sup35p forms amyloid fibrils and cannot perform its normal translation termination activity, full-length Ade1 is produced by stop-codon read through of ribosomes. Thus, [*PSI*$^+$] cells are white on YPD and can grow on −Ade plates.

PrD-GFP as a model substrate for amyloid

The Sup35p is made up of three domains: Q/N-rich N-terminal domain (N) required for [*PSI*$^{+}$] formation, highly charged middle domain (M) and the C-terminal domain (C) necessary for translation termination [72] (Fig 3). The N-terminal domain (N) is 1-114 residues long but to study the prions, many researchers use 1-253 long sequence including the highly charged middle domain (M) which makes this peptide more soluble and easy to handle [60]. The combined sequence of N and M domain of Sup35p is called as "NM" or "PrD". A GFP fusion protein of Sup35p prion domain (PrD-GFP) provides a visually tractable prion model to study the amyloid-like properties of [*PSI*$^{+}$] in yeast [65].

During *de novo* prion induction and maturation, the PrD-GFP fusion is deposited in three different stages of prions termed as Diffuse, Rings/Ribbon and Dot [65] [65]. Initially, during prion induction, PrD-GFP is expressed as a soluble form which shows diffuse fluorescence (Diffuse state). The soluble PrD-GFP can be converted to prion state in the presence of [*PSI*$^{+}$] prion inducer, called [*PIN*$^{+}$/*RNQ*$^{+}$]. In this stage, PrD-GFP amyloid aggregates appear as bundles of long fibrils at the cell periphery, often intersecting with the IPOD (Ring state). The molecular chaperone Hsp104 cleaves these long fibrils, and bundles of short fibrils become visible at the IPOD. This indicates the final mature state of PrD-GFP (Dot state) [65, 73]. Thus PrD-GFP can be used as a model amyloid substrate to study amyloid biology in yeast.

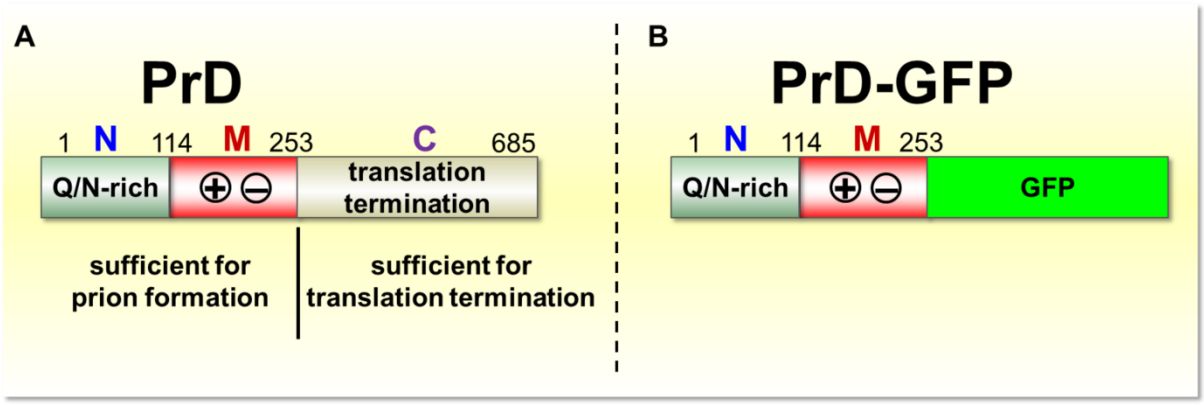

FIGURE 3: Protein domain organization of Sup35p– (**A**) The Sup35p has three domains: Q/N-rich N-terminal domain (N), highly charged middle domain (M) and the C-terminal domain (C). The NM or PrD domain is sufficient for [*PSI*$^{+}$] formation while the C-terminal domain is necessary and sufficient for translation termination. (**B**) A GFP fusion protein of Sup35p prion domain (PrD-GFP) serves as a model amyloid substrate to study the amyloid-like properties of [*PSI*$^{+}$] in yeast [65].

1.3. Components of the protein quality control network

Inside the cell, proteins often get misfolded due to several proteotoxic stresses, mutations or translational errors [55, 74]. These misfolded proteins normally have a tendency to aggregate which might have a toxic 'gain-of-function' to the cells [75]. In order to eliminate protein aggregates, cells have evolved a highly sophisticated cellular protein quality control machinery that maintains the proteome integrity and cell viability [74]. Several components of this protein quality control network work collaboratively to promote native folding of nascent polypeptides, degradation of misfolded proteins prior to aggregation or removal or deposition/sequestration of aggregates once they have formed [55, 74]. Molecular chaperones are the key players of this quality control network that determine the fate of misfolded/aggregated proteins in various ways.

1.3.1. Molecular chaperones involved in protein disaggregation

Molecular chaperones are an essential group of proteins that facilitate the proper folding, refolding and macromolecular assembly/disassembly of client proteins either through substrate binding and release cycles in an ATP-dependent manner or an ATP-independent 'holdase' mode [76, 77]. Although chaperones are very abundant cellular proteins, their intracellular levels are further increased during many stress conditions. The chaperones are classified into five major families based on their molecular weights: Hsp60, Hsp70, Hsp90, Hsp100 and the small heat shock proteins (sHSPs) [4, 78, 79]. Among them, some chaperones such as Hsp100, Hsp90, Hsp70 and Hsp60 proteins are ATP-dependent chaperones while sHSPs are ATP-independent chaperones [77]. The small heat shock proteins (sHSPs), the Hsp70 system and Hsp100 disaggregases are the major families of chaperones involved in aggregate handling in the cell. Therefore, the focus of this thesis is on those families of chaperones.

The Hsp70 chaperone family

The Hsp70 family of chaperones recognizes exposed hydrophobic amino acid side-chains of unfolded/partially folded proteins and promote *de novo* folding and refolding through substrate release cycles in an ATP-dependent manner [80-82]. The Hsp70/DnaK system is composed of Hsp70 (in yeast) or DnaK (in bacteria) with its two co-chaperones, a J-domain protein (Hsp40 in yeast and DnaJ in bacteria) and a nucleotide exchange factor (NEF) [55, 77, 83, 84]. Hsp70 is the most ubiquitous and conserved chaperone that exists in different cellular compartments. It drives various cellular functions including folding, assembly, and translocation of newly synthesized

proteins across organelle membranes and disaggregation of aggregated proteins [78, 85]. Hsp70 contains two domains: (I) a substrate-binding domain and (II) an ATPase domain. Hsp70 chaperone activity depends on dynamic interactions of these domains with its co-chaperones such as J-domain protein/Hsp40 (which delivers substrates to ATP-bound Hsp70 and accelerates ATPase activity of Hsp70) and nucleotide exchange factor (NEF) [78, 85].The ATP-bound Hsp70 (low substrate affinity state), binds with the exposed hydrophobic patches of unfolded/partially folded proteins via its substrate-binding domain [7, 85]. After ATP hydrolysis, the substrate is released by nucleotide exchange factors (NEFs) that trigger the exchange of ADP by ATP during the Hsp70 cycle. Hsp70 also works together with Hsp104 disaggregases, as described below for the disaggregation of large aggregates [67, 78].

The Hsp100 chaperone family

Hsp100 chaperones extract single polypeptides from aggregated species through its ATP-driven threading activity to either degrade them in cooperation with an associated protease or to refold them together with Hsp70. The Hsp100 disaggregase (ClpB in bacteria and Hsp104 in yeast) belongs to the Clp/Hsp100 family of the AAA+ (ATPases associated with various cellular activities) chaperones [86]. The Hsp100 disaggregases were initially identified as essential factors for cell survival when cells are exposed to extreme temperatures. This phenomenon is also referred to as heat-induced thermotolerance [87]. Later it was shown that such a thermotolerance is a consequence of the reactivation of aggregated proteins by a system called as Hsp100/Hsp70 bi-chaperone system [67, 88, 89]. This Hsp100/Hsp70 bi-chaperone system is composed of hexameric Hsp100 disaggregase and the Hsp70 system that facilitates in re-solubilization of the aggregated proteins in an ATP-dependent manner. Remarkably, cooperative action of both chaperone systems is necessary for proper protein disaggregation. Either system alone is unable to rescue the aggregated proteins.

The mechanism of protein disaggregation by this bi-chaperone system (Fig 4) involves several steps. Initially, the Hsp70 system recognizes misfolded protein aggregates and later recruits the hexameric Hsp100 disaggregase (ClpB/Hsp104). Fueled by ATP hydrolysis, ClpB/Hsp104 extracts polypeptides from aggregates by a threading activity through its central pore [55, 90]. A puling force generated by ATP hydrolysis promotes the translocation of the unfolded protein through the central pore of ClpB/Hsp104 hexamer [55]. Finally, the extracted unfolded polypeptide is subjected to the protein quality control network for either refolding or degradation. Besides the action of Hsp100/Hsp70 bi-chaperone system on disaggregation of heat-induced amorphous aggregates, this bi-chaperone system is also involved in prion (amyloids) fragmentation and propagation [77].

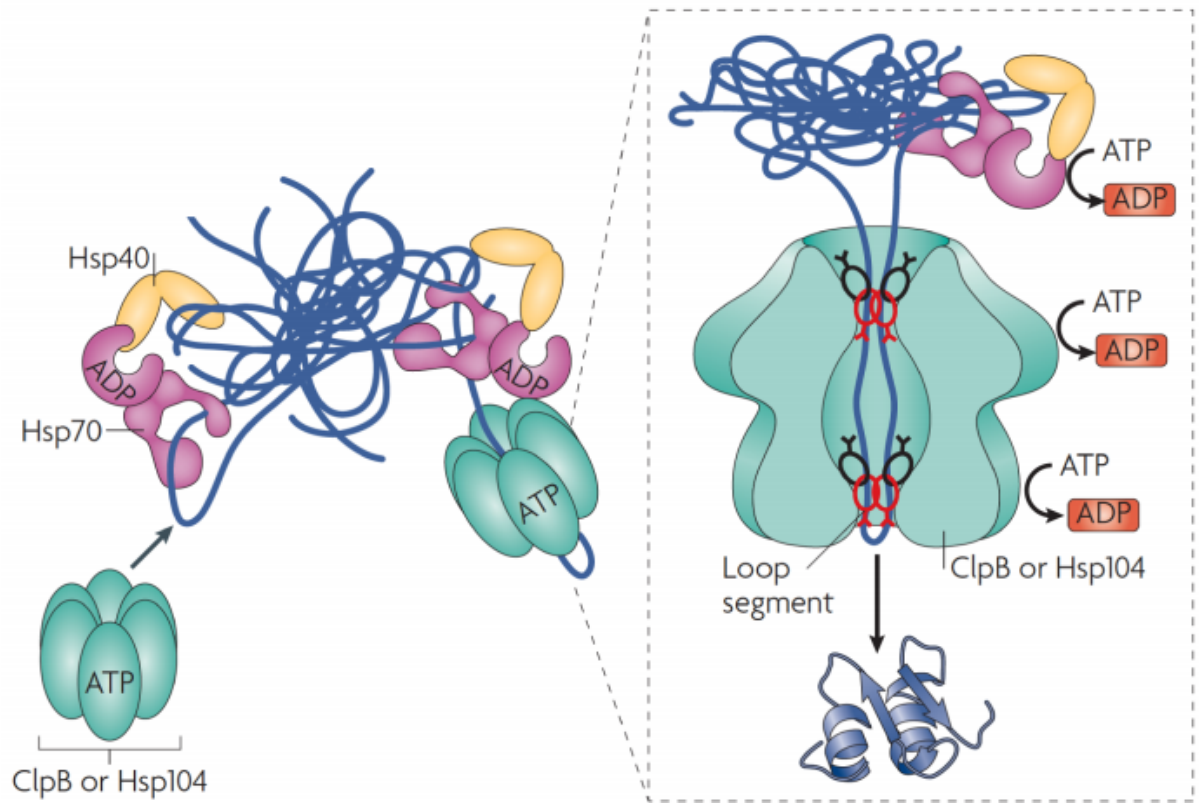

FIGURE 4: Mechanism of protein disaggregation by the ClpB/Hsp104-Hsp70 bi-chaperone system–The Hsp70 system (Hsp70 plus its co-chaperone Hsp40) initially recognizes the misfolded protein aggregates and later transfers them to the Hsp100 disaggregase (ClpB in bacteria and Hsp104 in yeast). The ClpB or Hsp104 hexamer extracts polypeptides from the aggregates by a threading activity, driven by ATP hydrolysis. The ATP hydrolysis generates a puling force to promote the translocation of single polypeptide chains from the aggregates through the central pore of the ClpB/Hsp104 hexamer. The unfolded protein is then refolded back to its native state by the Hsp70 system. The figure was adapted from [55].

The sHSP family

sHSPs are low molecular weight (15-42 kDa) ATP-independent chaperones which modulate the architecture of protein aggregates and facilitate their disaggregation. sHSPs generally function as ‘holdase’. Yeast harbors 2 known sHSP’s, namely Hsp26 and Hsp42 are known sHSPs. During stress conditions, these sHSPs (the high substrate affinity state) directly interact with misfolded/aggregated proteins and form a stable sHSP–substrate complex [55, 91]. This complex does not allow to release bound misfolded proteins spontaneously. Therefore, it creates a temporary reservoir of aggregated proteins inside the cytosol. The sHSPs-misfolded protein

complex then recruits either Hsp100/Hsp70 bi-chaperone system or Hsp70 system for the disaggregation of aggregated proteins [55].

1.3.2. Degradation and clearance of misfolded protein aggregates

Removal of damaged or misfolded proteins is an important task within the cellular quality control network and is mediated by different degradation machineries. Specialized recognition of damaged proteins for their degradation is ensured in organisms from all kingdoms of life, although it is accomplished by different ways in different organisms. Aggregated proteins can be degraded in two ways: (I) either as soluble single polypeptide chain extracted from an aggregate or (II) as entire protein aggregate. In the first case, single misfolded polypeptide chains have to be extracted first by specialized disaggregases such as Hsp104 (see section 1.3.1) before they can be turned over for example by the proteasome as described below.

The ubiquitin-proteasome system (UPS)

In eukaryotic cells, the ubiquitin-proteasome system (UPS) (Fig 5) confers a major cytosolic proteolytic activity by which mostly the short-lived proteins are first ubiquitinated and then targeted to the proteasome for their degradation. The protein ubiquitination is catalyzed by a cascade of three enzymatic reactions that conjugate the ubiquitin moiety (8.5 kDa) to lysine residues of the substrate. First, ubiquitin is activated by the ubiquitin-activating enzyme (E1). Subsequently, the activated ubiquitin is handed over to the ubiquitin-conjugating enzyme (E2). In the last step, the ubiquitin ligase (E3) binds both the substrate protein and E2~Ub and catalyzes the Ub transfer from E2~Ub onto the amino group of a lysine reside of the target protein [92, 93]. The E3 ligases recognize one or several specific proteins from the cytosolic proteome. Therefore, E3's provide the substrate selectivity for the UPS. Additional Ub moieties can be attached to the first Ub moiety to polyubiquitinated substrates. The polyubiquitinated proteins are then turned over by the 26S proteasome.

The 26S proteasome is composed of one 20S core particle and two 19S regulatory particle/cap subunits. The 20S core particle (made up of two times two heptameric rings, α1-7 and β1-7) is a proteolytic chamber that harbors three different proteolytic activities (chymotrypsin-like, trypsin-like, and peptidyl glutamyl-like) [94, 95]. The 19S regulatory particle recognizes polyubiquitinated proteins, removes the ubiquitin chain by 19S-cap associated deubiquitinases (DUBs) [96] and unfolds the substrate to translocate it into the interior of the 20S proteolytic core [92, 97]. Finally, the substrate is cleaved into oligopeptides. Targeting of cellular proteins for effective degradation needs to be controlled, independently of the nature of the substrates. Polyubiquitination is considered as a key degradation mark for substantial

proteasomal substrates, although ubiquitin-independent proteasomal degradation is also known for a few substrates [98]. Degradation of misfolded proteins via the UPS system uses specific E3 ligases. In yeast, the most prominent ones are: Ubr1 [99] and Ubr2 [100] in the cytosol and San1 in the nucleus [101]. Nuclear San1 was shown to degrade cytosolic misfolded proteins (ΔssCPY*-GFP substrate) with a parallel action of cytosolic Ubr1 [102]. Both Ubr1 and San1 can compensate for each other's function. Therefore, cytosolic misfolded substrates (tGnd1-GFP, ΔssCPY*-GFP) are not ubiquitinated/degraded in the absence of these E3 ligases [102, 103]. Remarkably, some preferred E2 enzymes such as Ubc4 and Ubc5 also involve in proteasome-mediated degradation of aberrantly folded cytosolic proteins. [104].

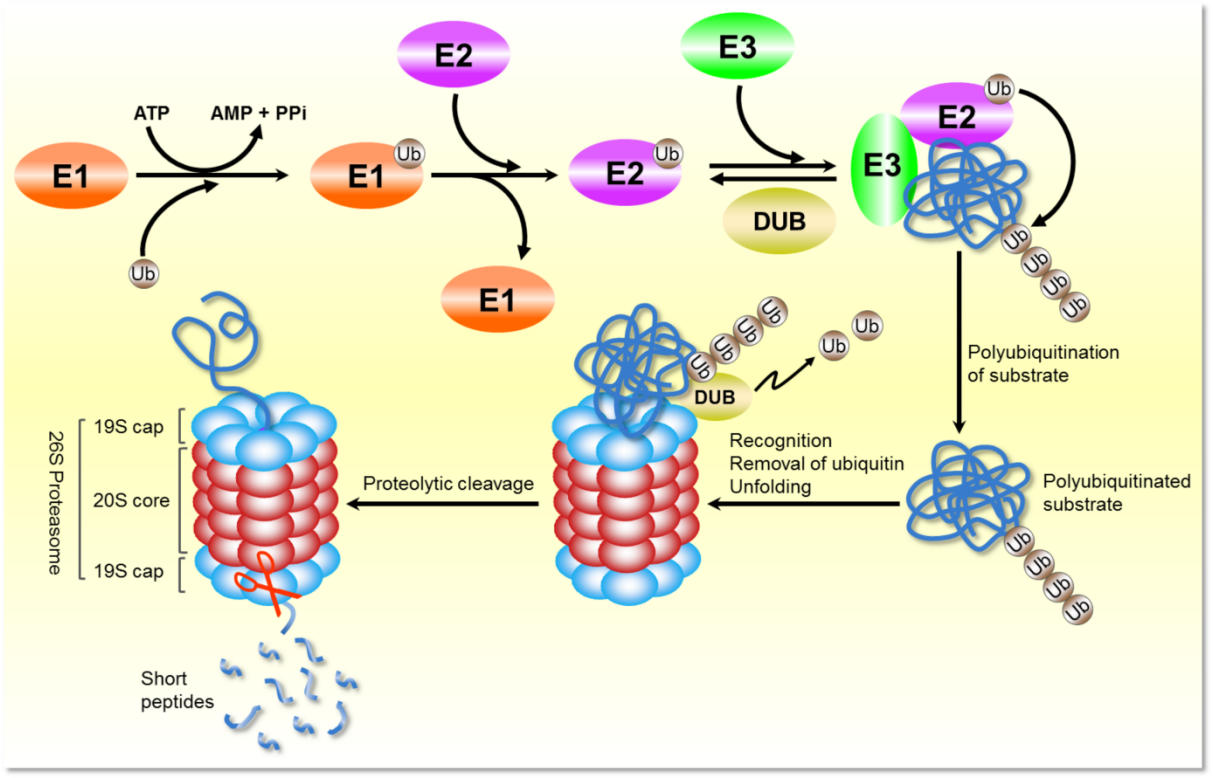

FIGURE 5: The ubiquitin–proteasome system (UPS) of protein degradation–The UPS is initiated by tagging the substrate protein with a highly conserved 76 amino-acid residue polypeptide, ubiquitin (Ub). This conjugation is an ATP-dependent process and is achieved by three enzymatic cascade reactions (E1–E3). The ubiquitin-activating enzymes (E1) first bind ubiquitin under ATP hydrolysis. Afterwards, the ubiquitin moiety is handed over to the ubiquitin-conjugating enzyme (E2). Subsequently, the ubiquitin ligase (E3) is attached with the substrate protein together with E2~Ub and catalyzes the transfer of Ub chain from E2~Ub onto an amino group of lysine residues of the target substrate protein. Multiple ubiquitin moieties are attached to the substrate protein destined for proteolytic turnover, resulting in polyubiquitin chains. The polyubiquitinated proteins are afterwards recognized by the 19S regulatory subunit (19S cap) of the 26S proteasome complex. Deubiquitinating enzymes (DUBs) that are associated with the 19S cap remove the ubiquitin chain before the substrate is unfolded and transferred into the interior core of the 20S cylindrical subunit (20S core) of the of the 26S proteasome complex. Finally, the substrate is cleaved into short peptides by the proteolytic activity of the 20S proteolytic core.

Autophagy

Autophagy ('self-eating') is a self-degradation system that efficiently removes nonfunctional cytoplasmic components under certain circumstances. Autophagy can also be involved in the turnover of aggregates and recycling of basic building blocks (i.e., amino acids) in response to nutrient starvation [105]. It is an evolutionary highly conserved cellular process that eliminates long-lived misfolded/aggregated proteins, damaged organelles (mitochondria, endoplasmic reticulum and peroxisomes) and intracellular pathogens [106-109]. The lysosomal (vacuolar) autophagy is the second major proteolytic degradation machinery in eukaryotes in addition to the UPS. This process mediates the bulk degradation of cytoplasmic components which are enwrapped into double-membrane vesicles termed autophagosomes. The autophagosome delivers these components into specific lytic compartments such as lysosomes in mammals and vacuoles in fungi and plants, for their proteolytic degradation. Thus, autophagy is an important cellular process that promotes cell viability by keeping the cellular environment free of aberrant proteins/organelles [110].

Based on cargo selection, two types of autophagy are described: non-selective (bulk) autophagy and selective autophagy [108, 111, 112] (Fig 6). The non-selective (bulk) autophagy degrades bulk cytoplasmic contents. [112]. The bulk autophagy is a nonspecific (non-selective) process that normally operates at a basal level, but can be induced upon starvation [111-114]. Thus, it is also termed starvation-induced autophagy [112, 115] that sequesters bulk cytoplasmic components to the growing autophagosomes. These autophagosomes further fuse with vacuole and release the bulk cytosolic contents into the vacuolar lumen for their degradation by resident acid hydrolases [112, 115]. In contrast, selective autophagy is a receptor-mediated process which degrades only specific cargoes (damaged mitochondria/peroxisomes, stress-induced ER, nucleus, proteasomes, pathogens and ribosomal/damaged proteins) by binding to specific autophagy receptors [112, 116-120].

In mammalian cells, ubiquitinated protein aggregates are internalized into lysosomes via selective autophagy (aggrephagy) that is mediated by specific autophagy receptors such as for example p62 and NBR1 [107, 121-124]. P62 or NBR1 directly bind to the autophagy marker protein LC3 (Atg8 in yeast) [121, 123] and recruits deposits of ubiquitinated protein aggregates to the lysosome. LC3 is a component of autophagic membranes, which enwrap these aggregates to form autophagosomes that subsequently fuse with the lysosome to release the aggregates into the lysosomal lumen for degradation by resident lysosomal proteases [107].

In yeast, vacuolar degradation of aggregated proteins has also been shown recently for some aggregates such as α-synuclein and polyQ-aggregates [125]. α-synuclein aggregates, formed upon overexpression, were found to be more stable in certain autophagy mutants than after proteasome inhibition [125]. This suggested that α-synuclein aggregates are efficiently degraded by an autophagic pathway in yeast

[125]. However, it did not become clear how these α-synuclein aggregates are recognized, transported and sequestered into the autophagosomes. Moreover, the Atg8 (LC3) adaptor protein CUE5 (human Tollip homolog) binds to ubiquitinylated PolyQ aggregates and links them to Atg8-phosphatidylethanolamine (Atg8–PE), present at the autophagosomes [126]. Deletion of the CUE5 adaptor protein leads to accumulation of PolyQ aggregates in the cytosol [126], suggesting PolyQ aggregates are removed by Cue5-mediated autophagy in yeast. In yeast, several autophagy-related (ATG) genes (33 ATG genes) are involved in the core machinery of both selective (CVT) and non-selective autophagy [127].

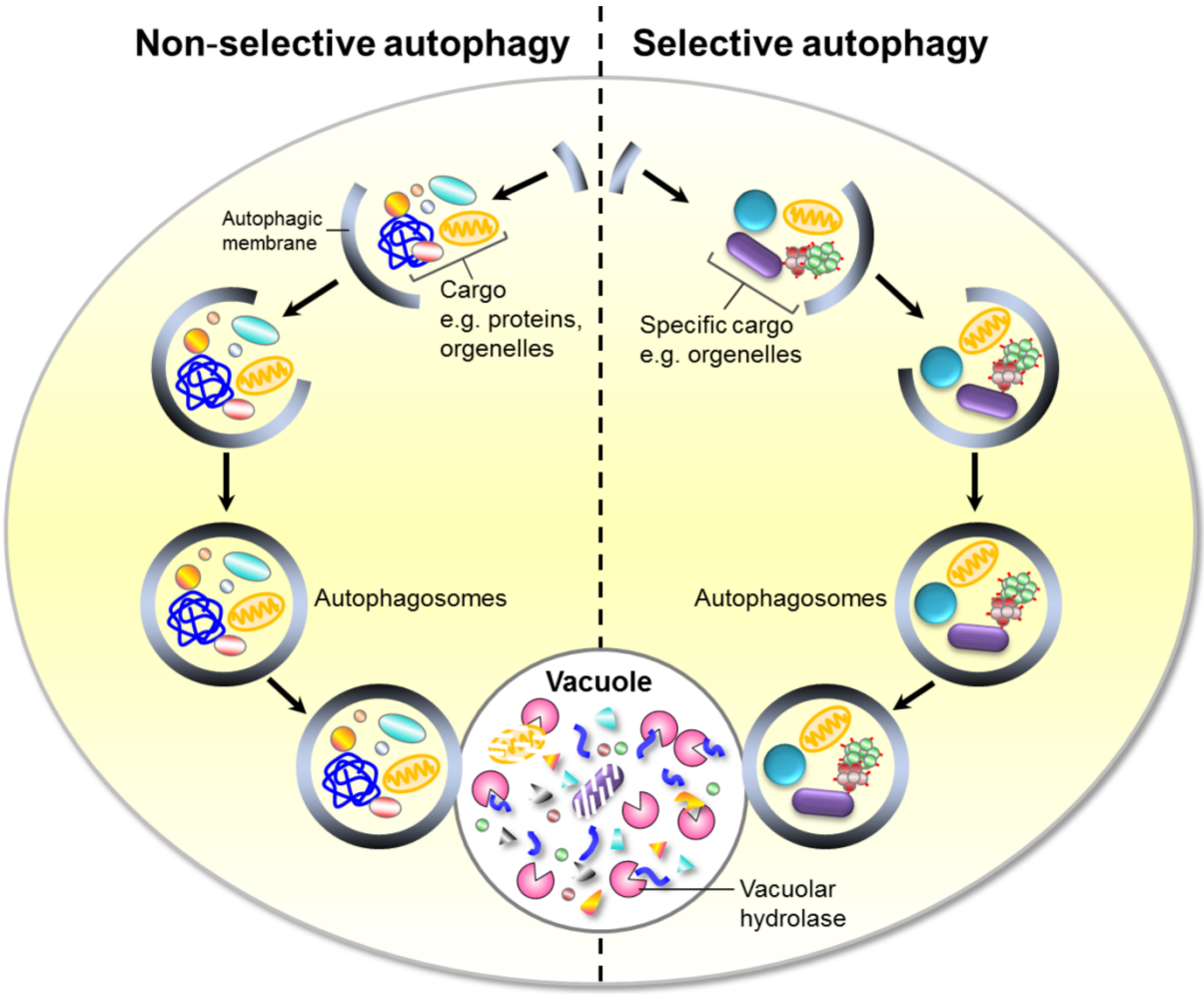

FIGURE 6: The non-selective (bulk) autophagy and selective autophagy in yeast – During non-selective (bulk) autophagy, bulk cytoplasm and other cytosolic constituents are randomly/non-selectively sequestered into the autophagosomes. The autophagosomes fuse with vacuole and release these cargos into the vacuolar lumen for their degradation by resident acid hydrolases. In contrast, selective autophagy is a receptor-mediated process which either degrades only specific cargoes (for example damaged mitochondria or peroxisomes) or delivers resident hydrolases aminopeptidase I (preApe1) and α-mannosidase (Ams1) into the vacuolar lumen for their maturation via the CVT (cytoplasm-to-vacuole targeting) pathway [112, 116-118].

The CVT pathway: a selective autophagy pathway in yeast

Selective autophagy is an important cellular quality control process that operates at a basal level under normal growth conditions and contributes to maintain cellular homeostasis. This process has the capacity to distinguish and recognize their substrates from the cytosolic pool by specific receptors. In yeast, the CVT (cytoplasm-to-vacuole targeting) pathway is a biosynthetic selective autophagy pathway that usually operates under non-starvation/nutrient-rich conditions [113, 116]. The CVT pathway delivers the resident precursor hydrolases aminopeptidase I (preApe1) and α-mannosidase (Ams1) from the cytosol into the vacuolar lumen for their maturation [112, 116-118]. Since it employs the core machinery of macroautophagy, it is also considered as a selective autophagy pathway in yeast.

The precursor aminopeptidase 1 (preApe1) is the primary cargo protein of this pathway. It oligomerizes in the cytosol to form dodecamers and higher order complexes of multiple dodecamers and is bound by the Atg19 receptor to form the CVT complex [113] [112, 114, 116, 127, 128]. The smaller oligomers of α-mannosidase (Ams1) also associate with this CVT complex [117, 118, 127]. This complex subsequently binds to the Atg11 adaptor, which links the complex to vesicles that contain the transmembrane protein Atg9 and are termed Atg9-vesicles. These Atg9 vesicles (containing preApe1, Atg19, Atg11 and Atg9) then associate with actin cables via unknown factors and are recruited to the Phagophore Assembly Site (PAS) adjacent to the vacuole [114] [115]. The PAS is a cellular site where cells initiate formation of double-membrane autophagosomes during autophagy and CVT vesicles during the CVT pathway (Fig 7). At the PAS, Atg8-phosphatidylethanolamine (Atg8–PE) conjugates bind to the Atg19 receptor and stay on the inner and outer membrane of the forming CVT vesicles [108, 109, 111, 129]. After fusion of these CVT vesicles with the vacuole, preApe1 is released into the vacuolar lumen and converted to its active mature form by proteolytic cleavage of the propeptide [113, 114]. Those Atg19 and Atg8–PE molecules that are located at the inner membrane of the CVT vesicles, are also degraded after this fusion event [109]. Although the CVT substrates preApe1 and Ams1 are delivered into the vacuole by their incorporation into CVT vesicles under normal growth conditions, CVT substrates can also be incorporated into autophagosomes under starvation conditions for their transport into the vacuole [115]. In yeast, the CVT pathway is studied extensively and serves as a model for selective types of autophagy. Its maturation kinetics can easily measure the degree of selective autophagy *in vivo*.

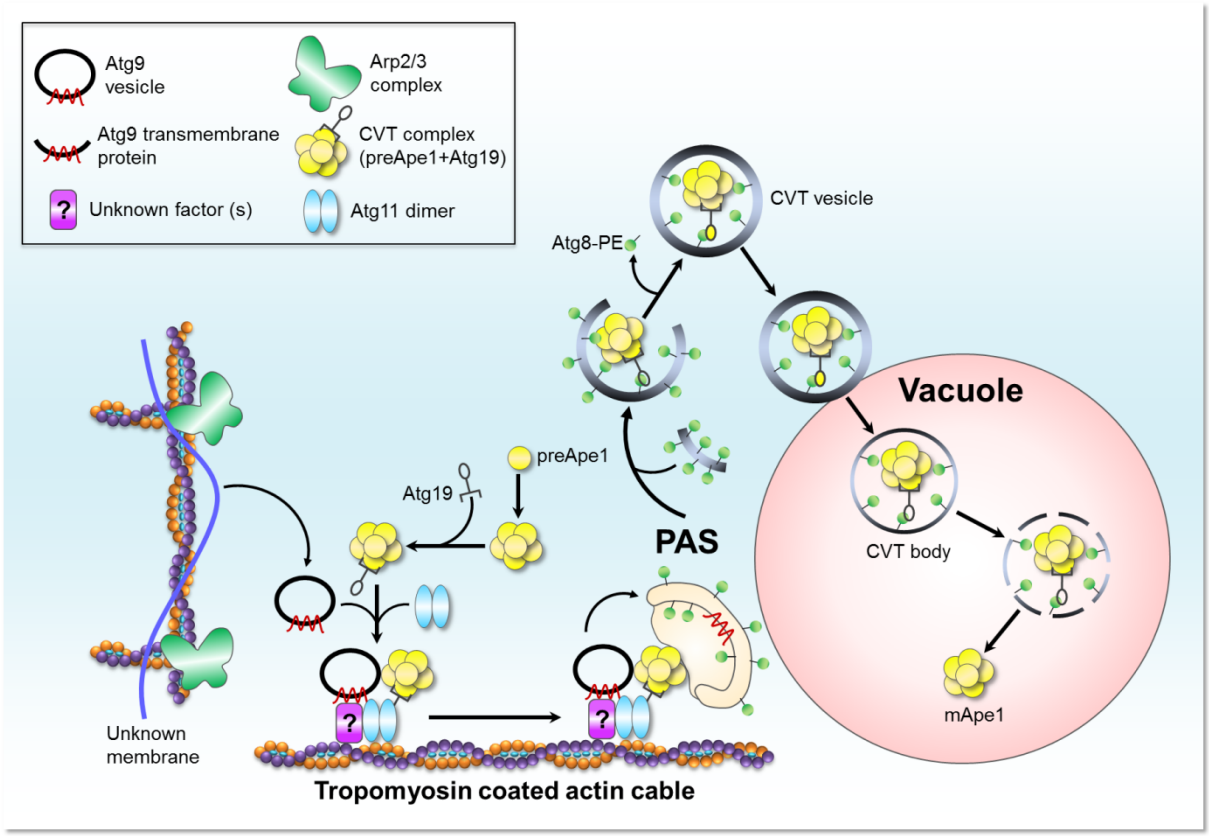

FIGURE 7: The CVT (cytoplasm-to-vacuole targeting) pathway is an example of a selective/specific autophagy in yeast – After synthesis, the precursor aminopeptidase 1 (preApe1) forms cytoplasmic oligomers that bind to its receptor Atg19 and forms the CVT complex. This complex further binds to Atg9-containing vesicles via the adaptor Atg11. These Atg9 vesicles (containing preApe1, Atg19 and Atg11) then associate with actin cables via an unknown linking factor and move to the phagophore assembly site (PAS), adjacent to the vacuole. At the PAS, preApe1 is enwrapped into double-membrane CVT vesicles which subsequently fuse with the vacuolar membrane and deliver preApe1 into the vacuolar lumen for its maturation. The figure was adapted and slightly modified from [114].

1.4. Spatial protein quality control network

Various stress conditions can cause proteins to misfold. Those misfolded proteins can accumulate in spatially distinct inclusions from bacteria to humans when refolding and degradation systems, dealing with the misfolded substrates, get overwhelmed [55]. It is assumed that such organized spatial quality control compartmentalization serves many favorable cellular purposes such as: (I) efficient protection of the cellular environment from the accumulation of potentially toxic aggregated species, (II) possible organization of protein quality control factors/chaperones acting on these aggregates, (III) supporting the triage process of refolding versus degradation of a misfolded protein and (IV) allow for asymmetric

inheritance of damaged/aggregation-prone species as a means to generate aggregate free progeny [74].

1.4.1. Aggregate deposition in bacteria

In bacteria, endogenous proteins can aggregate upon heat or oxidative stress. Overexpression of certain heterologous proteins in bacteria can cause stress. Consequently, these proteins form amorphous aggregates which are spatially compartmentalized into inclusion bodies (IBs) that are formed predominantly at the cell poles. Therefore, IBs are considered as temporary storages to deal with the overload of misfolded/aggregated species [130]. These protein aggregates recruit the disaggregation system ClpB/DnaK/DnaJ, also termed the bi-chaperone system (compare section 1.3.1). However, the actual mechanism by which aggregated and misfolded proteins are transported into peripheral inclusions, is still under debate. The polar localization of inclusions is not an active process but could be explained by a passive mechanism due to large nucleoid occlusion, which forces aggregates/inclusions to move towards the poles [55]. This polar localization allows for asymmetric inheritance of protein aggregates and rejuvenation of daughter cells without inclusions [131, 132]. This asymmetric inheritance of aggregates is lost when cytosolic aggregation is artificially targeted to the inner membrane [132], demonstrating that such spatial compartmentalization facilitates asymmetric inheritance of inclusion bodies.

1.4.2. Aggregate deposition in mammals

In the mammalian cytoplasm, specialized inclusion bodies, termed “aggresomes” are formed which deposit misfolded cytosolic proteins upon expression of heterologous proteins, various disease conditions or impairment of proteasomes [133]. These aggresomes are formed temporally at a perinuclear site termed microtubule-organizing center (MTOC). Aggresomes are surrounded by a cage of the intermediate filament vimentin [133]. The histone deacetylase HDAC6 functions as an adaptor that binds to Lys^{63}-linked polyubiquitin chains on misfolded proteins on the one hand and the minus-end microtubule motor protein dynein on the other hand, which drives the active transport of aggregates along microtubules towards the MTOC [134]. Therefore, ubiquitination mediated by Parkin/CHIP or other related E3 ubiquitin ligases [135, 136], seems to serve as a recognition signal to target misfolded proteins to the aggresome, though it was not shown for all aggresome substrates [137]. Disruption of microtubules or dynein motor function and inhibition of HDAC6 prevents aggresome formation and can lead the accumulation of misfolded protein aggregates as dispersed foci in the cytoplasm [133, 134]. Thus aggresomes protect the cell from the accumulation of potentially toxic aggregation-prone proteins in the cytoplasm. Furthermore, it facilitates the selective autophagic clearance of

these proteins. For autophagic degradation, protein aggregates bind to autophagic receptors p62 or NBR1 via their ubiquitin chains. These receptors also bind to the light chain 3 (LC3), a mammalian homologue of yeast Atg8 [123, 138]. This complex is enwrapped into double-membrane autophagosome which subsequently fuses with the lysosome and releases ubiquitylated substrates into the lysosomal lumen for degradation by hydrolytic enzymes (Fig 8).

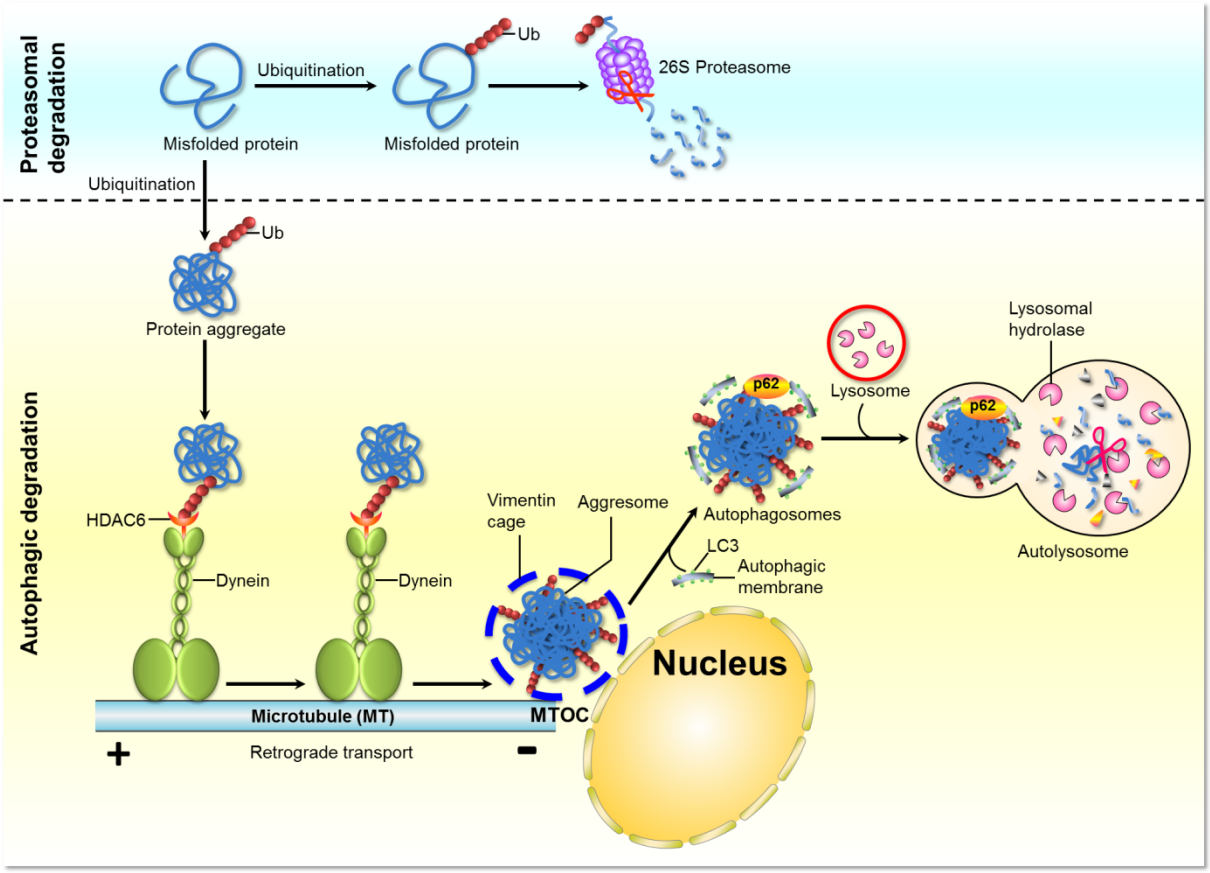

FIGURE 8: The aggresome–autophagy pathway (aggrephagy) in mammalian cells - In mammalian cells, misfolded proteins are initially ubiquitinated and degraded by the ubiquitin-26S proteasome system (UPS). When this UPS system failed or is overwhelmed, misfolded proteins form oligomers and small aggregates that can cause cytotoxicity. Under conditions of proteasomal impairment, these polyubiquitinated aggregates are recognized by the adaptor protein histone deacetylase HDAC6 which subsequently links these protein aggregates to the dynein motor protein. Aggregated proteins are transported by dynein motor protein complexes in a microtubule dependent manner towards the microtubule-organizing center (MTOC), adjacent to the nucleus. At the MTOC, these small aggregates coalesce to form large aggregates termed “aggresomes”, which are surrounded by a vimentin-cage of intermediate filaments. Ubiquitinated aggregates at the aggresomes are recognized by autophagic receptors p62 or NBR1 which facilitate the recruitment of autophagic membranes to the aggresome for autophagosome formation. Subsequently, the autophagosome fuses with the lysosome to form autolysosomes that allow the degradation of aggregated proteins by lysosomal hydrolases.

1.4.3. Deposition of Aggregates in *Saccharomyces cerevisae*

When components of the protein quality control system such as molecular chaperones and the ubiquitin–proteasome system (UPS)/autophagy degradation systems are overwhelmed or declined, protein aggregation is increased [74]. To deal with the overload of aggregated/damaged proteins, cells evolved additional spatial quality control strategies by which aggregated species are sequestered into specialized subcellular compartments, and such sequestration also facilitates asymmetric distribution of aggregates from mother to daughter cells [55, 74, 103, 139].

Asymmetric inheritance of protein aggregates

In *S. cerevisiae*, protein aggregates, particularly oxidatively damaged proteins, are retained in the mother cells during cell division. In the absence of the histone deacetylase Sir2, this process is compromised and accelerates the ageing processes and damage inheritance of protein aggregates by daughter cells [35, 139]. In addition, the disaggregase Hsp104 is also directly involved in the asymmetric segregation process [35, 140]. The mechanism of how Hsp104 works in the asymmetric segregation of damaged protein is still controversial. One study [141] showed that Hsp104 binds to aggregated proteins and tethers them to actin cables. Due to actin cable flow from the buds to the mother cells, aggregates are retrogradely transported and retained in the mother cell. The other study [140] showed that Hsp104 modulates the polarity of the actin cytoskeleton by binding with the components of the actin cytoskeleton or the septin machinery. Since the actin cytoskeleton facilitates asymmetric segregation of damaged proteins, deletion of HSP104 may have an indirect effect on aggregate segregation.

The cellular rejuvenation effect during asymmetric aggregate segregation was also observed in *S. pombe* and *E. coli,* suggesting that asymmetric inheritance is an evolutionarily conserved mechanism [142]. Different mechanistic perspectives were controversially discussed for asymmetric aggregate distribution: On the one hand, Sir2 and Hsp104 dependent actin-based active retrograde transport along cables clear the buds of damaged proteins [141] while on the other hand, the formation of aggregate-free buds was explained via passive diffusion of aggregates due to cell geometry and solubilization/disaggregation of aggregates in the buds by Hsp104 [143]. A passive asymmetric segregation was also observed in *S. pombe*, where heat-induced small Hsp104-GFP aggregates fuse into a large entity, which is asymmetrically inherited during budding through one of the daughter cells while leaving the other daughter cell free of aggregates. This fusion event is mediated by the small heat shock protein Hsp16 during the asymmetric segregation process [144]. In *S. cerevisiae*, the formation of specialized deposition sites for different types of

aggregates, INQ/JUNQ and IPOD (described in more detail in the next section), was suggested to facilitate asymmetric aggregate segregation [145, 146]. In human HEK293 cells, aggresome-like inclusions formed by an EYFP-tagged expanded polyglutamine segment (HDQ119-EYFP) were retained in only one of the daughter cells during their asymmetric inheritance [147]. In addition, such asymmetric inheritance of misfolded/aggregated proteins was also observed in mammalian cells where JUNQ-inclusion bodies (VHL substrate) were inherited asymmetrically while inheritance of IPOD like inclusions (HttQ97 substrate) was less stringently asymmetric [148].

Distinct aggregate deposition sites in yeast

In *Saccharomyces cerevisae*, misfolded/aggregated proteins are deposited at three major subcellular sequestration sites as described: INQ (*i*ntra*n*uclear *q*uality control compartment) [earlier JUNQ (*ju*xta*n*uclear *q*uality control compartment)], IPOD (*i*nsoluble *p*ro*t*ein *d*eposit) and CytoQ [56, 103] (Fig 9). Aggregated proteins require the nuclear factor Btn2 for deposition at the INQ [103, 149, 150]. Alternatively, they can be targeted to a newly discovered peripheral deposit termed as Cyto Q with the aid of the cytosolic small heat shock protein Hsp42 [151-154]. The IPOD, a perivacuolar deposition site, predominantly sequesters amyloidogenic protein aggregates [56, 65], terminally aggregated proteins [56] including carbonylation-sensitive proteins [65] and inactive 26S proteasomes [155], suggesting IPOD sequesters the high-molecular-weight aggregates/protein complexes before they are processed.
It was proposed that formation of INQ requires an intact actin cytoskeleton [153] but it was not clear if IPOD formation requires an intact actin cytoskeleton as well. For studying these deposition sites, different misfolded model substrates, degraded via the UPS, are commonly used. Those are a thermosensitive variant of the SUMO E2 enzyme Ubc9, Ubc9ts [156] and the human von Hippel-Lindau tumor suppressor protein (VHL), which is an E3 ligase that only properly folds when its cofactors Elongin B and C are present. In the absence of these co-factors, VHL is constantly misfolded and targeted for proteasomal degradation [157]. To study the IPOD, next to Ubc9ts and VHL, amyloidogenic substrates such as yeast prion Rnq1 [158] and the polyQ-rich protein Htt, amongst others, were used [56].

INQ (*i*ntra*n*uclear *q*uality control compartment)/ JUNQ (*ju*xta*n*uclear *q*uality control compartment)

JUNQ was originally suggested as a *ju*xta*n*uclear cytosolic deposition site since it was adjacent to DAPI staining [56]. However, DAPI stains only the chromatin, not the entire nucleus. Therefore missing co-localization of JUNQ and DAPI could not exclude a nuclear localization of JUNQ. Recently, Miller and coworkers showed that under the standard published protocol (heat shock at 37°C + proteasome inhibition

by MG132) [56, 153], JUNQ substrates, Ubc9ts and VHL are localized inside the nucleus when nucleus was visualized by the nuclear envelope/ring markers, Nup49 and Nsp1 [103]. A similar observation was made when VHL-GFP was co-expressed with Nup49-RFP. In this situation, misfolded VHL foci after heat shock were localized inside the Nup49 nuclear ring [150]. Taken together, JUNQ resides inside the nucleus, and it was subsequently renamed as INQ (*i*ntra*n*uclear *q*uality control compartment) [103]. The INQ/JUNQ also holds proteasomal subunits and the protein disaggregase Hsp104. The conditions leading to the formation of the INQ/JUNQ are similar to the mammalian aggresome. However, INQ/JUNQ was not found in the vicinity of the spindle pole body (SPB) that is equivalent to the mammalian microtubule-organizing center (MTOC) where aggresomes are formed. FLIP (Fluorescence Loss in Photobleaching) experiments show that INQ/JUNQ exchanges substrate proteins constantly with the surrounding pool [56, 153]. Initially, ubiquitination was proposed as a sorting signal for deposition of misfolded proteins at the INQ/JUNQ. Since the INQ/JUNQ also comprises proteasomes, it was recognized at first as deposition site for degradation of misfolded proteins [56]. In line with this, it was shown that either overexpressing a deubiquitinating enzyme (DUBs) or knocking out the two quality control E2 enzymes Ubc4 and Ubc5, which both results in less ubiquitination of misfolded proteins, sequester a JUNQ substrate at the IPOD instead of the JUNQ [56]. However, recent studies show that sorting of misfolded protein substrates to the INQ/JUNQ does not require ubiquitination [103].

CytoQ

Yeast has an additional subcellular aggregate deposition site termed as CytoQ (former Q body/peripheral aggregates/foci) that sequesters amorphous aggregates during heat stress [103, 152, 153]. Dissolution of CytoQ's requires the Hsp104-dependent disaggregation machinery [153]. Upon heat stress, initially, multiple peripheral foci/CytoQs are formed that coalesce into few larger inclusions over time [103]. Interestingly, these peripheral aggregates/CytoQs do not randomly diffuse in the cytoplasm, but formed in a coordinated manner along an intact cortical endoplasmic reticulum (ER) [152]. Formation of CytoQs is not required for degradation but seems to maintain the cellular fitness by sequestering misfolded species.

IPOD (*i*nsoluble *pro*tein *d*eposit)

Another subcellular deposition site identified in yeast is the IPOD. At the IPOD, insoluble aggregates such as terminally misfolded proteins, potentially oxidatively damaged proteins and amyloid aggregates (Htt103Q), the yeast prions [*RNQ*] and [*URE3*] [55, 56] and inactive proteasomes [155] accumulate. More recently, the IPOD was shown to serve as an intermediate sorting center for the damaged proteasomes before they are degraded by autophagy [155]. The IPOD exists adjacent to the

vacuole and is associated with the Hsp104 disaggregase. It is, however, striking that upon impairment of the ubiquitin-proteasome system (UPS) by deleting both E2 ubiquitin-conjugating enzymes Ubc4–Ubc5 (causes loss of ubiquitination of misfolded proteins), INQ/JUNQ substrates can be targeted to the IPOD, whereas introduction of a ubiquitin moiety to the bona fide IPOD substrate (Rnq1) allows for partial redistribution of the protein to the INQ/JUNQ [56]. In contrast to INQ/JUNQ, IPOD is quite stable and does not exchange substrate with the cytosol [56, 153]. The IPOD compartment also co-localizes with a bona fide autophagy marker, Atg8/LC3, but the possible physiological role for this is still unclear [56]. It is also unclear what the possible fate of substrates of IPOD is.

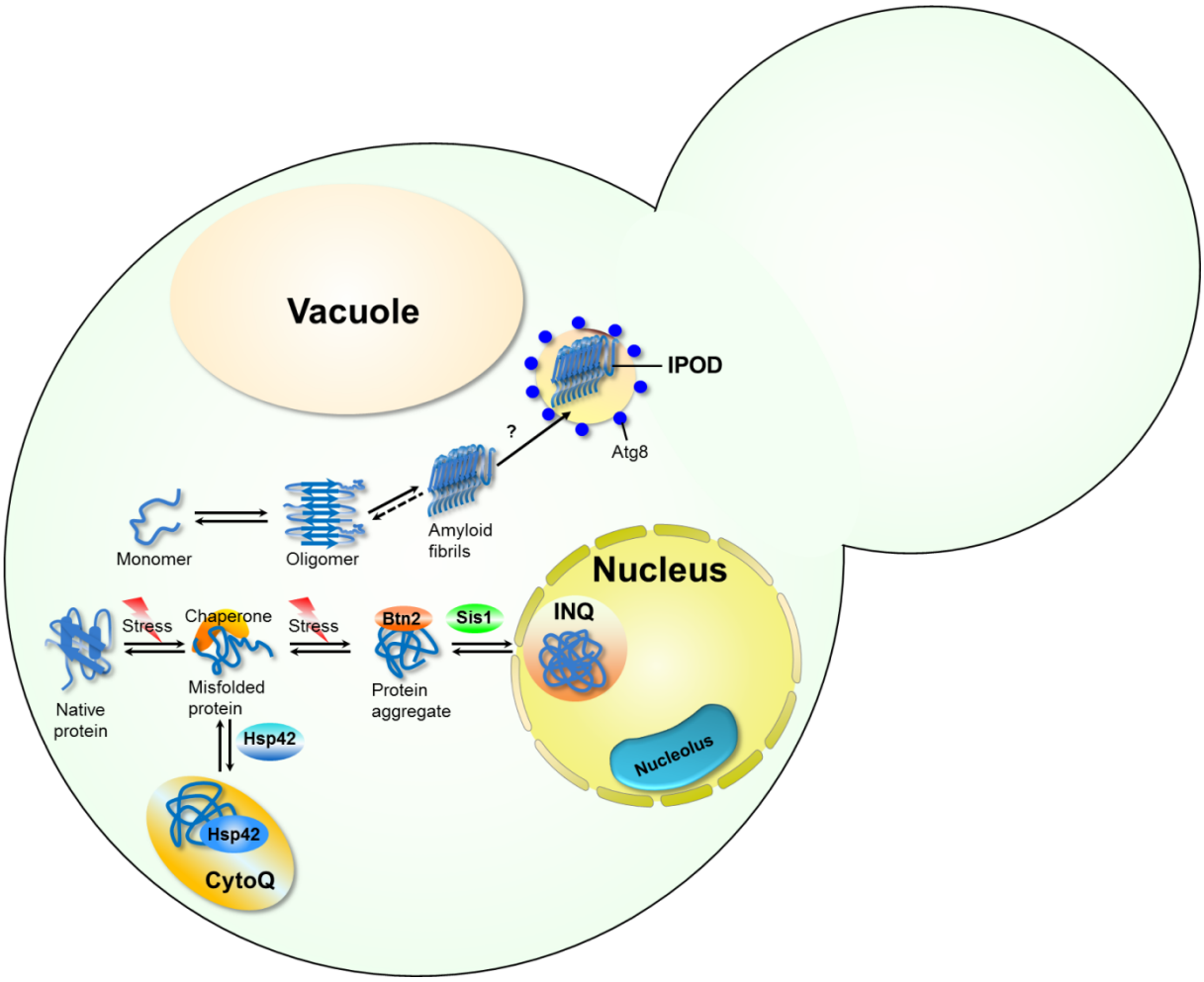

FIGURE 9: *S. cerevisae* sorts misfolded proteins into three distinct quality control compartments - Upon stress, misfolded proteins are either targeted for degradation or refolding with the aid of different molecular chaperones. Soluble protein aggregates are targeted either to the INQ with the nuclear sorting factor Btn2, or they are targeted to a peripheral deposition site termed as Cyto Q with the aid of cytosolic small heat shock protein Hsp42. Amyloidogenic aggregates (shown as an array of β-sheets) predominantly accumulate at the IPOD, a perivacuolar deposition site.

Factors determining deposition of misfolded proteins

The presence of three different aggregate deposition sites in yeast asks for cellular factors that specifically guide a misfolded/aggregated protein to the respective site. In *Saccharomyces cerevisae,* different substrate-independent sorting factors were identified that sequester amorphously misfolding proteins into spatial deposition sites. The first aggregate-sorting factor is the cytosolic small heat shock protein Hsp42 which is required for deposition of these aggregates at the Cyto Q [151-154]. Deletion of HSP42 results loss of Cyto Q but does not affect the formation of INQ/JUNQ upon cellular stress conditions [153]. Remarkably, an intact actin cytoskeleton is required for INQ/JUNQ formation since disruption of the actin cytoskeleton by latrunculin A (LatA) leads to increased foci of mCherry-VHL aggregates in both WT and *hsp42*Δ cells [153].

A second aggregate sorting factor is Btn2, which was originally identified as a factor acting in an unrelated biological process, which is late endosome to Golgi transport of specific proteins [159]. Btn2 is a short-lived nuclear protein which is rapidly degraded under standard growth conditions [149]. It interacts with v-SNAREs (**v**esicle -**SNA**P (Soluble NSF Attachment Protein) **RE**ceptor) and transports proteins via late endosome-Golgi trafficking [149, 159]. Btn2 is closely associated with another protein-sorting factor termed Cur1. Both factors are stress-inducible and interfere with each other during prion propagation. However, in contrast to Cur1, Btn2 directly regulates spatial protein quality control. Cells lacking Btn2 form peripheral protein aggregates (now CytoQ) upon stress, but not the INQ/JUNQ [149]. Btn2 interacts with Hsp40 chaperone Sis1 [149]. Therefore, it was suggested that Sis1 may promote sorting of misfolded cytosolic proteins to the INQ/JUNQ. However, since depletion of Sis1 does not entirely block the sequestration of misfolded proteins at the INQ/JUNQ, other factors were hypothesized to act together with Sis1 [103]. Alternatively, Sis1 was also suggested to have an indirect effect on the INQ/JUNQ formation as its depletion can reduce the capacity of the protein quality control system which then would lead to more aggregation.

The amyloidogenic substrates (Htt103Q, Rnq1 or the NM (PrD) domain of Sup35) are deposited at the perivacuolar deposition site IPOD under all conditions [56, 65]. However, the molecular mechanism underlying this deposition process is still unknown. No targeting factor till now had been identified which is required for deposition of amyloids at this site. A model of misfolded protein deposition in *S. cerevisiae* is shown in Fig 9.

2

Aims

The protein quality control system is an important cellular strategy that maintains proteome integrity by removing or sequestering misfolded proteins at specific deposition sites. Such sequestration strategy protects the cellular environment from potentially toxic misfolded species. In *Saccharomyces cerevisae,* three distinct deposition sites have been identified: INQ/JUNQ, Q body/CytoQ and the IPOD. Misfolded proteins are deposited at the INQ/JUNQ with the nuclear sorting factor Btn2 [103, 149, 150] or they are deposited to a peripheral site termed as Q body/CytoQ with the aid of the cytosolic small heat shock protein Hsp42 [151-154]. Amyloidogenic protein aggregates such as prions are deposited at the IPOD, a perivacuolar deposition site, but the mechanism by which amyloid aggregates are recognized and deposited at this site is unknown. The IPOD is located adjacent to the Phagophore Assembly Site (PAS) [56, 65] where the cell initiates autophagy and the Cytoplasm-to-Vacuole Targeting (CVT) pathway. Formation of the IPOD is independent of Hsp42, suggesting that both amyloidogenic substrates and misfolded protein substrates are handled differently [153]. Earlier, it was hypothesized that formation of INQ requires an intact actin cytoskeleton [153] but it was not clear if IPOD formation requires an intact actin cytoskeleton.
Within my PhD thesis, I focused on understanding the molecular mechanism that is involved in the recruitment of prion amyloid aggregates to the IPOD and investigated the fate of amyloid depositions in the vicinity of the PAS. I addressed the following key questions:

1. Which are the factors that are involved in recognition and targeting of amyloid substrates to the IPOD?
2. What is the molecular mechanism of recruitment of amyloid substrates to the IPOD?
3. What is the fate of amyloids deposited at the IPOD?

I approached this task by employing a fishing approach for amyloid binding factors using immobilized prion amyloid fibers and microscopy of fluorescently tagged amyloid fibers. For studying the fate of amyloid depositions at the IPOD, I employed pulse-chase type of experiments.

3

Results

3.1. Identification of PrD-GFP amyloid binding partners

In 2008, two distinct types of aggregate deposition sites have been described in *S. cerevisiae*: JUNQ and IPOD [56]. IPOD is a perivacuolar compartment and mainly sequesters amyloidogenic protein aggregates such as Ure2, Rnq1 and HttQ103 [56]. In addition, a GFP fusion protein of Sup35p prion domain (PrD-GFP) was also shown to co-localize with the Rnq1 prion and deposit at the IPOD, suggesting that PrD-GFP can serve as a model amyloidogenic substrate to study amyloid deposition at the IPOD in yeast [65]. However, the molecular machinery underlying the recognition and recruitment of these amyloidogenic substrates to the IPOD is not known.

Therefore, I employed the prion domain (PrD) of Sup35 [160-162] for identifying amyloid binding factors from yeast cell lysates that are involved in recognition and recruitment of amyloid aggregates to the IPOD. To do so, I used a fishing approach with yeast cell lysates and *in vitro* assembled recombinant biotin-labeled PrD amyloid fibrils immobilized to streptavidin coated magnetic beads.

3.1.1. Purification of recombinant PrD proteins from *E. coli*

To use PrD-fibers as amyloid bait, 10xHis-Sumo-PrD-AviTag and 10xHis-Sumo-PrD-STOP constructs were used. The two constructs were available in the Tyedmers Lab (Fig 10A and 10B). The construct that allows for biotinylation of the PrD domain was pHis10-Sumo-PrD-TEV-Avi. The AviTag is a biotinylation tag that efficiently biotinylates any protein by a co-expressed biotin ligase *in vivo and in vitro*. To synthesize non-biotinylated PrD, the pHis10-Sumo-PrD-STOP construct was used. In both constructs, a Ulp1 protease cleavage site was included between pHis10-Sumo and PrD to be able to remove the 10xHis-sumo tag by Ulp1 digestion. To make PrD-fibers, I did not use only 10xHis-Sumo-PrD-AviTag since it could bind very tightly to

streptavidin beads and may then disturb the interaction of PrD-binding partners. Therefore, I also included the non-biotinylated (10xHis-Sumo-PrD-STOP) construct to produce mixed PrD fibers with a few molecules of biotinylated PrD and excess molecules of non-biotinylated PrD (1:50 ratio).

I expressed these constructs in *E. coli* BL21 (DE3) harboring a biotin ligase from an IPTG-inducible pBirAcm plasmid. I purified biotin-labeled 10xHis-Sumo-PrD-AviTag and unlabeled 10xHis-Sumo-PrD-STOP recombinant PrD proteins from *E. coli* using a Ni-NTA resin (Fig 10C-D). Finally, PrD-Avitag and PrD-STOP were obtained after removal of the 10xHis-Sumo tag with Ulp1 digestion (Fig 10E, lane 3 and lane 6). The cleaved His-sumo tag was removed by a second incubation with Ni-NTA resin (see section 5.2.8 for detail). I prepared biotin labeled PrD heterofibers by mixing purified PrD-Avitag to PrD-STOP at a ratio of 1:50 and incubating overnight at room temperature with a slow rotation (Fig 11A, lane1). The PrD heterofibers were then sonicated for 5 min in order to gain short fibers which were found in the pellet after centrifugation (Fig 11A, lane3). I confirmed the formation of amyloid fibers by electron microscopy (EM) after negative staining with 2 % aqueous uranyl acetate on 100 mesh carbon-coated copper TEM grids (Fig 11B). The average length of sonicated PrD heterofibers was ~300 nm (Fig 11C).

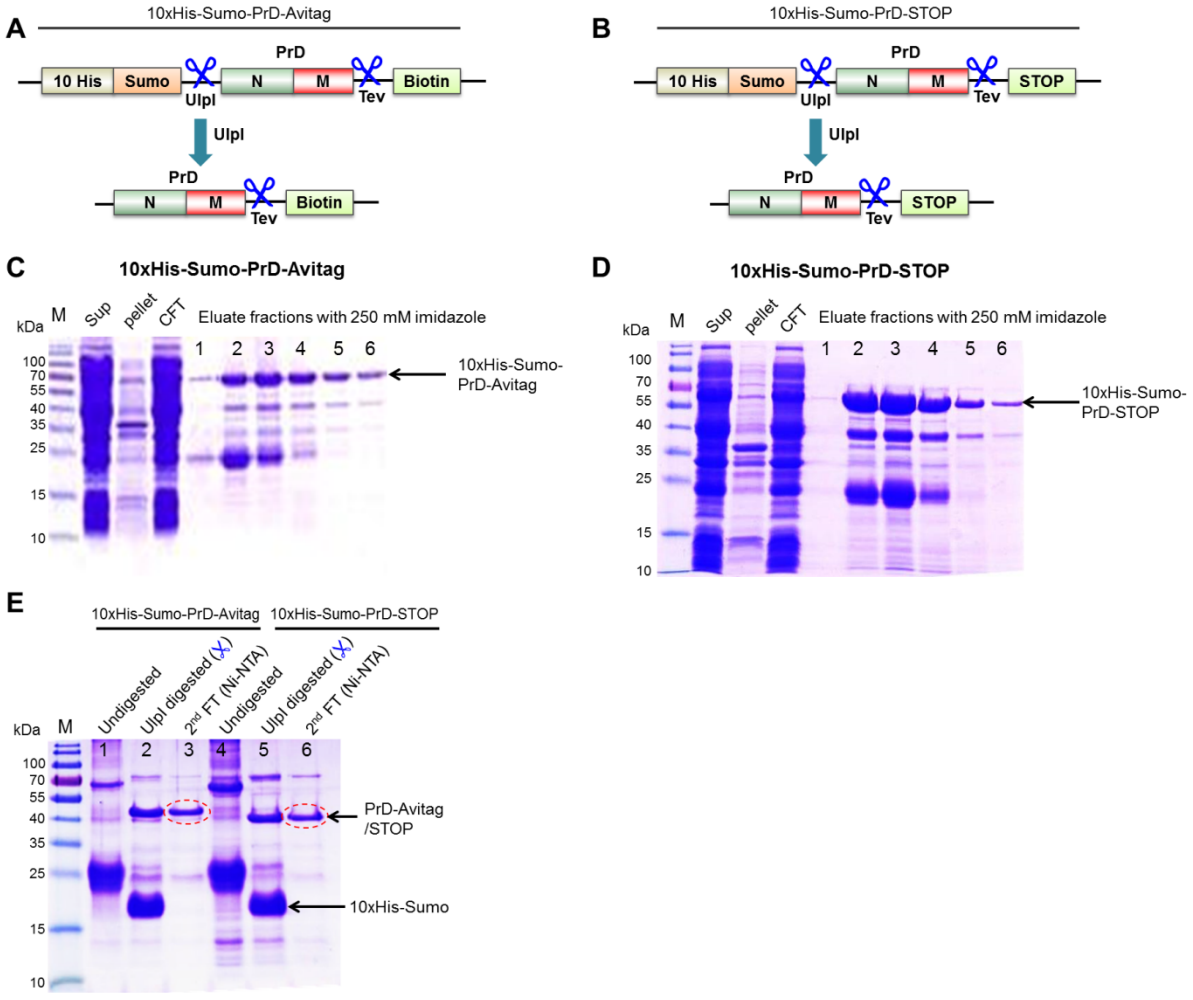

FIGURE 10: Purification of 10xHis-Sumo-PrD-Avitag and 10xHis-Sumo-PrD-STOP by $Ni2^{+}$-affinity chromatography and removal of 10xHis-Sumo by UlpI digestion – (**A, B**) Cartoon of 10xHis-Sumo-PrD-Avitag (A) or 10xHis-Sumo-PrD-STOP (B) constructs used to generate the amyloid bait. Both constructs contain an UlpI protease cleavage site to remove the His-sumo tag after purification. PrD-Avitag/Biotin generates biotin labeled PrD whereas PrD-STOP is used to generate unlabeled PrD. (**C**) 10xHis-Sumo-PrD-Avitag was expressed in *E. coli* BL21 (DE3) and purified with a Ni-NTA column and 250 mM of imidazole for elution. (**D**) Same as (C) but with the 10xHis-Sumo-PrD-STOP construct. (**E**) Removal of the 10xHis-Sumo tag from the purified 10xHis-Sumo-PrD-Avitag and 10xHis-Sumo-PrD-STOP proteins after cleavage by an UlpI protease. PrD-Avitag (biotinylated) or PrD-STOP (non-biotinylated) were collected in the flow through (FT) after incubating UlpI digested 10xHis-Sumo-PrD-Avitag/STOP with Ni-NTA beads. The PrD-Avitag/STOP proteins were further used to form the biotin-labeled PrD heterofibers.

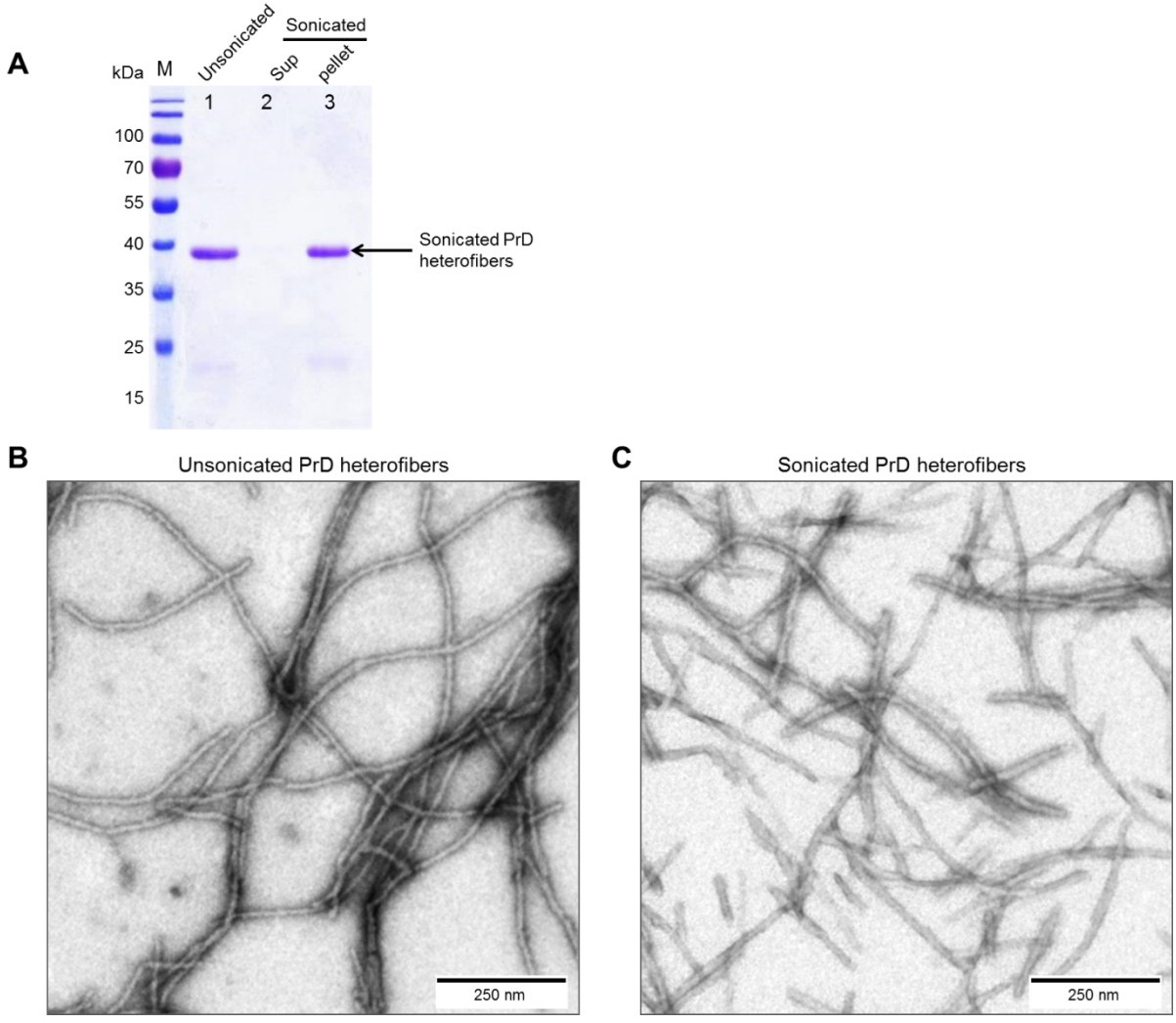

FIGURE 11: Analysis of biotin-labeled PrD heterofibers – (**A**) SDS-PAGE with biotin-labeled PrD heterofibers after sonication for 5 min. Sonicated fibers were centrifuged at 14000 rpm for 30 min. The supernatant and pellet was loaded onto an SDS-PAGE to check if the fibers are still in the pellet fraction after sonication. (**B**) Electron Microscopy (EM) of PrD amyloid fibers prepared from biotin-labeled and unlabeled recombinant PrD at a ratio of 1:50 after negative staining with uranyl acetate at 50000X magnification. (**C**) Same as (B) but after 5 min of sonication. Scale bar, 250 nm.

3.1.2. Binding of biotin-labeled PrD heterofibers to streptavidin beads

I immobilized the sonicated PrD heterofibers with streptavidin beads for ~ 1-2 h at 4°C. The beads with immobilized PrD fibers were further incubated with [*PSI*$^{+}$] yeast cell lysates at 4°C over night under gentle agitation (Fig 12A). Streptavidin beads without any immobilized PrD were taken as negative control. After overnight incubation, potential PrD amyloid binding partners were eluted by boiling the beads in 2X Laemmli sample buffer at 95°C and separated by SDS-PAGE (Fig 12B) prior to mass spectrometry (MS) analysis at the Core Facility for Mass Spectrometry & Proteomics/ZMBH, Heidelberg. In brief, In-gel tryptic digestion and LC-MS/MS analysis was used. Samples on the Coomassie stained gel were first reduced and alkylated before the trypsin digestion. Single lane containing proteins was excised and cut into two slices from the entire lane with a fresh scalpel. Subsequently, peptides were extracted, concentrated in a vacuum centrifuge concentrator and diluted to 30 µl with 0.1% TFA. 25 µl of peptides were injected into a nanoHPLC system (nanoAcquity, Waters) coupled to an ESI LTQ Orbitrap mass spectrometer (Thermo Fisher). The uninterrupted MS/MS spectra were searched against “The Swissprot_2014_04 *Saccharomyces Cerevisiae* Database” (for details please refer the paper [163]).

A

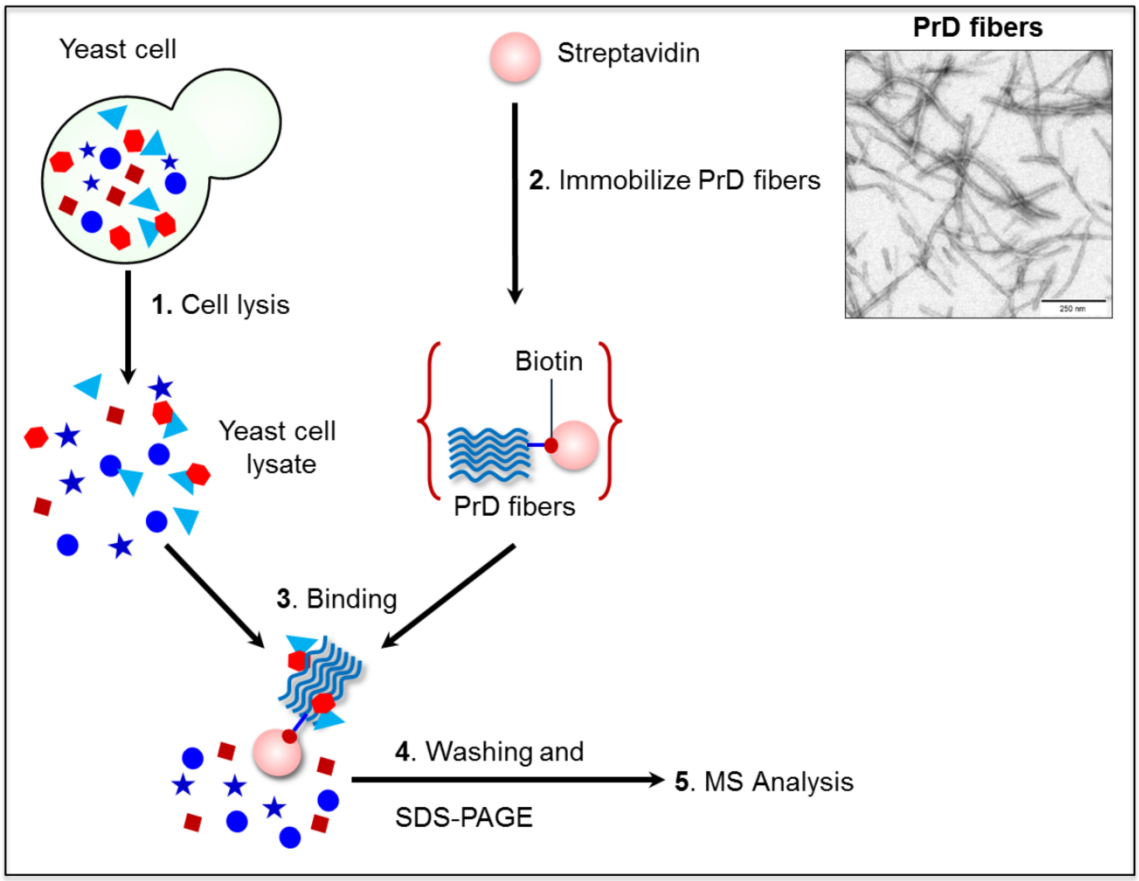
Yeast cell
Streptavidin
PrD fibers
2. Immobilize PrD fibers
1. Cell lysis
Biotin
Yeast cell lysate
PrD fibers
3. Binding
4. Washing and
SDS-PAGE
5. MS Analysis

B

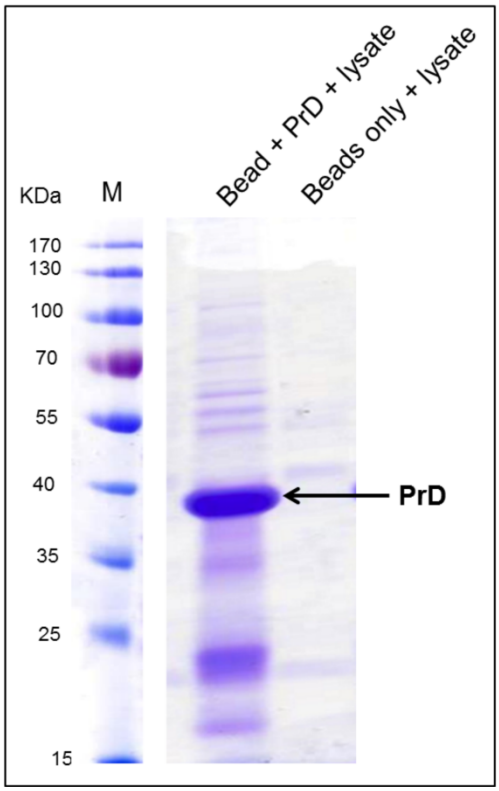
Bead + PrD + lysate
Beads only + lysate
KDa
M
170
130
100
70
55
40
35
25
15
PrD

FIGURE 12: Fishing of prion amyloid binding proteins from yeast cell lysates – (**A**) A cartoon of the fishing approach with [*PSI*$^{+}$] yeast cell lysates and *in vitro* assembled recombinant biotin-labeled PrD amyloid fibers immobilized to streptavidin coated magnetic beads. Proteins bound to the resin were eluted by boiling in 2X SDS sample buffer and separated by SDS-PAGE followed by Coomassie staining prior to mass spectrometry (MS) analysis. (**B**) SDS-PAGE with eluate from a resin immobilized with PrD fibers (left lane) and a negative control where just beads without immobilized PrD fibers were incubated with yeast lysates (right lane).

From my fishing approach, 64 proteins were ≥2-fold enriched in the column with PrD fibers as compared to the control (without fibers). These proteins were considered as potential as PrD interactors. They belong to various functional groups such as actin cytoskeleton-modulating proteins (Tpm1 and Tpm2), proteins involved in the endocytic secretory pathway/autophagy (Sec4, Sec14, Sec21 and Ykt6 and Ypt1), chaperones (Sis1, Saa1/2, Sec18 and Sgt2) and stress granule-associated RNA binding proteins (Pub1 and Pab1). Among them, I found several proteins that were previously shown to interact with Sup35 or its PrD [164-169]. These proteins were: The Hsp40 chaperones Sis1 and Ydj1, the Hsp70 chaperones Saa1/2, the amyloid sensor Sgt2, the mRNA binding proteins Pub1 and Pab1 and the actin binding and organizing protein Sla2. The identification of these known interaction partners of Sup35 or its PrD, highlighted in green in Fig 13, indicated that my fishing approach worked. I note that I did not find all known [*PSI*$^{+}$] aggregate interactors in my fishing approach, which demonstrates that the method is not quantitative. Interestingly, however, I found proteins that were not previously described as PrD binding partners, such as tropomyosin1/2 and several SEC genes (Fig 13).

List of proteins identified to bind to PrD (SUP35) fibers

Ribosomal proteins

PAB1
PUB1
RPL2A
RPS3
RPS6A
RPS17A
HRP1
RPS4a
RPL5
RPL6B
RPL20A
RPS1A

Metabolic enzymes

LYS12
PSA1
ADH1
IDH2
AAH1
PRS3
PDR16
IDH1
PRO3

Nuclear transport

NSR1

Transcription/Transalation

DHH1
SUA7
HYP2
ASC1
KTI12
NPL3
NRD1

Cytoskeleton

TUB2
DNM1
TPM1
TPM2
SLA2
LSB3
GCS1

Other

CHA1
VMA2
VMA8
FUS3
SNO1
GSP2
APT2
SEC53
RHB1
NEW1
ULP1
SMT3

Chaperones

NAP1
SIS1
YDJ1
SSA1
SSA2
SGT2
SEC18
GET3

Endocytic vesicular transport and/or autophagy

YKT6
RVS161
YPT1
SAR1
SEC4
SEC14
SEC21

Mitochindrial

ATP2

FIGURE 13: Functional grouping of hits identified in fishing of PrD binding proteins from yeast cell lysates – The strongest hits (see also Appendix Table 1) which were bound to PrD fibers on column and were ≥2-fold enriched compared to the control (without fibers) in the fishing approach, were grouped according to their role in biological processes. The hits are categorized based on the corresponding descriptions in the SGD database (http://www.yeastgenome.org/).

3.1.3. Co-localization of identified binding partners with PrD-GFP

In yeast, tropomyosin has two isoforms Tpm1 and Tpm2, which bind and stabilize actin cables/filaments, thereby influencing several transport processes such as organelle segregation and cell polarization along tropomyosin-decorated actin cables [170]. Earlier, it was shown that INQ formation requires an intact actin cytoskeleton [153], but it was unclear if amyloid substrate recruitment to the IPOD also requires an intact actin cytoskeleton. To test a possible role of Tpm1/2 in IPOD biogenesis, I

tested first whether the protein was bound to the column only in traces or in significant amounts. For testing this, I repeated the fishing experiment with PrD as amyloid bait as described before, but with a lysate from a yeast strain that carried Tpm2 with an HA-tag. This tag allowed me to ask whether the protein bound to the immobilized PrD was present in amounts detectable by Western Blotting. I found that Tpm2 was bound to PrD fibers *in vitro* in detectable amounts (Fig 14A). Next, I asked whether an interaction between Tpm1/2 and PrD may also occur *in vivo*? To do so, I designed a co-localization experiment for investigating if Tpm1/2-mCherry interacts with PrD-GFP *in vivo*. As a positive control, I also included mCherry fusions of known PrD interactors such as Ssa1 [167, 168], Pub1 [166] and Pab1 [164]. The latter three indeed co-localized with PrD-GFP at the IPOD, however Tpm1/2-mCherry did not accumulate with PrD-GFP at the IPOD (Fig 14B). This left the possibility that such a putative interaction could be more transient, for example during the recruitment of PrD-GFP aggregates to the IPOD.

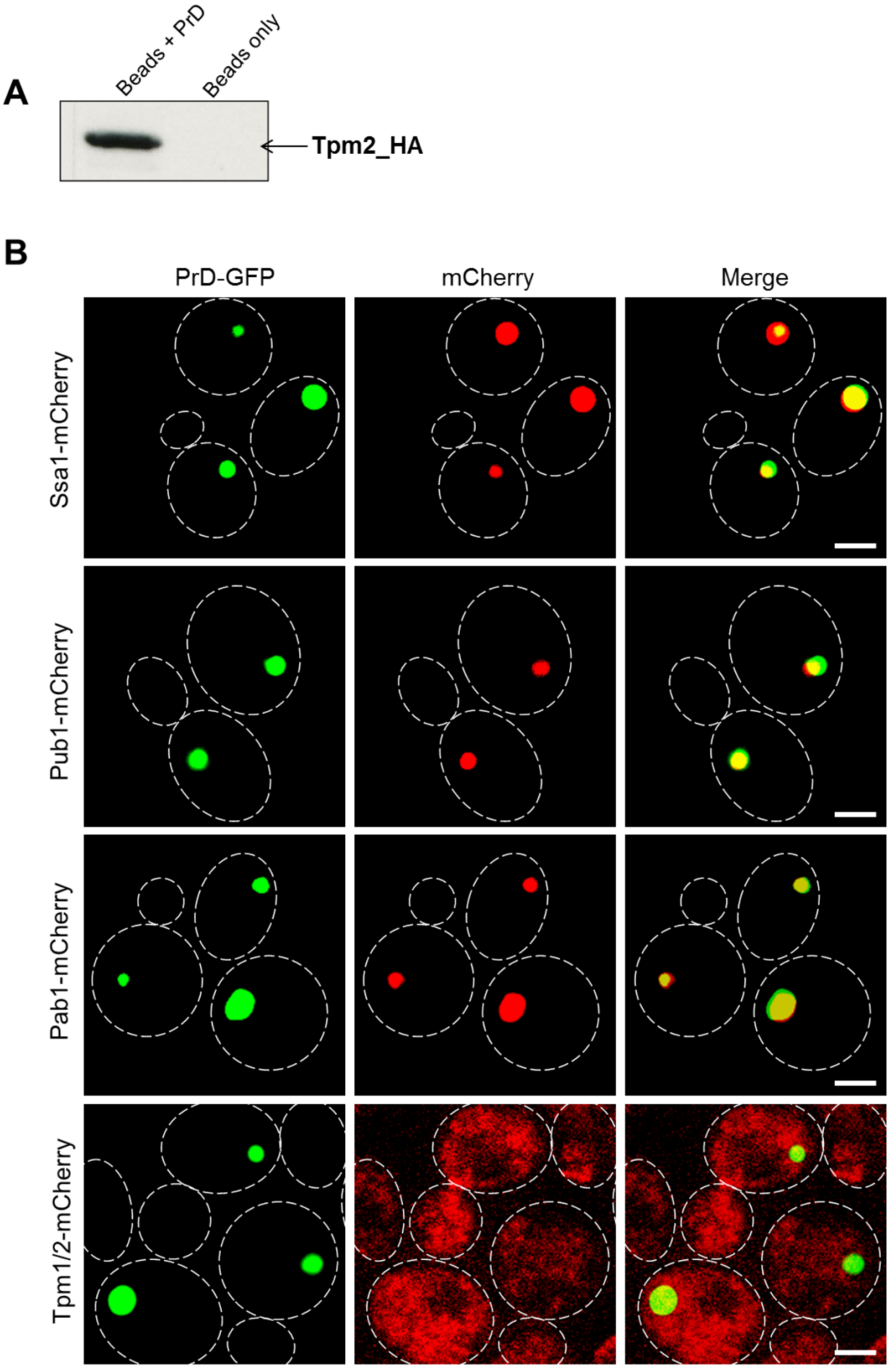
A
Beads + PrD
Beads only
Tpm2_HA
B
PrD-GFP
mCherry
Merge
Ssa1-mCherry
Pub1-mCherry
Pab1-mCherry
Tpm1/2-mCherry

FIGURE 14: Test for binding of Tpm1/2 with PrD *in vitro* and *in vivo* – (**A**) Fishing experiment as in Fig 12A, but with yeast cell lysates from a strain that carried a deletion in TPM1 and an aid-degron tagged Tpm2. The aid-degron-tag contained additionally an HA-tag. After elution of the bound fraction, the samples were subjected to SDS-PAGE followed by Western Blotting with an antibody against the HA-tag to detect Tpm2-aid-HA in the eluate. (**B**) Logarithmic growth phase culture of 74D-694-ΔPrD (SUP35) [*PrD-GFP*$^{+}$] that contained C-terminal mCherry fusions of different genes identified as PrD-fiber binding proteins in the fishing experiment described in Fig 13. Cells were subsequently fixed with 4% of formaldehyde (PFA) and analyzed by fluorescence microscopy as described in methods. After deconvolution, a merged image of the z-stacks taken in the GFP- and the mCherry channels, respectively, were overlaid. Scale bar, 2 µm.

3.2. Characterization of the molecular mechanism of recruitment of prion amyloids to the IPOD

3.2.1. Tropomyosin, Myo2 and Calmodulin functions are required for proper recruitment of PrD-GFP to the IPOD

Since both Tpm1/2 were found to interact with PrD-GFP *in vitro*, but did not co-localize at the IPOD *in vivo*, I wondered if tropomyosins may interact transiently with PrD-GFP aggregates, for example during a recruitment step to the IPOD deposition site. If that was the case and was a crucial step in the recruitment, depletion of these proteins should interfere with proper targeting of PrD-GFP aggregates to the IPOD. For testing this, I used a [*PSI*$^{+}$] strain expressing PrD-GFP under control of a galactose inducible promoter. Since both Tpm1 and Tpm2 have overlapping functions and the double deletion of both tropomyosins is lethal [171], I conditionally depleted Tpm2 in a tpm1-knock out strain (tpm1Δ) employing the well-established "Auxin Inducible Degron (aid)" tag system [172]. For this, Tpm2 was tagged with a degron-tag (aid) and the plant E3 ligase SCF-TIR1 was co-expressed. Upon addition of the plant hormone auxin, auxin binds to E3 ligase SCF-TIR1 that promotes the interaction between SCF-TIR1 and the "aid" tagged protein. The target protein is then polyubiquitinated and efficiently degraded by the 26S proteasome. I induced the PrD-GFP in galactose-based media for 6 hours in the absence and presence of auxin. After PrD-GFP induction and Tpm2 depletion, I withdrew an aliquot, fixed the cells with PFA and visualized the aggregation pattern of PrD-GFP under the fluorescence microscope. In the control, more than 95% of the cells showed one single large PrD-GFP dot/IPOD (Fig 15A and 15B) as formerly described [65]. In contrast, 61 % (Fig 15D) of the cells showed multiple PrD-GFP foci upon depletion of tpm1/2 (Fig 15C, right panel). The wild-type (wt) strain that lacks an aid-tag showed only one single large PrD-GFP dot/IPOD per cell even in the presence of auxin (Fig 15A and 15B), suggesting that the multiple PrD-GFP foci phenotype was due to the conditional depletion of the tropomyosin function and not due to a side effect of auxin. Depletion

of Tpm2 in [*PSI*$^{+}$] tpm1Δ strain was confirmed by Western Blot analysis with an antibody against an HA tag attached to the “aid” degron tag (Fig 15I). Short-term depletion of Tpm2 for 6 hrs was not lethal for the cells (Fig 15J).

It was recently shown that tropomyosins decorate actin filaments for efficient interaction and movement of class-V myosins such as Myo2 along actin filaments [173, 174]. In addition, Myo2 was shown to interact genetically with another actin-binding protein termed calmodulin (Cmd1), which is involved in proper organization of actin cables and polarized growth [175]. Furthermore, it has been shown that tropomyosin along with Myo2 and Cmd1 are required for retaining Htt103Q- and heat-induced protein aggregates asymmetrically in the mother cells during cell division [139, 141, 176]. Thus, I extended my studies to Myo2 and Cmd1 due to this functional association. Since these two actin-binding proteins are essential, I applied the same “aid system” to greatly deplete their levels temporarily. Similar to Tpm2, I fused both proteins with a degron-tag (aid) [172] and performed the experiment in the same way as for Tpm2 depletion. I observed a similar multiple PrD-GFP foci phenotype upon depletion of Myo2 and Cmd1 (Fig 15E and Fig 15G) as for Tpm1/2 depletion, suggesting that these proteins are also involved in the recruitment of PrD-GFP aggregates to the IPOD. Depletion of Myo2 and Cmd1 was confirmed by Western Blot analysis with an antibody against an HA tag attached to the “aid” degron tag (Fig 15I). Short-term depletion of these proteins for 6 hrs did not have a negative effect on cell viability (Fig 15J).

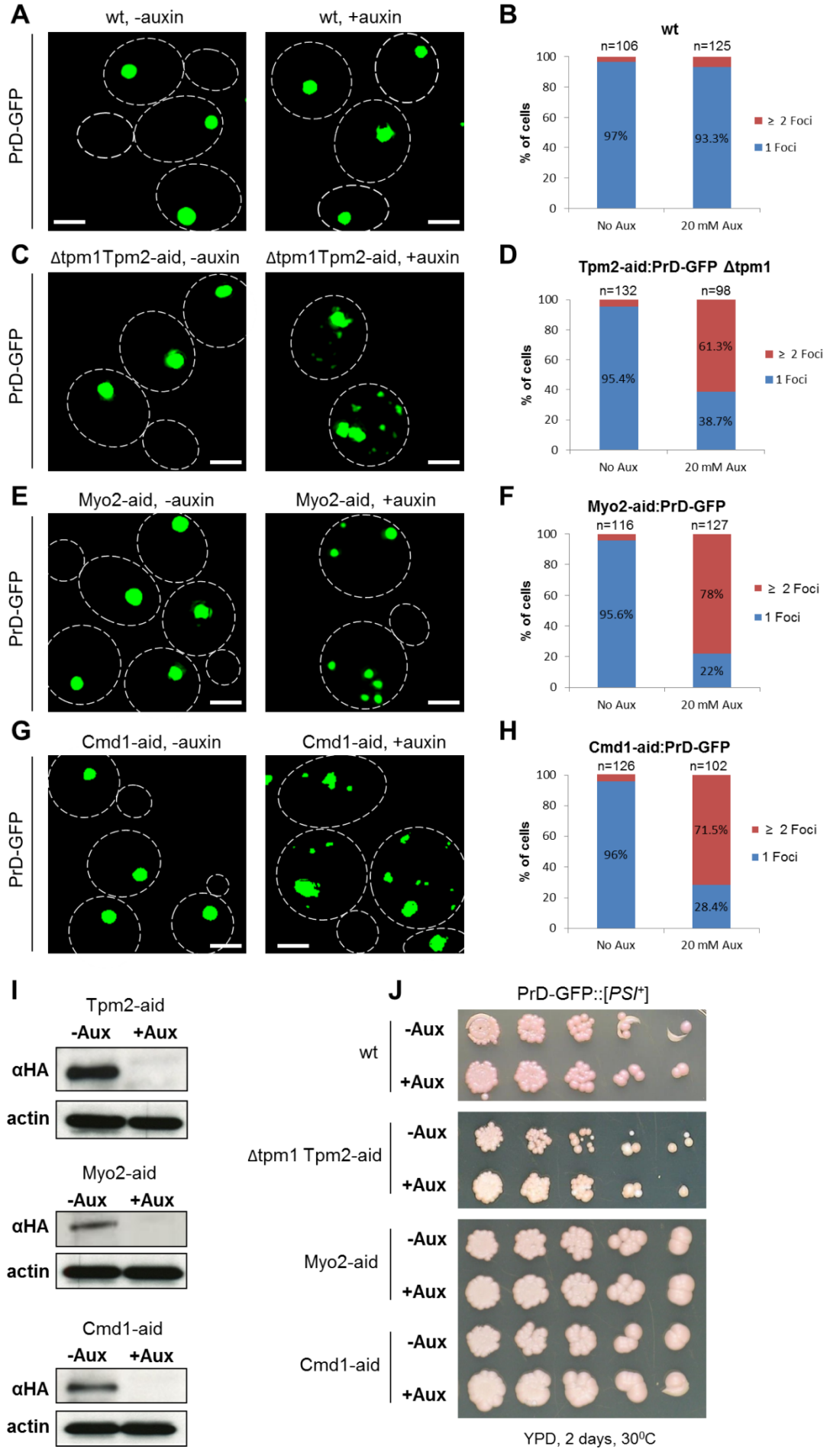
A
wt, -auxin
wt, +auxin
PrD-GFP
B
wt
n=106
n=125
% of cells
97%
93.3%
≥ 2 Foci
1 Foci
No Aux
20 mM Aux
C
Δtpm1Tpm2-aid, -auxin
Δtpm1Tpm2-aid, +auxin
D
Tpm2-aid:PrD-GFP Δtpm1
n=132
n=98
95.4%
61.3%
38.7%
E
Myo2-aid, -auxin
Myo2-aid, +auxin
F
Myo2-aid:PrD-GFP
n=116
n=127
95.6%
78%
22%
G
Cmd1-aid, -auxin
Cmd1-aid, +auxin
H
Cmd1-aid:PrD-GFP
n=126
n=102
96%
71.5%
28.4%
I
Tpm2-aid
-Aux
+Aux
αHA
actin
Myo2-aid
Cmd1-aid
J
PrD-GFP::[PSI+]
wt
Δtpm1 Tpm2-aid
Myo2-aid
Cmd1-aid
YPD, 2 days, 30°C

FIGURE 15: Tropomyosin, Myo2 and calmodulin are essential for proper accumulation of PrD-GFP at the IPOD – (**A, C**) PrD-GFP was induced with galactose for 6 hours in a [*PSI*$^{+}$] wild-type strain (**A**) or in a strain containing a deletion of Tpm1 and a C-terminal aid tag in Tpm2 (**C**), in the absence or presence of 20 mM of auxin as indicated. Cells were fixed with PFA and analyzed by fluorescence microscopy. (**B, D, F, H**) Quantification of PrD-GFP foci in the wild-type strain (B) and upon depletion of Tpm1/2 (D) or Myo2 (F) or Cmd1 (H) is shown. Frequencies of cells with 1 single focus or more than 1 foci are given in %. (**E, G**) Same experiment as in (C), but in a [*PSI*$^{+}$] strain with C-terminal aid-tag in MYO2 (**E**) or CMD1 (**G**). (**I**) Western blot of the *tpm1Δ* Tpm2-aid, Myo2-aid and Cmd1-aid strains after auxin treatment as in (C, E, and G) with an antibody against an HA-tag present in the aid-tag. An anti-actin antibody served as loading control. (**J**) Wild-type (wt), *tpm1Δ* Tpm2-aid, Myo2-aid and Cmd1-aid strains were treated as in (A) prior to serial dilution and a spotting test for cell viability. Cells were grown on YPD plates for 2-3 days. Scale bar, 2 µm.

3.2.2. Myo2 and Calmodulin functions are required for the formation of ring- and ribbon-shaped aggregates of PrD-GFP

While PrD-GFP is present at the IPOD in the mature [*PrD-GFP*$^{+}$] prion state, the protein was found in ring- and ribbon-shaped aggregates during *de novo* induction of the prion state when PrD-GFP was overexpressed in [*psi*$^{-}$] cells [65, 167, 177]. Therefore, I also tested if auxin-induced depletion of Myo2 and Cmd1 would impair the formation of these ring- and ribbon-shaped aggregates. Rings/ribbon-shaped PrD-GFP aggregates were induced with galactose for 24 hours in a [*psi*$^{-}$] strain [65] carrying either an aid tag in Myo2 or Cmd1, in the absence or presence of 20 mM of auxin. Upon auxin addition, these mutants did not form proper rings/ribbon-shaped aggregates but formed multiple punctate aggregates (Fig 16A top middle and bottom right panels). A wild-type (wt) strain (without any aid tag) displaying rings/ribbon-shaped aggregates of PrD-GFP in [*psi*$^{-}$] cells did not show any auxin effect (Fig 16A top right panel). The viability was not yet affected by this prolonged presence of auxin for 24 hrs (Fig 16B). Together, these data demonstrate that essential components of the actin cable -based transport machinery, Myo2, Cmd1 and Tpm1/2, are crucial for the formation of ring- and ribbon-shaped aggregates of PrD-GFP.

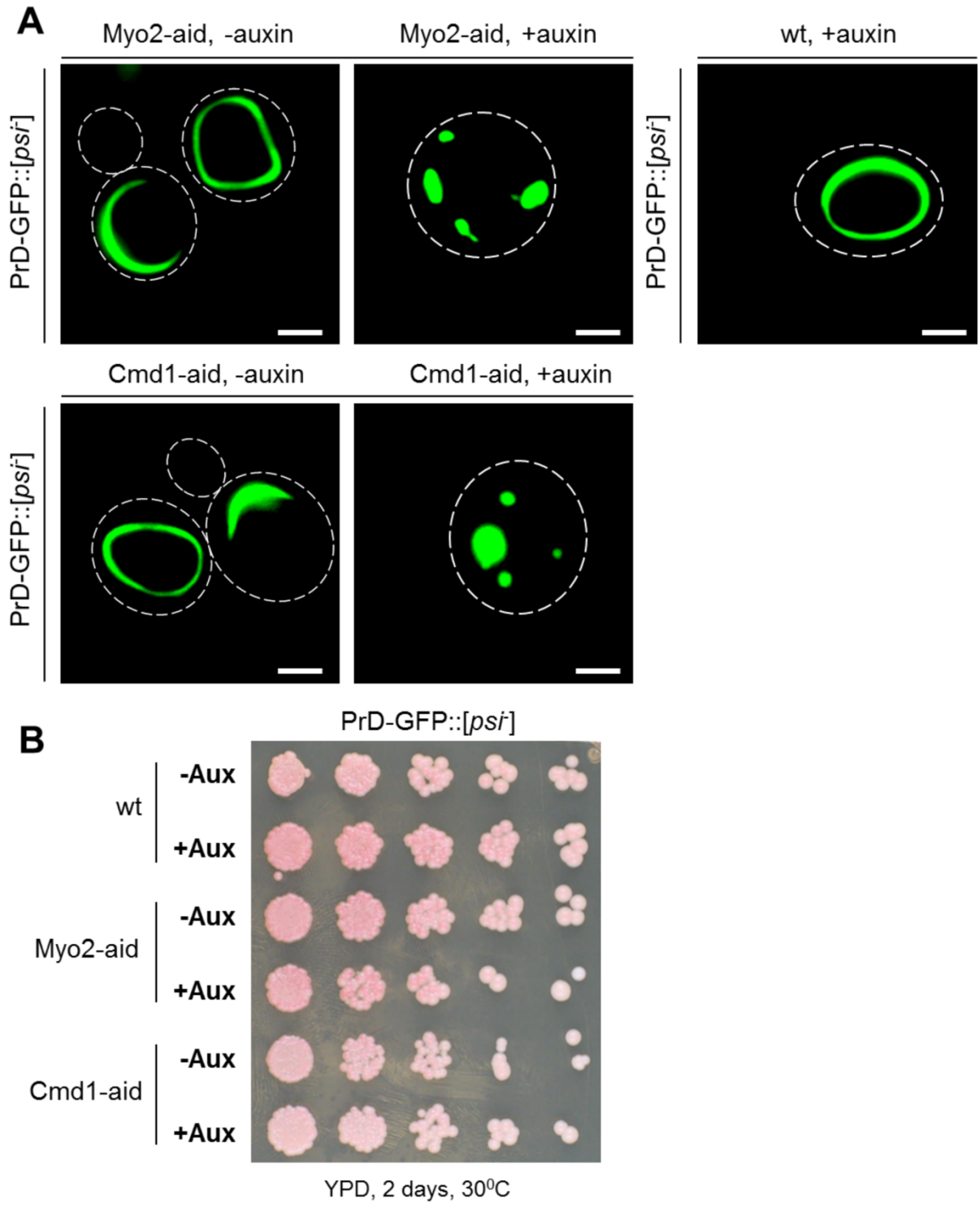

FIGURE 16: Myo2 and calmodulin are essential for formation of ring- and ribbon-shaped aggregates – (**A**) PrD-GFP was induced with galactose for 24 hours in a 74D-694 [*psi⁻*] strain that either carried a C-terminal aid-tag in MYO2 and in CMD1 or was wild-type (wt). While one culture was left untreated (control, top and bottom left panel), 20 mM of auxin was added for 24 hours during PrD-GFP induction (top middle, top right and bottom right panel) to the other one. Cells were subsequently fixed with PFA and analyzed by fluorescence microscopy as described in the methods. (**B**) Wild-type (wt), Myo2-aid and Cmd1-aid strains were treated as described in (A) before subjecting them to serial dilutions followed by a spotting test for cell viability after the auxin treatment. Cells were subsequently grown on YPD plates for 2 days at 30 °C. Scale bar, 2 µm.

3.2.3. Washout of auxin restores Myo2 function and causes re-localization of PrD-GFP aggregates to the IPOD

Loss of tropomyosin, Myo2 and Cmd1 function led to formation of multiple PrD-GFP foci in the cytoplasm rather than recruiting these aggregates to one single IPOD site. If these proteins are involved in the coalescence and recruitment of PrD-GFP aggregates to the central IPOD deposition site, washout of auxin should readily restore the targeting defect. Since auxin-induced depletion of these functionally linked proteins caused a similar multiple PrD-GFP foci phenotype, I focused on Myo2 in the following experiments. To test if the defect in PrD-GFP localization could be restored, I washed out auxin from Myo2-depletd cells that expressed PrD-GFP under control of a galactose-inducible promoter and incubated the cells in glucose-based media without auxin to monitor the pre-existing multiple PrD-GFP foci. Already after 1 hour of auxin removal, 93% of the cells had one single PrD-GFP IPOD again (Fig 17A, right panel and 17B). In addition, for further confirmation that all multiple fluorescence foci really refused again to one central IPOD rather than being degraded, I performed a time-lapse microscopy experiment. In brief, after induction of PrD-GFP with galactose and auxin addition, cells were pelleted and placed on an agarose pad on a microscope slide without auxin, but with glucose instead of galactose. Z-stack images were acquired every 2-5 min over a period of 1 hr. Within 1 hour of auxin removal in glucose-based media, pre-existing multiple PrD-GFP foci directly refused to one central IPOD deposition site (Fig 17C and Fig 17D). This suggests that PrD-GFP foci represent transport intermediates that are trapped on the way to the IPOD deposition site if the actin–tropomyosin–myosin-based transport machinery is impaired.

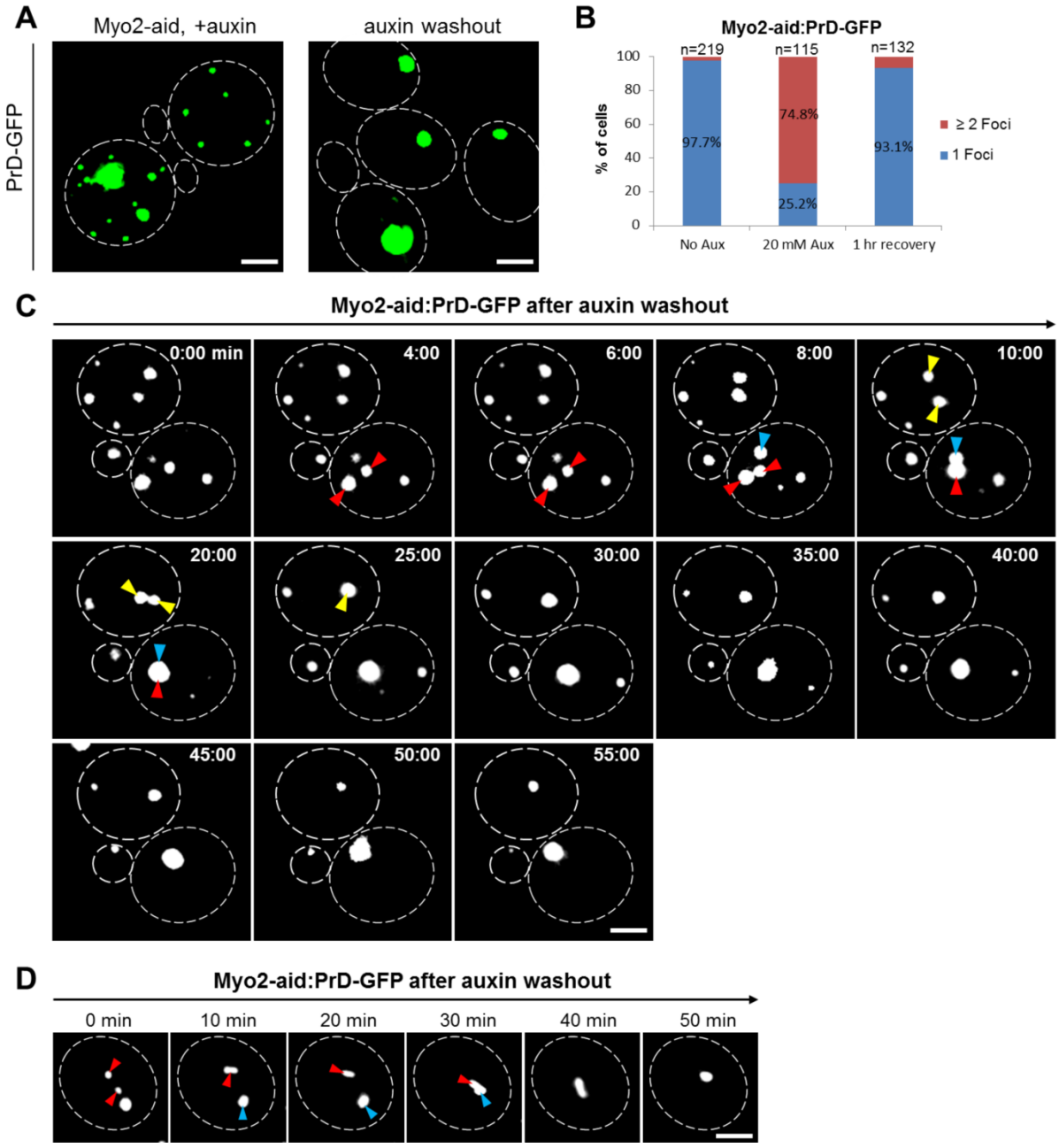

FIGURE 17: Washout of auxin restores Myo2 function and localization of PrD-GFP at the IPOD – (**A**) PrD-GFP was induced with galactose for 6 hours in the presence of 20 mM auxin in a [*PSI*$^{+}$] strain with a C-terminal aid-tag in MYO2 (left panel). Subsequently, cells were pelleted, resuspended in YPD without auxin to rescue Myo2 function and further incubated for 60 min prior to fixation and fluorescence microscopy (right panel). (**B**) Quantification of PrD-GFP localization in either 1 or more than 1 foci in % in the absence or presence of 20 mM auxin or after auxin washout (1 hr recovery). (**C**) Microscopy images from a time-lapse microscopy experiment as in A, but after removal of auxin. In brief, after induction of PrD-GFP and auxin addition for 6 hours, cells were pelleted and placed onto an agarose pad containing glucose instead of galactose on a microscope slide for time-lapse microscopy. A z-stack with a step width of 0.3 µm was taken every 2-5 min (**D**) A single cell from an experiment as in C to highlight direct refusion events of PrD-GFP foci. Scale bar, 2 µm.

3.2.4. Myo2 depletion impairs proper recruitment of PrD-GFP to the IPOD rather than IPOD integrity

Myo2 and tropomyosins were shown to deliver different cargoes along actin cables during many cellular transport processes [178]. Therefore, the most likely explanation for the multiple foci phenotype upon Myo2 depletion was an impaired recruitment of PrD-GFP to the central IPOD site. However, at this point of time, I could not exclude the possibility that Myo2 and tropomyosins are involved in maintaining the IPOD integrity instead recruiting PrD-GFP aggregates to this single IPOD site. In such a case, Myo2 depletion would lead to a loss of the integrity of the IPOD and the deposition site would fall apart (fragment) into multiple smaller aggregates, which would also give the multiple PrD-GFP foci phenotype I observed upon Myo2 and Tpm1/2 depletion (see Fig 17A, left panel). Therefore, to differentiate these two possibilities, I first pre-formed the PrD-GFP IPOD with galactose induction for 6 hours without depleting Myo2, then removed the galactose media and incubated the cells with the preformed IPODs in glucose-based media in the presence of auxin to deplete Myo2 for 6 more hrs and subsequently monitored the pre-existing single IPODs over time for 6 hours. Aliquots were withdrawn every 2 hours (0, 2, 4 and 6 hours) for fluorescence microscopy (Fig 18A) and cells with one PrD-GFP or multiple foci were quantified (Fig 18B). I did not observe any fragmentation/disruption of pre-existing single PrD-GFP IPOD upon Myo2 depletion, suggesting that Myo2 is involved in the recruitment of the PrD-GFP at the IPOD rather than maintaining the IPOD integrity. However, I observed that the pre-existing PrD-GFP dot was slowly and progressively decaying over time, which is followed up upon and explained in more detail in Fig 29A.

In second set of experiments, I further ruled out the possibility that Myo2 is involved in maintaining the IPOD integrity by looking if Moy2 depletion causes immediate appearance of multiple PrD-GFP foci or one single and transient IPOD before multiple PrD-GFP foci would appear. For testing this idea, I induced PrD-GFP with galactose in the presence of auxin for 6 hours. After 2, 4 and 6 hours, I withdrew aliquots for fluorescence microscopy (Fig 18C) and quantified the cells with one or multiple PrD-GFP foci (Fig 18D). A great majority of cells showed multiple PrD-GFP foci (68% - 78%) at all time points (Fig 18D), strongly favoring the hypothesis that Myo2 is involved in the recruitment of the PrD-GFP aggregates to the IPOD rather than maintaining IPOD integrity.

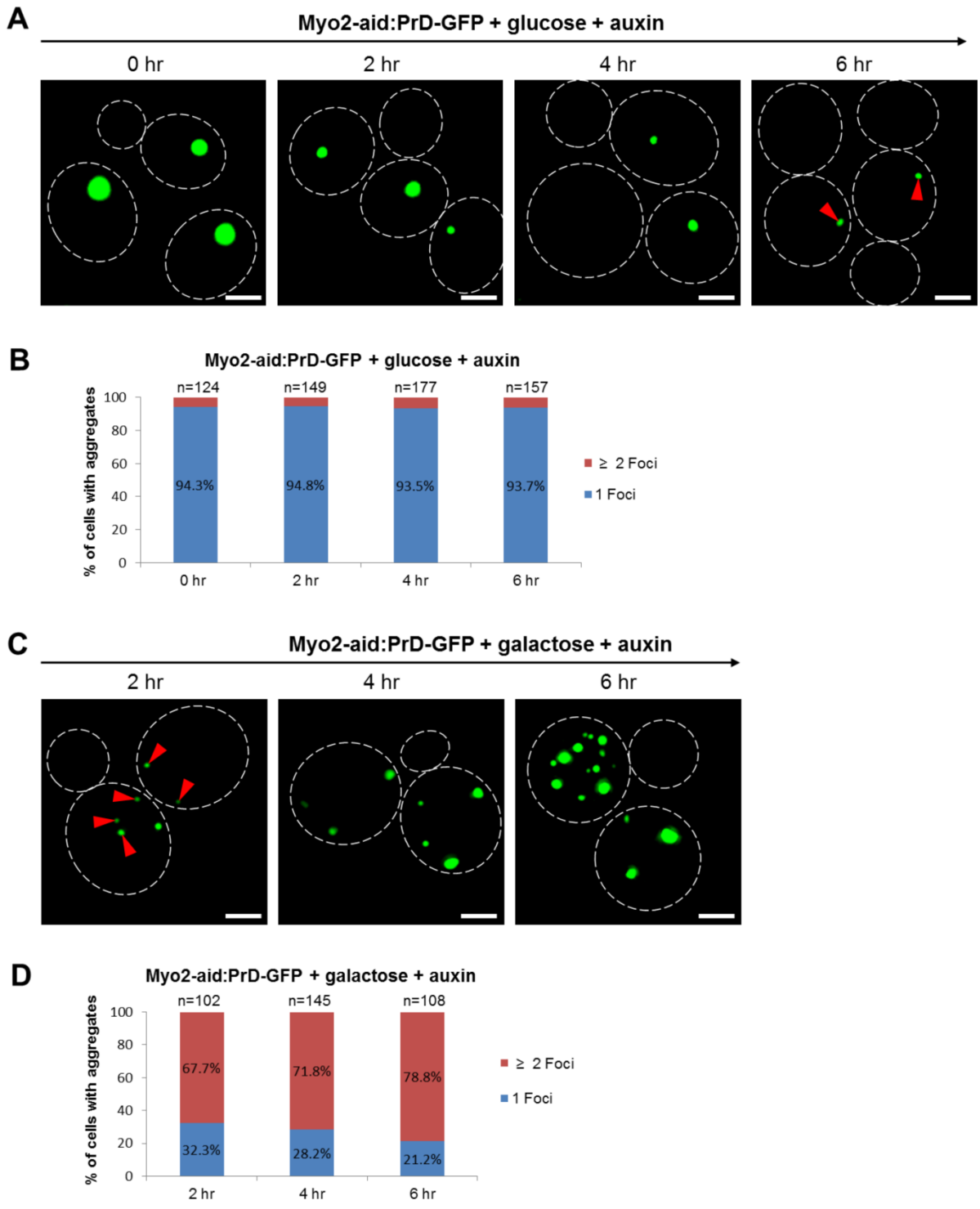

FIGURE 18: Myo2 depletion impairs proper recruitment of PrD-GFP to the IPOD rather than IPOD integrity – **(A)** PrD-GFP was induced with galactose for 6 hours without auxin in a [*PSI*$^{+}$] Myo2-aid strain to allow for IPOD formation. Subsequently, cells were pelleted and resuspended in YPD media with 20 mM auxin and incubated further. Aliquots were withdrawn every 2 hours, fixed and analyzed by fluorescence microscopy. **(B)** Quantification of PrD-GFP localization from experiment A. PrD-GFP localization in either 1 or more than 1 foci was determined from cells that still carried PrD-

GFP aggregates and plotted as %. **(C)** PrD-GFP was induced with galactose in the presence of 20 mM auxin in a [*PSI*$^+$] Myo2-aid strain. After the indicated times, aliquots were withdrawn, fixed and analyzed by fluorescence microscopy. **(D)** Quantification of PrD-GFP localization from experiment C. PrD-GFP localization in either 1 or more than 1 foci was determined and plotted as %. Scale bar, 2 µm.

3.2.5. Myo2 depletion results in co-accumulation of Atg8 together with PrD-GFP foci

Depletion of the Tpm1/2 and Myo2 resulted in a reversible defect in deposition of multiple PrD-GFP foci at one single IPOD deposition site near the vacuole. The IPOD is known to be in close proximity to the PAS [56, 65] where the cells initiate formation of autophagosomes and CVT vesicles [113, 128]. Atg8 was shown to co-localize with the IPOD [56] and was also found to co-localize with PrD-GFP at the IPOD [65]. At the same time, it is the most commonly used PAS marker. Atg8 was suggested to be recruited to the PAS via the actin cytoskeleton, as disruption of actin filaments by Latrunculin A (LatA) blocked Atg8 sorting to the PAS [179]. To understand a possible correlation between the IPOD, it's vicinity to the PAS and the involvement of Myo2 in PrD-GFP recruitment to the IPOD, I introduced the PAS marker RFP-Atg8 into a Myo2-aid [*PSI*$^+$] strain with the Gal-inducible PrD-GFP construct and tested if the recruitment of Atg8 to the PAS and its co-localization with PrD-GFP aggregates is affected upon Myo2 depletion. In short, PrD-GFP was induced with galactose for 6 hours with or without auxin in the [*PSI*$^+$] Myo2-aid strain that carried a plasmid coding for RFP-Atg8. Cells were fixed with PFA and analyzed by fluorescence microscopy in the GFP and mCherry channels. In the absence of auxin, 79 % of the single PrD-GFP IPODs showed a co-localization with Atg8 PAS marker, as expected [56, 65] (Fig 19A, upper panel). Remarkably, I observed that upon Myo2 depletion, RFP-Atg8 formed multiple foci, which co-localized with the multiple PrD-GFP foci in 89 % of the case (Fig 19A, lower panel). This result left two possibilities: First, PrD-GFP aggregates could have attracted/co-aggregated the PAS marker proteins, as amyloids tend to be sticky [180], and due to the multiple PrD-GFP foci phenotype, I observed multiple PAS marker foci. Secondly, recruitment of Atg8 to the PAS also depends on Myo2 based transport along actin cables and both, PrD-GFP and RFP-Atg8, use a similar recruitment machinery (track) to accumulate at the neighboring IPOD and PAS respective sites. Consequently, the PAS marker would co-accumulate with the multiple PrD-GFP foci. To differentiate between these two possibilities, I applied two independent approaches. In the first approach, I incubated the PrD-GFP and RFP-Atg8 expressing Myo2-aid strain with 5 mM GdnHCl, which abolishes the prion state (termed curing) and leads to diffuse PrD-GFP fluorescence throughout the cytoplasm [65, 66]. The cured cells still formed one RFP-Atg8 focus in the absence of auxin (Fig 19B, upper panel), whereas Myo2-depleted cured cells showed multiple RFP-Atg8 foci (Fig 19B, lower panel), suggesting that PrD-GFP and RFP-Atg8 foci can be formed independently. In the second approach, I introduced a galactose-

inducible genomic N-terminal GFP fusion to endogenous Atg8 in a Myo2-aid [PSI^+] strain that did not express any PrD-GFP. Multiple GFP-Atg8 fluorescent foci (Fig 19C, middle panel) were observed upon Myo2 depletion for 6 hours with auxin in this strain, which were subsequently refused to one PAS focus after auxin washout (Fig 19C, right panel and Fig 19D). In addition, a clear and direct re-fusion event of pre-existing multiple GFP-Atg8 foci was monitored by time-lapse microscopy immediately after removal of auxin (Fig 19E), suggesting that the PAS marker RFP-Atg8 forms multiple foci upon Myo2 depletion independently of the IPOD or the PrD-GFP substrate.

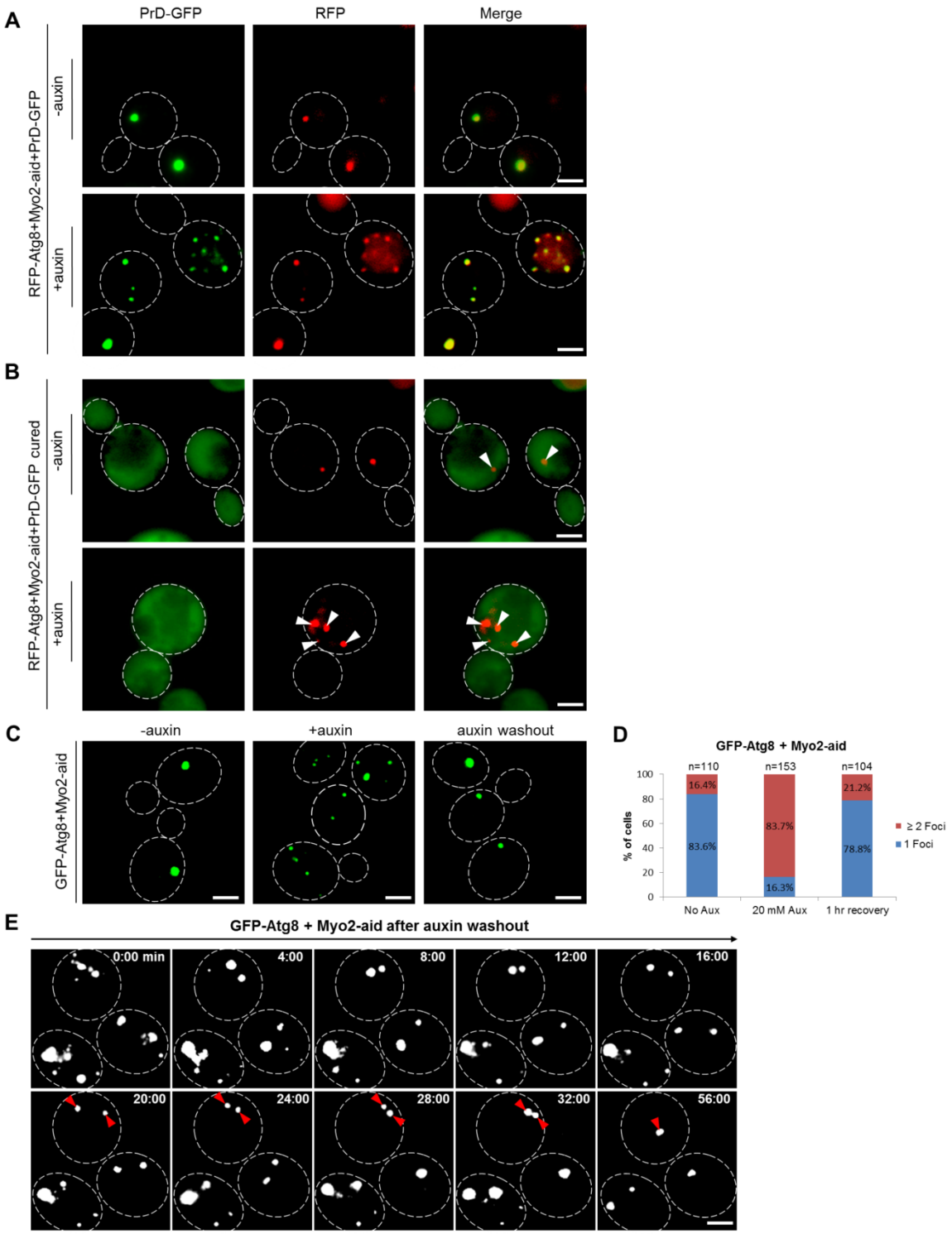

FIGURE 19: Myo2 depletion results in co-accumulation of RFP-Atg8 together with PrD-GFP foci – (**A**) PrD-GFP was induced with galactose for 6 hours in the absence or presence of 20 mM auxin in a [*PSI*$^+$] Myo2-aid strain that carried a plasmid coding for RFP-Atg8. Cells were fixed with PFA and analyzed by fluorescence microscopy in the GFP and mCherry channels. Co-localization: –auxin: 79 %, n=114 foci; +auxin: 89 %, n=96 foci. **(B)** Same experiment as in (A) in the same strain after curing of the [*PSI*$^+$] prion with GdnHCl. **(C)** Same experiment as in (A), but in a [*PSI*$^+$] Myo2-aid strain that did not express PrD-GFP, but GFP-Atg8 as a genomic fusion under control of the Gal1 promoter. In brief, GFP-Atg8 was induced with galactose for 6 hours in the absence or presence of 20 mM auxin.

Subsequently, cells were pelleted, resuspended in YPD without auxin to restore Myo2 function and incubated further for 60 min (auxin washout, right panel) prior to fixation and fluorescence microscopy. **(D)** Quantification of GFP-Atg8 foci in the absence or presence of auxin or after auxin washout (1 hr recovery). Frequencies of cells with 1 single focus or more than 1 foci are given in %. **(E)** Microscopy images from a time-lapse microscopy experiment as in C, but after removal of auxin. In brief, after induction of GFP-Atg8 and auxin addition for 6 hours, cells were pelleted, resuspended in YPD in the absence of auxin to restore Myo2 function and placed onto a microscope slide with an agarose pad for time-lapse microscopy. Z-stacks with a step width of 0.2 µm were acquired every 4 min. Scale bar, 2 µm.

3.2.6 Myo2 depletion results in co-accumulation of preApe1 together with PrD-GFP foci

After my observation that Myo2 depletion impairs the sorting of Atg8 to the PAS site, I wondered how preApe1, a substrate of the CVT pathway, is affected by Myo2 depletion. Precursor preApe1 is sorted to the PAS along actin cables [114]. At the PAS, preApe1 accumulates as multimeric complex and is enwrapped into the double-membrane CVT vesicles that subsequently fuse with the vacuolar membrane and deliver preApe1 into the lumen for its maturation (See the Fig 7). Therefore, for testing the effect of Myo2 depletion on this CVT substrate, I introduced a preApeI-mCherry fusion into Myo2-aid [*PSI*$^{+}$] cells expressing galactose-inducible PrD-GFP and performed a similar experiment as described in Fig19A. For this, PrD-GFP was induced with galactose for 6 hours with or without auxin in this strain. Fixed cells were analyzed by fluorescence microscopy in the GFP and mCherry channels. In the absence of auxin, 60 % of single PrD-GFP IPODs showed a co-localization with preApe1 PAS marker (Fig 20A, upper panel) while upon Myo2 depletion, 65 % of multiple PrD-GFP foci co-localized with multiple preApe1-mCherry foci (Fig 20A, lower panel). Here, I expected co-localization of almost all PrD-GFP IPODs with a preApe1 PAS marker focus [56, 65] just as with with RFP-Atg8 (compare Fig 19A). The lower degree of co-localization (only 60 %) compared to RFP-Atg8 was perhaps due to the following reasons: (I) interference of the mCherry tag with the preApe1 structure/conformation that led to failure of targeting to the PAS (II) the preApre1-mCherry fusion was present in low amounts such that the accumulation of preApe1 at the PAS could be detected technically in every cell.

Next, I further validated that preApe1 is mistargeted upon Myo2 depletion in the absence of any potentially sticky PrD-GFP amyloid aggregates. For testing this, I generated a galactose-inducible genomic N-terminal GFP-preApe1 fusion in a Myo2-aid [*PSI*$^{+}$] strain that did not express any PrD-GFP. 49 % of the cells (Fig 20C) showed multiple GFP-preApe1 fluorescent foci (Fig 20B, right panel) after Myo2 depletion compared to the control cells without auxin (Fig 20B, left panel), suggesting that Myo2 is required for sorting the CVT substrate preApe1 to the PAS.

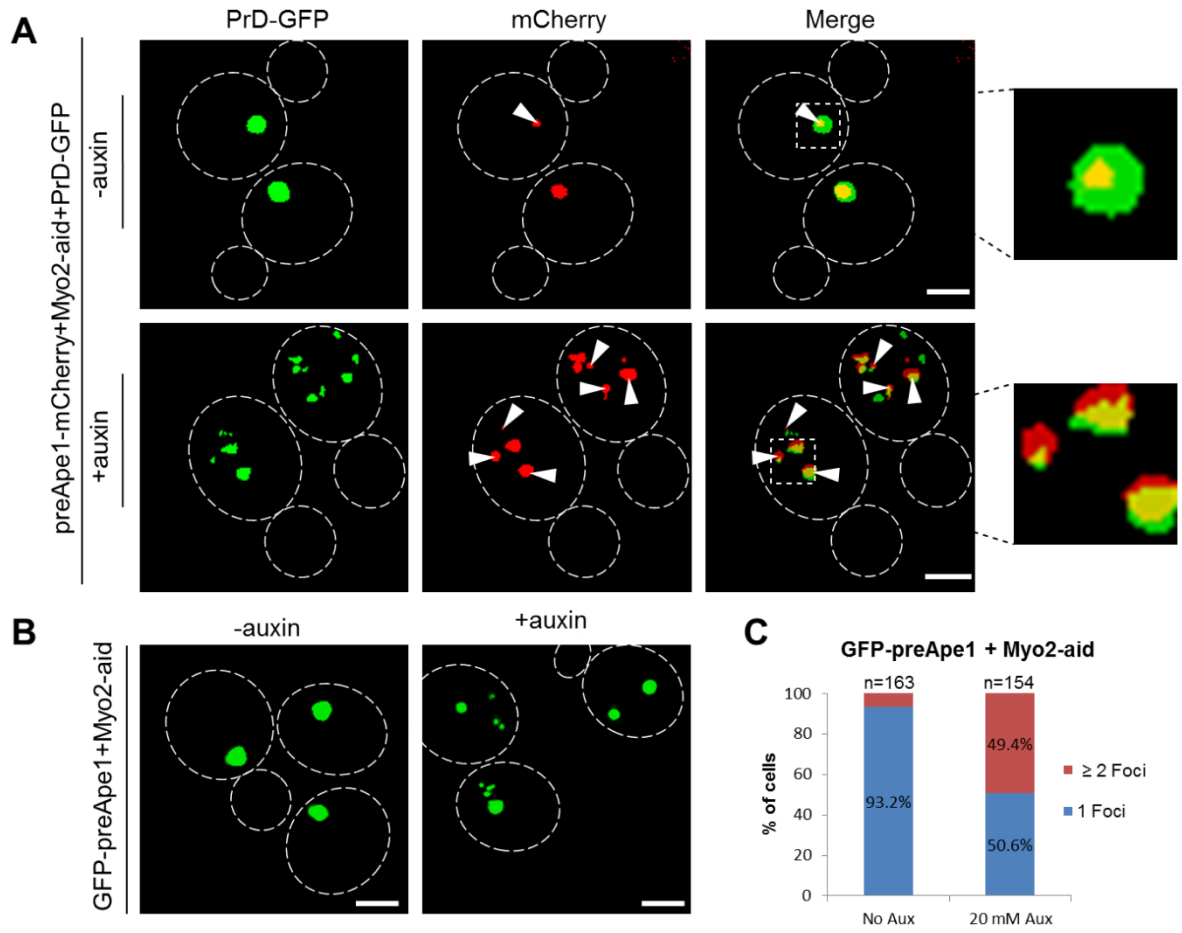

FIGURE 20: Myo2 depletion results in co-accumulation of preApe1-mCherry together with PrD-GFP foci – (**A**) PrD-GFP was induced with galactose for 6 hours in the absence or presence of 20 mM auxin in a [*PSI*$^{+}$] Myo2-aid strain with a genomic C-terminal mCherry fusion to preApe1. Cells were fixed with PFA and analyzed by fluorescence microscopy in the GFP and mCherry channels. Co-localization of existing PrD-GFP foci with at least 1 preApe1-mChery focus: –auxin: 60 %, n=98 foci; +auxin: 65 %, n=234 foci. (**B**) Same experiment as in (A), but in a [*PSI*$^{+}$] Myo2-aid strain that did not express PrD-GFP, but a genomic N-terminal GFP fusion to preApe1 controlled by a Gal promoter. (**C**) Quantification of GFP-preApe1 foci upon depletion of Myo2 is shown in the right panel. Frequencies of cells with 1 single focus or more than 1 foci are given in %. Scale bar, 2 µm.

3.2.7. Myo2 is also essential for proper accumulation of different amyloid substrates (Rnq1, Ure2 and Htt103Q) at the IPOD

Since Myo2 is involved in sorting of both, the IPOD substrate PrD-GFP to the IPOD- and the CVT pathway substrate preApe1 to the adjacent PAS destination site, I wondered whether Myo2 is also required for targeting of additional bona fide IPOD substrates such as Ure2, Rnq1 and HttQ103 [56] to the IPOD? For exploring this, I repeated a similar experiment as compared to PrD-GFP (compare Fig 15) by

introducing galactose-inducible Rnq1-GFP, Ure2-YFP and Htt103Q-CFP constructs into Myo2-aid mutants in [*PSI*$^{+}$] cells instead of PrD-GFP. In brief, I induced the corresponding IPOD substrates with galactose for 6 hours in a [*PSI*$^{+}$] Myo2-aid strain or a wild-type (wt) strain, in the absence or presence of auxin and withdrew aliquots for fluorescence microscopy. Subsequently, cells were resuspended in YPD (glucose chase) without auxin and incubated further for 60 min (auxin washout) prior to PFA fixation and fluorescence microscopy. All corresponding Myo2-aid strains expressing these IPOD substrates displayed one single IPOD in the absence of auxin (no Myo2 depletion), but a multiple foci phenotype upon auxin-based depletion of Myo2, just like PrD-GFP did auxin (Fig 21A, E, and I, middle panels). The control strains without the Myo2-aid tag did not show any multiple foci phenotypes, confirming again that the observed effect was due to the depletion of Myo2 (Fig 21C,D, G, H, K and L). These pre-existing multiple foci of different IPOD substrates were again refused to one central IPOD after removal of auxin (Fig 21A, E, and I, auxin washout panels), suggesting that Moy2 is involved in general in the recruitment of different IPOD substrates to the IPOD.

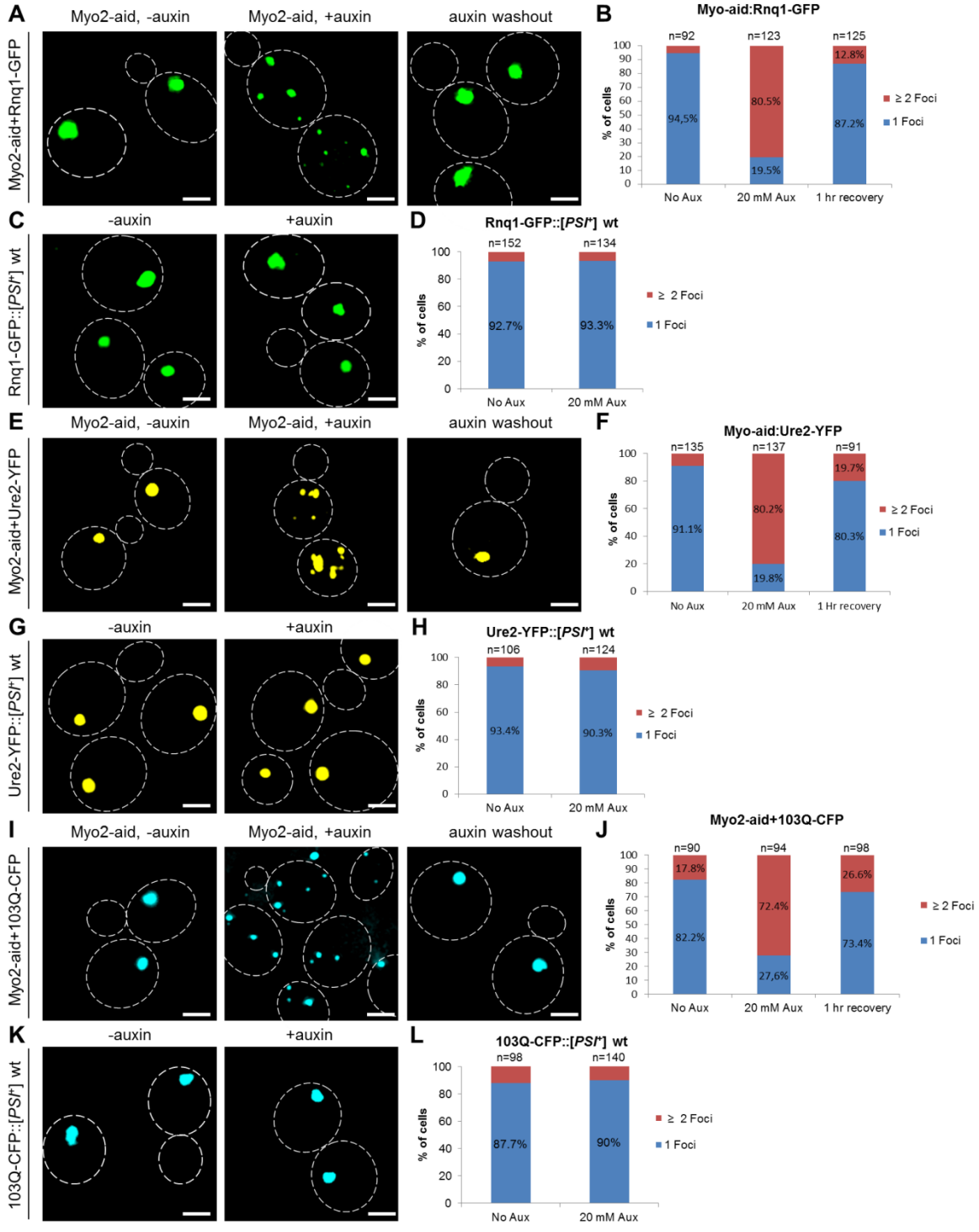

FIGURE 21: Myo2 is also essential for proper accumulation of different amyloid substrates (Rnq1, Ure2 and Htt103Q) at the IPOD – (**A, C**) Rnq1-GFP (integrated into genome) was induced with galactose for 6 hours in a [*PSI*$^{+}$] strain with a C-terminal aid-tag in MYO2 (left and middle panel) (A) or a wild-type (wt) strain (C), in the absence or presence of 20 mM of auxin as indicated. Subsequently, cells were pelleted, resuspended in YPD (glucose chase) without auxin to restore Myo2 function and incubated further for 60 min [auxin washout, right panel, (A)] prior to fixation and fluorescence microscopy. (**B, D**) Quantification of Rnq1-GFP foci upon depletion of Myo2 (B) or in the wild-type (wt) (D) is shown. Frequencies of cells with 1 single focus or more than 1 foci are given in %.

(**E, G**) Same experiment as in (A), but in a [*PSI*$^{+}$] Myo2-aid strain (E) or a wild-type strain (G) with a Ure2-YFP construct integrated into the genome under control of the Gal1 promoter. (**F, H**) Quantification of Ure2-YFP foci upon depletion of Myo2 (F) or in the wild-type (H) is shown. Frequencies of cells with 1 single focus or more than 1 foci are given in %. (**I, K**) Same experiment as in (A), but in a [*PSI*$^{+}$] Myo2-aid strain (I) or a wild-type strain (K) with a Htt103Q-CFP construct integrated into the genome under control of the Gal1 promoter. (**J, L**) Quantification of Htt103Q-CFP foci upon depletion of Myo2 (J) or in the wild-type (L) is shown. Frequencies of cells with 1 single focus or more than 1 foci are given in %. Scale bar, 2 µm.

3.2.8. Depletion of Myo2 impairs proper recruitment of IPOD substrates (Rnq1, Ure2 and Htt103Q) to the IPOD rather than the integrity of the IPOD

In Fig 21, I showed that Moy2 is required in general for sorting of different IPOD substrates to the IPOD. To confirm that Moy2 is required for recruitment of these different substrates to the IPOD rather than being required for maintaining IPOD integrity (compare Fig 18), I performed a similar experiment with galactose-inducible Rnq1-GFP in a [*PSI*$^{+}$] Myo2-aid strain as shown for PrD-GFP in Fig 18A. In brief, I first pre-formed the single Rnq1-GFP IPOD with galactose without Myo2 depletion and subsequently monitored this pre-existing single IPOD for 6 hours in glucose-based media containing auxin to deplete Myo2. I withdrew aliquots every 2 hours for fluorescence microscopy (Fig 22A) and quantified the cells with one or multiple Rnq1-GFP foci (Fig 22B). Again, I did not observe any fragmentation of pre-existing single Rnq1-GFP IPODs upon Myo2 depletion, suggesting that Myo2 is involved in sorting the Rnq1-GFP aggregates to the IPOD rather than in maintaining IPOD integrity.

Next, I asked whether two different IPOD markers expressed in the same cell are recruited simultaneously to the same IPOD site. For this, I used a [*PSI*$^{+}$] Myo2-aid strain expressing galactose-inducible Ure2-YFP and Htt103Q-CFP. I induced both substrates with galactose for 6 hours in the absence or presence of 20 mM auxin. After auxin-based Myo2 depletion, I observed multiple foci of both Ure2-YFP and Htt103Q-CFP markers (Fig 22C, middle panel) that co-localized with each other, while without auxin, the cells showed one IPOD with both substrates as expected [56, 65] (Fig 22C, upper panel). Interestingly, these pre-existing multiple foci of the two IPOD substrates Ure2 and Htt103Q sorted back to one central IPOD after restoration of Myo2 function by auxin washout (Fig 22C, lower panel). From these data, it is concluded that Myo2-based transport along actin cables is crucial for sorting different amyloids substrates to the IPOD instead of maintaining the IPOD morphology.

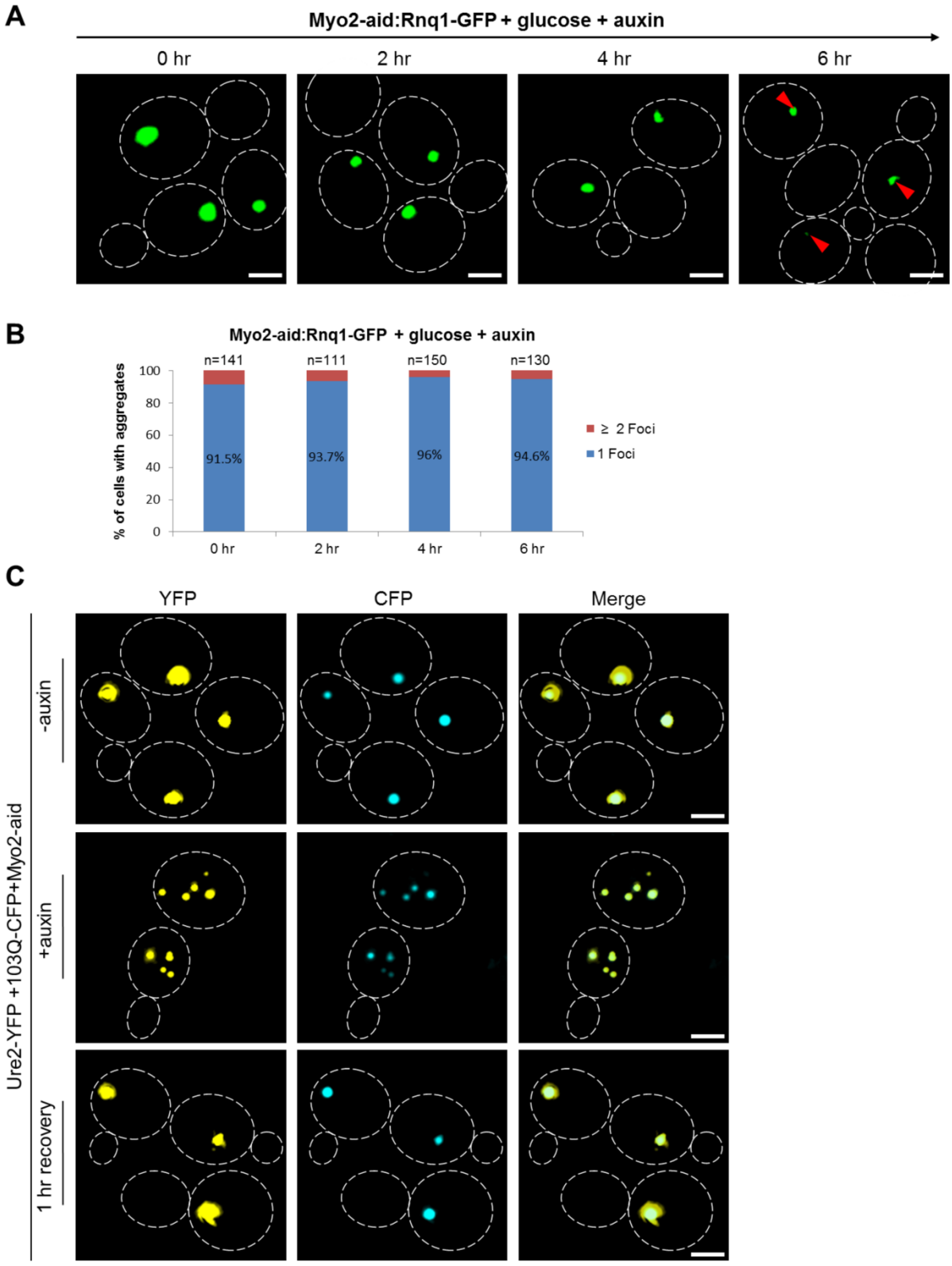

FIGURE 22: Depletion of Myo2 impairs proper recruitment of IPOD substrates (Rnq1, Ure2 and Htt103Q) to the IPOD rather than interfering with maintenance of the IPOD integrity – **(A)** Rnq1-GFP was induced with galactose for 6 hours in the absence of auxin in a [*PSI*$^{+}$] Myo2-aid strain. Subsequently, cells were pelleted and resuspended in YPD media in the presence of 20 mM auxin

and incubated further. Aliquots were withdrawn every 2 hours, fixed and analyzed by fluorescence microscopy. (**B**) Quantification of Rnq1-GFP foci from experiment A. Rnq1-GFP localization in either 1 or more than 1 foci was determined from cells that still carried Rnq1-GFP aggregates and plotted as %. (**C**) Co-localization of Ure2-YFP with Htt103Q-CFP. Both Ure2-YFP and Htt103Q-CFP in the same strain were induced with galactose for 6 hours in the absence or presence of 20 mM auxin in a [*PSI*$^{+}$] Myo2-aid strain (upper and middle panel). Subsequently, cells were pelleted, resuspended in YPD without auxin to restore Myo2 function and incubated further for 60 min (auxin washout, bottom panel) prior to fixation and fluorescence microscopy. Co-localization: –auxin, +auxin and auxin washout: 100 %, n=100-150 foci. Scale bar, 2 µm.

3.2.9. Myo2 depletion results in co-accumulation of Atg9 with PrD-GFP foci

Recruitment of preApe1, a substrate of the CVT pathway, involves formation of the so called CVT complex. The CVT complex consists of preAp1 and its receptor Atg19 [114]. It is loaded onto Atg9 transport vesicles and moves to the PAS along actin cables [114] in normal growth conditions. Atg9 is a multispanning transmembrane protein which exists in small cytoplasmic membrane vesicles termed as Atg9 vesicles [181] (see Fig7). Thus, disruption of actin filaments blocks the transport of both preApe1 and Atg9 vesicles to the PAS [179]. However, the linkage between these transport vesicles and actin cytoskeleton is unknown. At the PAS, preApe1 is enwrapped into the double-membrane CVT vesicles that subsequently deliver preApe1 into the lumen of the vacuole for its maturation (see Fig 7 for detail). Since PrD-GFP and preApe1 both use a similar targeting route for their sorting to the IPOD and PAS respectively, I wondered if PrD-GFP aggregates may also be associated with such Atg9 vesicles during recruitment to the IPOD deposition site. For testing this hypothesis, I labeled Atg9 with 3X-mCherry and introduced it into the previously used [*PSI*$^{+}$] Myo2-aid strain expressing galactose-inducible PrD-GFP and performed a co-localization experiment. In the autophagy field, it is known that there is a large pool of Atg9 vesicles in the cytoplasm, but only a subfraction of this pool co-localizes with the preApe1 PAS marker [182]. Atg9 vesicles also co-localize with Atg8 during the PAS formation [183]. PrD-GFP was induced with galactose for 6 hours in the absence or presence of 20 mM auxin in a [*PSI*$^{+}$] Myo2-aid strain that carried a C-terminal 3xmCherry-tag in the endogenous ATG9. Cells were fixed with PFA and analyzed by fluorescence microscopy in the GFP and mCherry channels. In the absence of auxin, 78 % of the single PrD-GFP IPODs showed co-localization with at least one of the multiple foci representing the pool of Atg9- 3X-mCherry (Fig 23, upper panel). Upon Myo2 depletion, I observed many more Atg9- 3X-mCherry foci. Nevertheless, 77 % of the multiple PrD-GFP foci observed under these conditions had at least one Atg9- 3X-mCherry focus co-localizing to them (Fig 23, lower panel). These above data suggest that PrD-GFP aggregates are associated with Atg9 transport vesicles, just like preApe1 is [182]. Thus these transport vesicles likely deliver both cargos to their destination sites, IPOD and PAS respectively, using the same targeting route, i.e. actin cables.

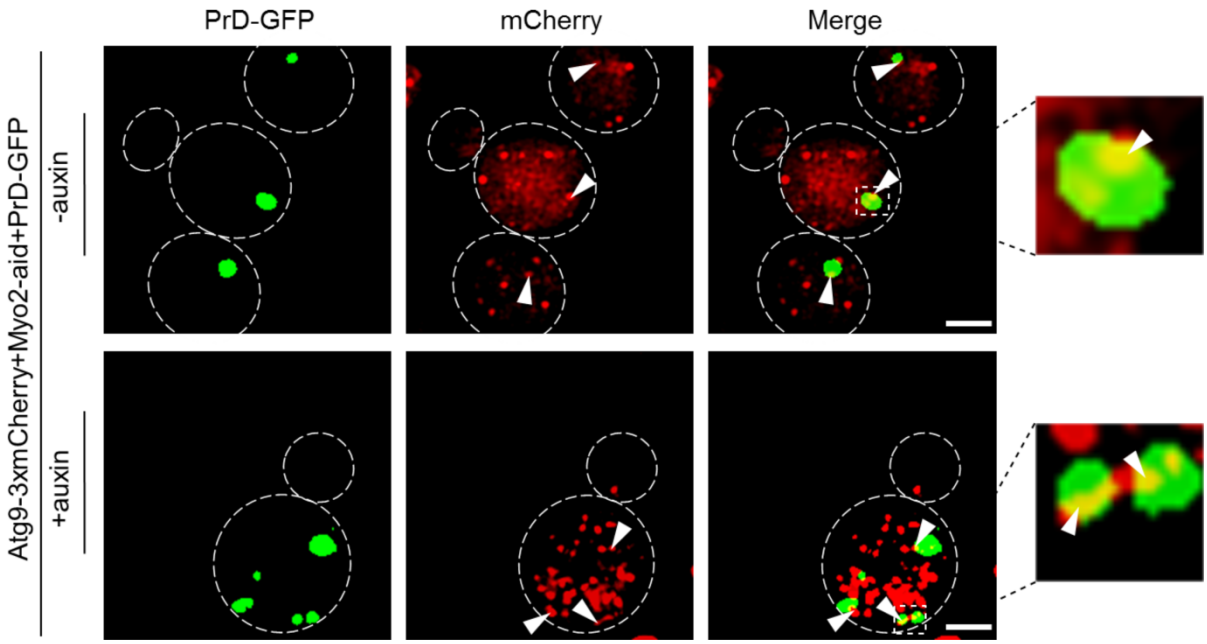

FIGURE 23: Myo2 depletion results in co-accumulation of Atg9 with PrD-GFP foci – PrD-GFP was induced with galactose for 6 hours in the absence or presence of 20 mM auxin in a [*PSI*$^{+}$] Myo2-aid strain with a C-terminal 3xmCherry-tag in the endogenous ATG9. Cells were fixed with PFA and analyzed by fluorescence microscopy in the GFP and mCherry channels. Co-localization of existing PrD-GFP foci with at least 1 Atg9-3xmCherry focus: –auxin: 78 %, n=116 foci; +auxin: 77 %, n=205 foci. Scale bar, 2 µm.

3.2.10. Depletion of Sec14, Sec18 and Sec21 also impairs the recruitment of PrD-GFP to the IPOD

Recently, it was shown that Sec proteins (Sec18 and Sec53) are required for asymmetric inheritance of Htt103Q and heat-induced protein aggregates together with Myo2/Cmd1/actin [139]. Since I also fished with immobilized PrD several Sec proteins (Sec4, Sec14, Sec18, Sec21, and Sec53) from yeast cell lysates (compare Fig 13), I decided to also investigate their possible role in the recruitment of the PrD-GFP aggregates to the IPOD. Sec4 is Rab family GTPase which associates with secretory vesicles and is involved in their polarized transport towards the site of cell growth in a Myo2-dependent manner along actin cables [184]. Sec4 is also involved in the transport of Atg9 vesicles to the PAS during autophagy/CVT pathway [185]. Sec14 is a phosphatidylcholine/phosphatidylinositol (PI/PC) transfer protein that is required for the transport of trans-Golgi-derived vesicles as well as for autophagy [186]. Sec18, a SNARE [**SNA**P (Soluble NSF (N-ethylmaleimide-sensitive factor) Attachment Protein **RE**ceptor] disassembly chaperone is required for several vesicular fusion events such as homotypic vacuole fusion and translocation of preApe1 into the vacuole [182, 187]. Sec18 has also been shown to be involved in the trafficking of Atg9 vesicles from peripheral sites to the PAS along with several

SNARE proteins such as Sso1/2, Sec9, Tlg2, Ykt6 and Sec22 [182]. Sec21, a COPI coatomer protein was found to associate with Vid (vacuole import and degradation) vesicles to deliver inactive fructose-1,6-bisphosphatase (FBPase) into the vacuolar lumen for its degradation [188].

Since all these Sec proteins (Sec4, Sec14, Sec18, Sec21 and Sec53) are essential, I applied the same auxin-based depletion system [172] to greatly deplete their levels temporally and monitored the distribution of PrD-GFP aggregates. I tested all Sec proteins except for Sec4, whose auxin-based depletion did not work due to technical reasons. However, I was able to observe the depletion effect of Sec14, Sec18, Sec21 and Sec53 proteins on PrD-GFP sorting to the IPOD. In short, I induced PrD-GFP with galactose for 6 hours in the absence and presence of auxin in [*PSI*$^{+}$] Sec14/18/21/53-aid strains. In response to auxin, I observed a similar reversible multiple PrD-GFP foci phenotype as observed with Myo2 depletion in most of the cells (70 % in the Sec14-aid strain, 83% in the Sec18-aid strain and 74 % in the Sec21-aid strain) (Fig 24 A-F). Since these proteins are known to be involved in vesicular transport processes, these results suggested that efficient recruitment of PrD-GFP to the IPOD involves vesicular transport. This would be consistent with a function of Myo2 in vesicle transport along actin cables, that has been described for other vesicular transport processes already [189]. Restoration of Sec14, Sec18 and Sec21 functions by auxin washout led to refusion of all pre-existing multiple foci to one central IPOD (Fig 24A, Fig 24C and Fig 24E, right panels). Depletion of Sec14, Sec18 and Sec21 was confirmed by Western Blot analysis with an antibody against an HA tag attached to the “aid” degron tag (Fig 24I). Short-term depletion of these proteins, such as Sec14 and Sec18 for 6 hrs had no effect on cell viability (Fig 24J). Taken together, above data suggest that Sec14, Sec18 and Sec21 are involved in proper targeting of PrD-GFP amyloids to the IPOD site. In case of the Sec53-aid strain, I did not observe any sorting defect for PrD-GFP aggregates (Fig 24G, right panel). I note, however, that the degree of depletion for this protein was very low (Fig 24 I). This suggests that Sec53 is either not involved in sorting of PrD-GFP aggregates to the IPOD or that its depletion was just not sufficient to display a phenotype (Fig 24I).

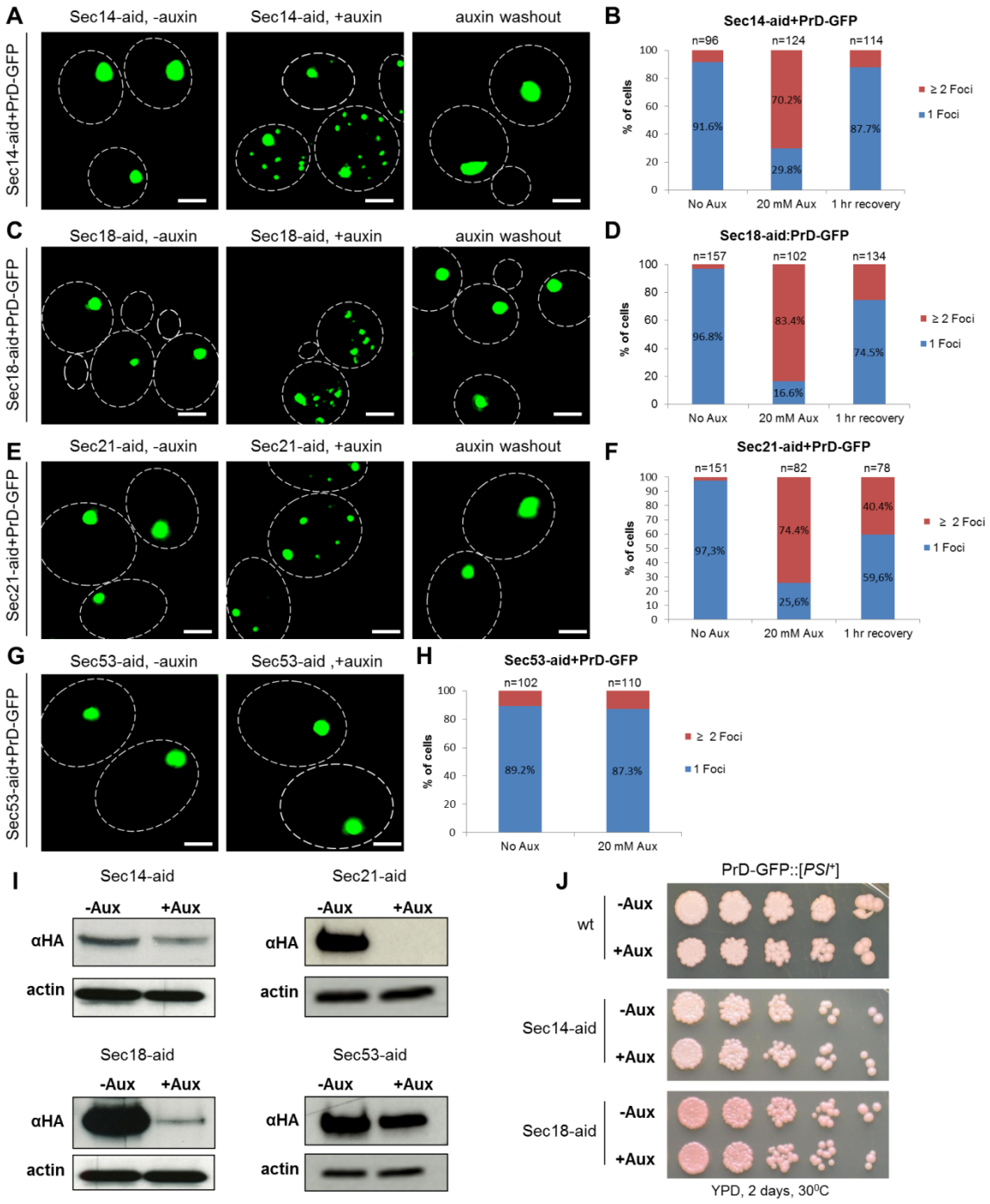

FIGURE 24: Depletion of Sec14, Sec18 and Sec21, but not Sec53, impairs the recruitment of PrD-GFP to the IPOD – (**A, C, E**) PrD-GFP was induced with galactose for 6 hours in the absence or presence of 20 mM auxin (left and middle panels) in a [*PSI*$^+$] strain with a C-terminal aid-tag in SEC14 (A) or SEC18 (C) or SEC21 (E) and aliquots were withdrawn for fluorescence microscopy analysis. Subsequently, cells were pelleted, resuspended in YPD (glucose chase) without auxin and incubated further for 60 min to restore Sec14, Sec18 and Sec21 functions (auxin washout, right panels) prior to PFA fixation and fluorescence microscopy. (**B, D, F, H**) Quantification of PrD-GFP foci upon depletion of Sec14 (B), Sec18 (D), Sec21 (F) or Sec53 (H) is shown. Frequencies of cells with 1 single focus or more than 1 foci are given in %. (**G**) Same experiment as in (A), but in a [*PSI*$^+$] strain with a C-terminal

aid-tag in SEC53. The experiment was performed without auxin washout. (**I**) Western blot analysis of the [*PSI*$^{+}$] Sec14-aid, Sec18-aid, Sec21-aid and Sec53-aid strains without (-Aux) or after depletion of Sec14, Sec18, Sec21 and Sec53 (+Aux) with an antibody against an HA-tag present in the aid-tag. An anti-actin antibody served as loading control. (**J**) A [*PSI*$^{+}$] wild-type (wt), Sec14-aid and Sec18-aid strains were treated as described in (A, C) before serial dilution and spotting onto YPD plates and growth for 2 days to test for viability. Scale bar, 2 µm.

3.2.11. Sec18 depletion results in co-accumulation of multiple mCherry-Atg8 foci together with PrD-GFP foci

Trafficking of Atg9 vesicles from peripheral sites to the PAS requires several SNARE proteins such as Sso1/2, Sec9, Tlg2, Ykt6 and Sec22 including Sec18 SNARE chaperone [182]. From my fishing approach, Sec18, a SNARE disassembly chaperone was found to bind PrD fibers *in vitro* (see Fig13). Sec18 is involved in several cellular processes such as: (I) ER to Golgi trafficking (secretory pathway) [190]; (II) endocytic pathway [191]; (III) homotypic vacuole fusion and vesicular fusion events [192]; (IV) autophagy [182]. I found evidence that PrD-GFP aggregates are associated with such Atg9 vesicles during their recruitment to the IPOD (see Fig 23). Interestingly, I found that Sec18 SNARE-mediated vesicular transport is required for reversible accumulation of PrD-GFP aggregates at the IPOD (see Fig 24C). Since I observed that PrD-GFP and PAS proteins use a similar machinery for their recruitment to the IPOD and PAS, respectively, I wondered whether Sec18 also mediates sorting of PAS markers to the PAS.

To investigate this, I transformed the mCherry-Atg8 PAS marker into [*PSI*$^{+}$] Sec18-aid strain expressing galactose-inducible PrD-GFP and asked if Atg8 sorting to the PAS and its co-localization with PrD-GFP aggregates is impaired upon Sec18 depletion. In the absence of auxin, 76 % of single PrD-GFP IPODs showed a co-localization with the Atg8 PAS marker, as expected [56, 65] (Fig 25A, upper panel). More interestingly, auxin-based depletion of Sec18 also caused multiple mCherry-Atg8 foci which were further co-localized with 79 % of the multiple PrD-GFP foci (Fig 25A, lower panel). However, to further rule out the possibility that multiple mCherry-Atg8 foci phenotype was a consequence of co-aggregation of the PAS marker with potentially sticky PrD-GFP aggregates, I cured this strain with 5 mM GdnHCl to abolish the prion state in PrD-GFP and repeated the same experiment (compare Fig 19B). After curing, these cells still formed one mCherry-Atg8 focus in the absence of auxin (Fig 25B, upper panel), whereas Sec18-depleted, cured cells showed multiple mCherry-Atg8 foci (Fig 25B, lower panel), suggesting that PrD-GFP and mCherry-Atg8 do not co-aggregate, but form multiple foci independently of each other. Furthermore, auxin-based Sec18 depletion also caused reversible multiple GFP-Atg8 fluorescent foci in 76 % of the cells (Fig 25C, middle panel and Fig 25D) when a galactose-inducible genomic N-terminal GFP-Atg8 fusion was used in a Sec18-aid [PSI^{+}] strain without any PrD-GFP. These GFP-Atg8 foci were re-localized to one PAS focus after auxin removal (Fig 25C, right panel).

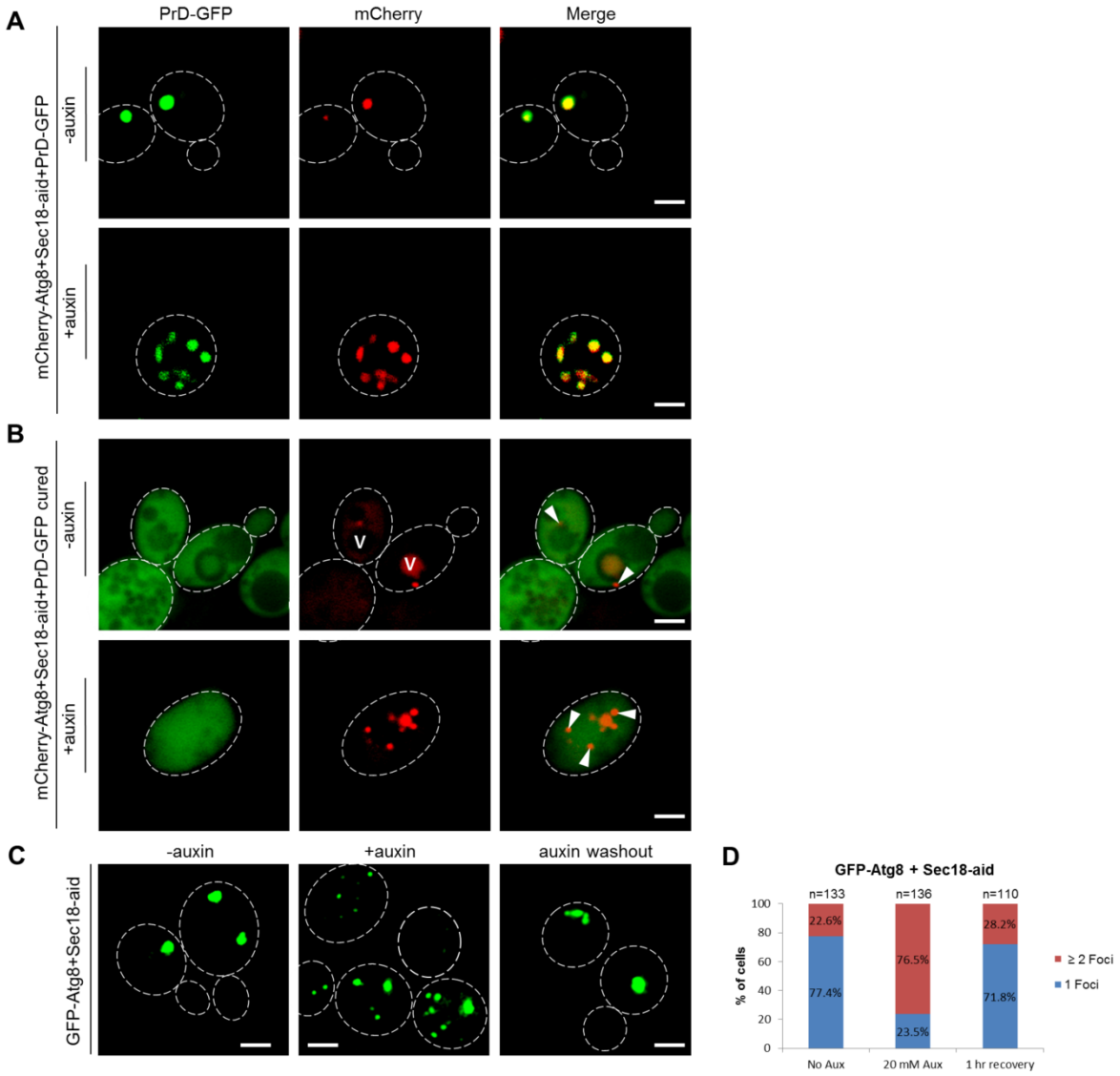

FIGURE 25: Sec18 depletion results in co-accumulation of multiple mCherry-Atg8 foci together with PrD-GFP foci – (**A**) PrD-GFP was induced with galactose for 6 hours in the absence or presence of 20 mM auxin in a [*PSI*$^{+}$] Sec18-aid strain with a plasmid carrying an N-terminal mCherry-Atg8 fusion under control of the Atg8 promoter prior to fixation and fluorescence microscopy in the GFP and mCherry channels. Co-localization of PrD-GFP foci with mCherry-Atg8 foci: –auxin: 76 %, n=105 foci; +auxin: 79 %, n=108 foci. **(B)** Same experiment as in (A) in the same strain after curing of the [*PSI*$^{+}$] prion with GdnHCl. V=vacuole (**C**) Same experiment as in (A), but in a [*PSI*$^{+}$] Sec18-aid strain that did not express PrD-GFP, but GFP-Atg8 as a genomic fusion under control of the Gal1 promoter. In brief, GFP-Atg8 was induced with galactose for 6 hours in the absence or presence of 20 mM auxin. Subsequently, cells were pelleted, resuspended in YPD without auxin and incubated further for 60 min to restore Sec18 function (auxin washout, right panel) prior to fixation and fluorescence microscopy. **(D)** Quantification of GFP-Atg8 foci in the absence or presence of auxin or after auxin washout (1 hr recovery). Frequencies of cells with 1 single focus or more than 1 foci are given in %. Scale bar, 2 µm.

3.2.12. Sec18 depletion leads to co-localization of Myo2 with PrD-GFP foci

Impairment of the actin-based transport machinery by depleting Myo2 and Tpm1/2 blocked proper recruitment of PrD-GFP and the PAS markers Atg8 and preApe1 to their adjacent destination sites, IPOD and PAS, respectively (see Fig 19 and 20). Furthermore, I found evidence that PrD-GFP and the PAS markers are loaded onto Atg9 vesicles (compare Fig 23). It is known that vacuolar vesicles/lobes are moved and inherited from the mother to daughter cells with the aid of Myo2 motor protein and specific adaptors/receptors along actin cables [193]. Therefore, I hypothesized that Myo2 might be the linking factor between the vesicular transport machinery and the actin cytoskeleton. Therefore, I tested whether Myo2 is present in PrD-GFP transport intermediates after Sec18 depletion. For that, I tagged the genomic copy of Myo2 with 3xmCherry in a [*PSI*$^{+}$] Sec18-aid strain expressing galactose-inducible PrD-GFP. Then, I induced PrD-GFP with galactose for 6 hours in the absence or presence of 20 mM auxin. After induction, I fixed the cells with and analyzed by fluorescence microscopy in the GFP and mCherry channels. The control cells without auxin showed a diffuse fluorescence of Myo2-3xmCherry (Fig 26A, upper panel), while after Sec18 depletion, Myo2-3xmCherry formed foci-like structures that co-localized in 74 % of the cases with the multiple PrD-GFP aggregates (Fig 26A, lower panel). From this, I concluded that Myo2 links the Atg9-vesicle based transport machinery to tropomyosin-coated actin cables to deliver PrD-GFP and preApe1 substrates to their recruitment sites IPOD and PAS, respectively.

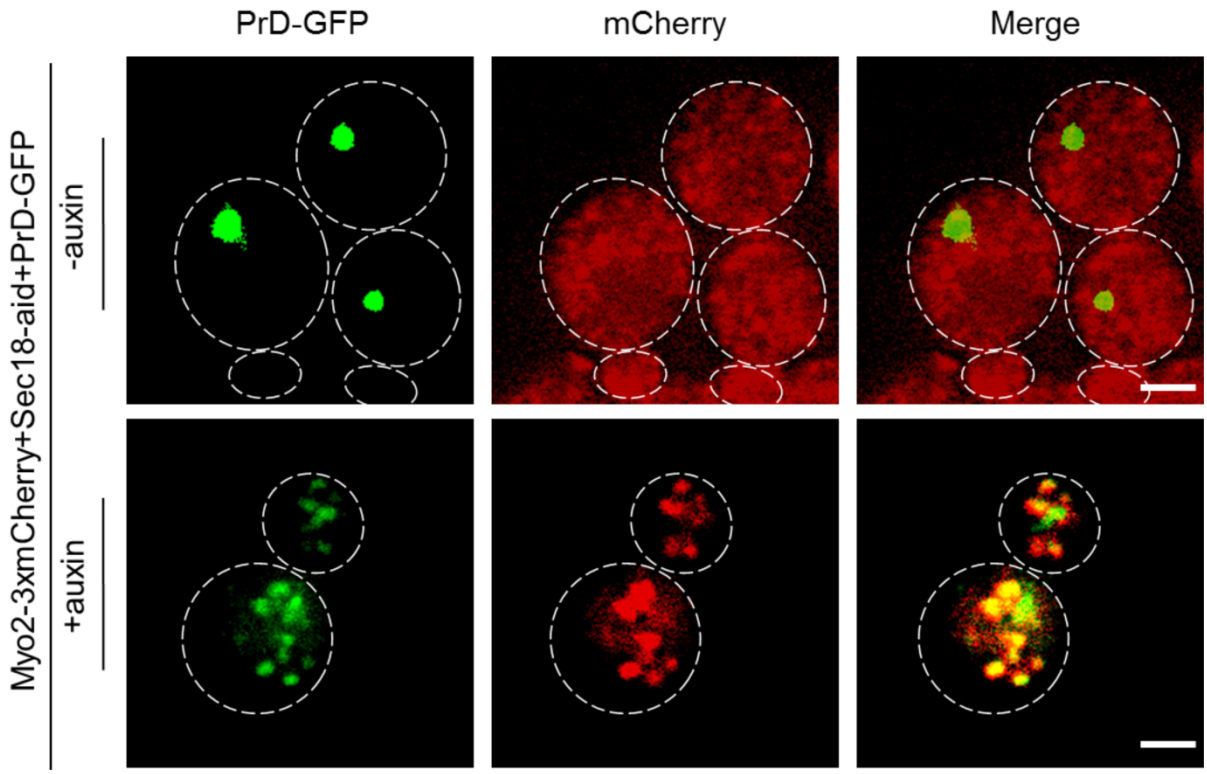

FIGURE 26: Sec18 depletion leads to co-localization of Myo2 structures with PrD-GFP foci – PrD-GFP was induced with galactose for 6 hours in the absence or presence of 20 mM auxin in a [*PSI*$^{+}$] Sec18-aid strain with a C-terminal 3xmCherry-tag in the endogenous MYO2. Cells were fixed with and analyzed by fluorescence microscopy in the GFP and mCherry channels. Co-localization of existing PrD-GFP foci with Myo2-mCherry structures: +auxin: 74 %, n=238 foci. Scale bar, 2 µm.

3.3. Investigating the fate of amyloid aggregates at the IPOD

3.3.1. PrD-GFP is not turned over via bulk autophagy

I observed that PrD-GFP aggregates are recruited to the IPOD using a similar vesicular transport machinery as preApe1 employs for its transport to the PAS. Not surprisingly then, both IPOD and PAS exist in close proximity to each other, because they seem to use the same tracks. At the PAS, preApe1 is enwrapped by a double-

membrane vesicle to form the CVT vesicle which subsequently delivers preApe1 into the vacuolar lumen for its maturation [127]. Therefore, I wondered if PrD-GFP amyloid aggregates are recruited in close proximity to the PAS for their enwrapping into double-membrane autophagosomes and possible autophagy-mediated turnover. This would resemble the situation in mammalian cells where aggresomes are degraded by autophagy [122]. For testing this idea, I used a strain that constitutively expresses PrD-GFP and accumulates PrD-GFP aggregates at the IPOD i.e. [*PrD-GFP*$^{+}$] and tested whether the protein levels of PrD-GFP would change when autophagy was either inhibited or induced [65]. I also included a strain expressing PrD-GFP in the non-prion (soluble) conformation i.e. [*prd-gfp*$^{-}$], where PrD-GFP shows diffuse fluorescence throughout the cytoplasm. This served as a positive internal control for successful induction of autophagy for the following reason: Induction of bulk autophagy results in enwrapping of random parts the cytoplasm into autophagosomes and degradation in the vacuole [113, 194]. In the strain with soluble PrD-GFP dispersed throughout the cytoplasm, some of the PrD-GFP should also be incorporated into autophagosomes along with the random parts of the cytoplasm and degraded in the vacuole. Since GFP that is released from GFP fusion proteins is quite stable in the vacuolar lumen [126, 195, 196], this should result in emergence of free GFP and reduced levels of PrD-GFP. After autophagy induction with 4 mM spermidine [197], I observed indeed a slight decrease in the PrD-GFP levels and the release of free GFP moiety in the [*prd-gfp*$^{-}$] strain (Fig 27A, lane 4) compared to the untreated wild-type cells (Fig 27A, lane 2), confirming that autophagy was induced successfully. If PrD-GFP aggregates were also turned over via autophagy, then the steady state levels of PrD-GFP should also decrease in the strain where the protein is aggregated and deposited at the IPOD, and a band of free GFP should emerge. However, upon autophagy induction, I could not observe such an appearance of the free GFP moiety or a change in the PrD-GFP levels (Fig 27A, lane 3). Thus PrD-GFP aggregates are not turned over in the vacuole to a detectable degree. When, I inhibited autophagy by adding 1 mM of PMSF in pep4 mutant background [119] of both strains, I did not see any increased PrD-GFP level in [*PrD-GFP*$^{+}$] (Fig 27A, lane 5) and [*prd-gfp*$^{-}$] strain (Fig 27A, lane 6), again arguing that there is no significant turnover of PrD-GFP aggregates in the vacuole under steady state conditions. In second experiment, I deleted essential components of the autophagy machinery [119], and looked whether these mutants show a difference in the steady-state level of PrD-GFP compared to wild-type (wt). In these mutants, I observed neither a significant difference in the levels of PrD-GFP compared to the wild-type cells (Fig 27B) nor in the morphology/intensity of PrD-GFP IPOD (Fig 27C). These above data suggest that PrD-GFP IPOD is not turned over via bulk autophagy in yeast.

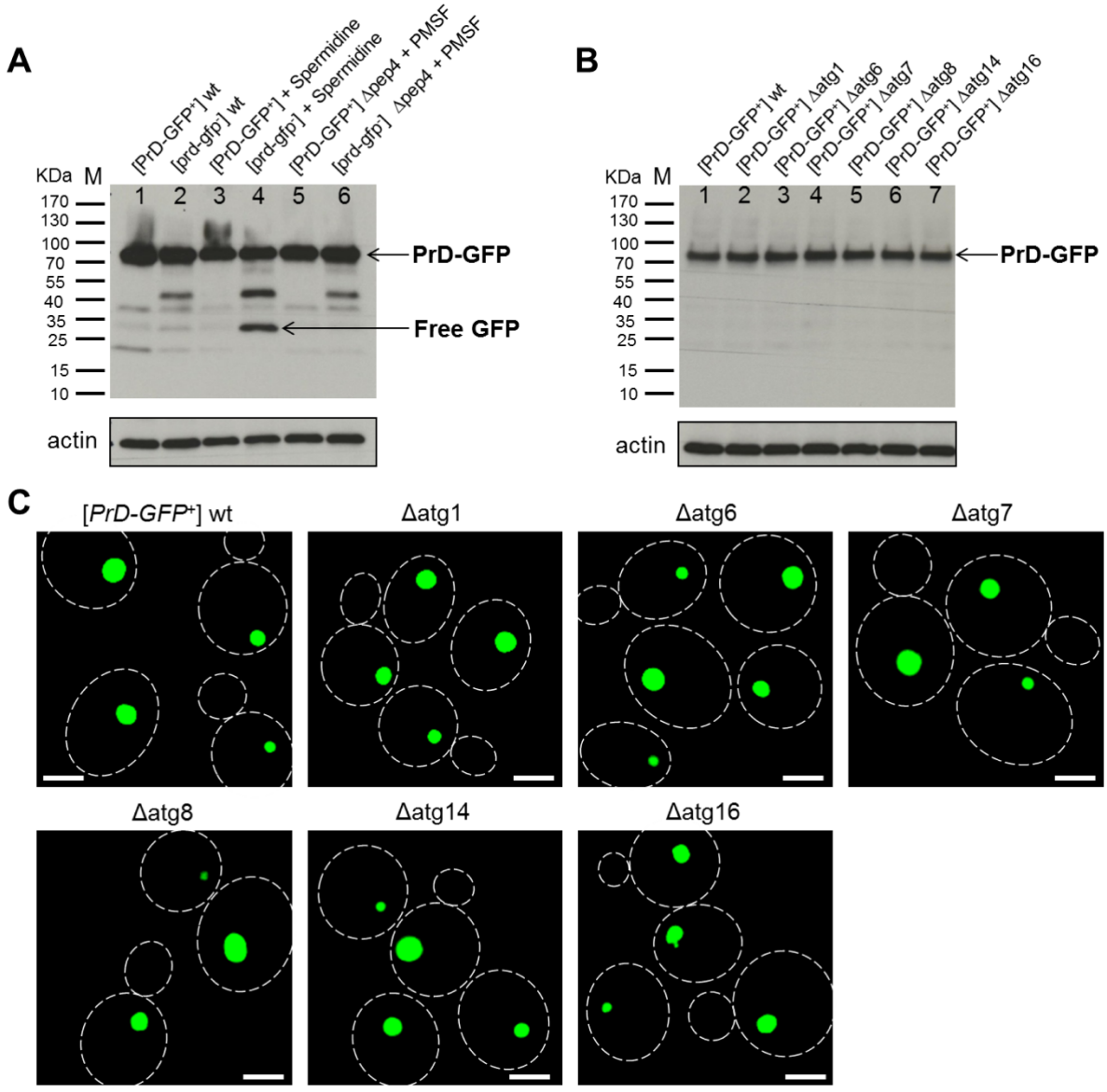

FIGURE 27:PrD-GFP is not turned over by bulk pathway – (**A**) Strains expressing PrD-GFP constitutively under control of the GPD promoter with a deletion in the endogenous prion domain in SUP35 were either in the prion state [*PrD-GFP*$^{+}$] or in the non-prion state [*prd-gfp*$^{-}$]. The PEP4 gene was deleted as indicated. Strains were grown to saturation, diluted to an OD_{600} of 0.15 and were further incubated untreated or in the presence of 4 mM spermidine (autophagy induction) or 1 mM PMSF (inhibition of vacuolar peptidases, no autophagic turnover of proteins) as indicated. After ~4 hours, cells were harvested, adjusted to identical cell numbers and subjected to Western Blot analysis using an anti-GFP antibody. Turnover of PrD-GFP is monitored by release of free GFP moiety. An antibody against actin was used as loading control. (**B**) Yeast strains as in (A) that propagated PrD-GFP in the prion state ([*PrD-GFP*$^{+}$]) but carried a different deletion in autophagy-related genes as indicated, were grown to logarithmic growth phase, adjusted to identical cell numbers and analyzed by Western Blotting with an anti-GFP antibody and an anti-actin antibody as loading control. (**C**) Same as (B) where logarithmic growth phase cells were fixed and subjected to fluorescence microscopy. Scale bar, 2 µm.

Role of substrates of the CVT pathway (preApe1 and Ams1) and different CVT pathway components (Atg9, Atg11 or Atg19) on PrD-GFP sorting to the IPOD

Both preApe1 and PrD-GFP aggregates use a similar actin-mediated Atg9 vesicle-based transport machinery for their recruitment at the IPOD and PAS, respectively. Loading of the CVT substrate preApe1 to the Atg9 vesicles is mediated by a specific receptor termed Atg19, and the adaptor Atg11 [114, 116, 127]. It was shown that another vacuolar hydrolase, α-mannosidase (Ams1) also employs the same CVT pathway as preApe1 to enter into the vacuole [127]. Therefore, I also tested whether any substrate of the CVT pathway or its receptor/adaptor is required for targeting of PrD-GFP aggregates to the IPOD. For testing these components of the CVT pathway, I deleted these genes in a [*PSI*$^+$] strain expressing galactose-inducible PrD-GFP. Then, I induced PrD-GFP with galactose for 6 hours in a [*PSI*$^+$] wild-type (wt) strain and deletion mutants of the components of the CVT pathway. However, these mutants did not show any difference in the morphology/intensity of PrD-GFP IPOD compared to the wild-type cells (Fig 28). These above data show that no CVT pathway components are required for recruitment of PrD-GFP to the IPOD.

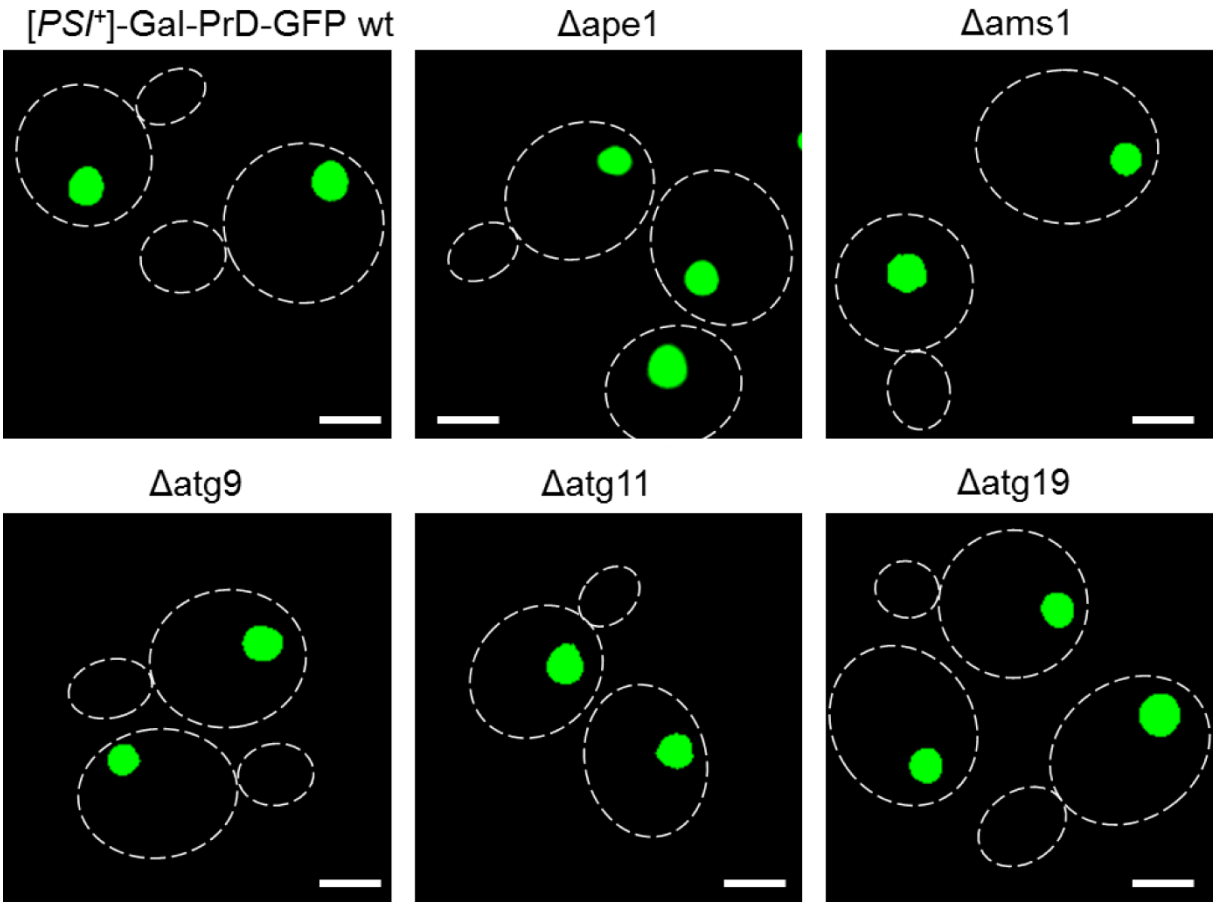

FIGURE 28: Neither the substrates of the CVT pathway (preApe1 and Ams1) nor different CVT pathway components (Atg9, Atg11 or Atg19) are crucial for PrD-GFP sorting to the IPOD – PrD-GFP was induced with galactose for 6 hours in a [*PSI*$^+$] wild-type (wt) strain or an identical strain, but

with the indicated deletions in CVT pathway substrates/components. Cells were fixed with PFA and analyzed by fluorescence microscopy. Scale bar, 2 µm.

3.3.2. PrD-GFP is slowly extracted from the IPOD by Hsp104 and progressively decays over time

Although I did not find any evidence for autophagic turnover of PrD-GFP aggregates, PrD-GFP IPODs slowly and progressively decayed over time (see Fig 18A) in a [*PSI*$^+$] Myo2-aid strain. To investigate how this decay is mediated, I performed such a decay experiment in the wild-type [*PSI*$^+$] strain expressing galactose-inducible PrD-GFP. First, I induced formation of the PrD-GFP IPOD with galactose for 6 hours. Subsequently, I chased the cells with this pre-existing single IPOD in glucose-based media for 8 hours and monitored the fate of the IPOD over time. I observed that the IPOD decayed and progressively became smaller and smaller over time (Fig 29A and 29B). This observation gave a hint that PrD-GFP aggregates are processed from the IPOD. In yeast, a well-known amyloid remodeling factor is Hsp104 [198-202], which was shown to interact *in vivo* with different IPOD substrates [167, 203]. To test if PrD-GFP aggregates at the IPOD are subjected to Hsp104-dependent processing, I induced the PrD-GFP IPOD with galactose for 6 hours and again chased the cells with this pre-existing IPOD over time in glucose-based media containing 5mM GdnHCl to inhibit Hsp104 activity [204]. After Hsp104 inhibition, the PrD-GFP IPOD did not decay at all, but retained even after 8 hours of glucose chase (Fig 29C and 29D). This suggests that PrD-GFP aggregates are extracted by the Hsp104 disaggregation machinery from the IPOD.

Next, I wanted to investigate the possible fate of PrD-GFP after extraction from the IPOD by Hsp104. One obvious possibility was that extracted PrD-GFP is degraded by the proteasome, since PrD-GFP was not degraded to a significant extend by bulk autophagy (see Fig 27 A). For testing this, I inhibited the proteasome with MG132 using a [*PSI*$^+$] strain with the Gal-inducible PrD-GFP construct that lacks a PDR5 gene to prevent pumping out of the proteasome inhibitor MG132. With this experiment, I also included as a positive control for proteasomal inhibition tGnd1-GFP as a known substrate for proteasomal degradation [103]. In short, I grew tGnd1-GFP expressing cells to mid-log phase and added 100 µg/ml of cycloheximide (CHX) to stop ongoing synthesis of tGnd1-GFP and further chased the protein for 8 hours in the absence and presence of proteasome inhibitor MG132 (Fig 29F, lane 2 and 3). After 8 hours of proteasome inhibition by MG132, tGnd1-GFP was greatly stabilized (Fig 29F, lane 3). Thus I repeated the PrD-GFP IPOD decay experiment as described below. In brief, I first induced formation of the PrD-GFP IPOD with galactose for 6 hours in a [*PSI*$^+$] Δpdr5 background strain and subsequently chased this pre-existing IPOD in glucose-based media (abolishment of galactose induced expression of PrD-GFP) in the absence of the proteasome inhibitor MG132 and in the presence of

MG132 or GdnHCl. After 8 hours of glucose chase, the levels of PrD-GFP were decreased in the absence of MG132 (Fig 29E, lane 2) as compared to the amount before the chase (Fig 29E, lane 1), while there was a clearly reduced decrease in PrD-GFP levels when I inhibited the proteasome (Fig 29, lane 3). Upon proteasome inhibition, however, the PrD-GFP levels did not reach to the levels before the glucose chase ("time 0h" of glucose chase) (Fig 29E, lane 1 and lane3), suggesting that extracted PrD-GFP is not only degraded by the proteasome. In contrast, after Hsp104 inhibition with GdnHCl, the PrD-GFP levels were the same as compared to "time 0h" of glucose chase (Fig 29E, lane 4). This was consistent with fluorescence microscopy analysis as shown in Fig 29C where also no decay of the PrD-GFP IPOD could be observed.

These above observations suggest that PrD-GFP can be degraded by the proteasome and perhaps additional cellular degradation pathways [205], but only after its slow and progressive extraction by Hsp104 from the IPOD. Thus accumulation of PrD-GFP amyloids at the IPOD might serve a temporary storage function when downstream cellular degradation systems are overwhelmed. Such temporary storage at the IPOD would sequester potentially toxic amyloids from the cytosol. In support of this idea, it was recently shown that non-amyloid substrates such as inactive proteasomes are temporally deposited at the IPOD before their vacuolar autophagic degradation [155].

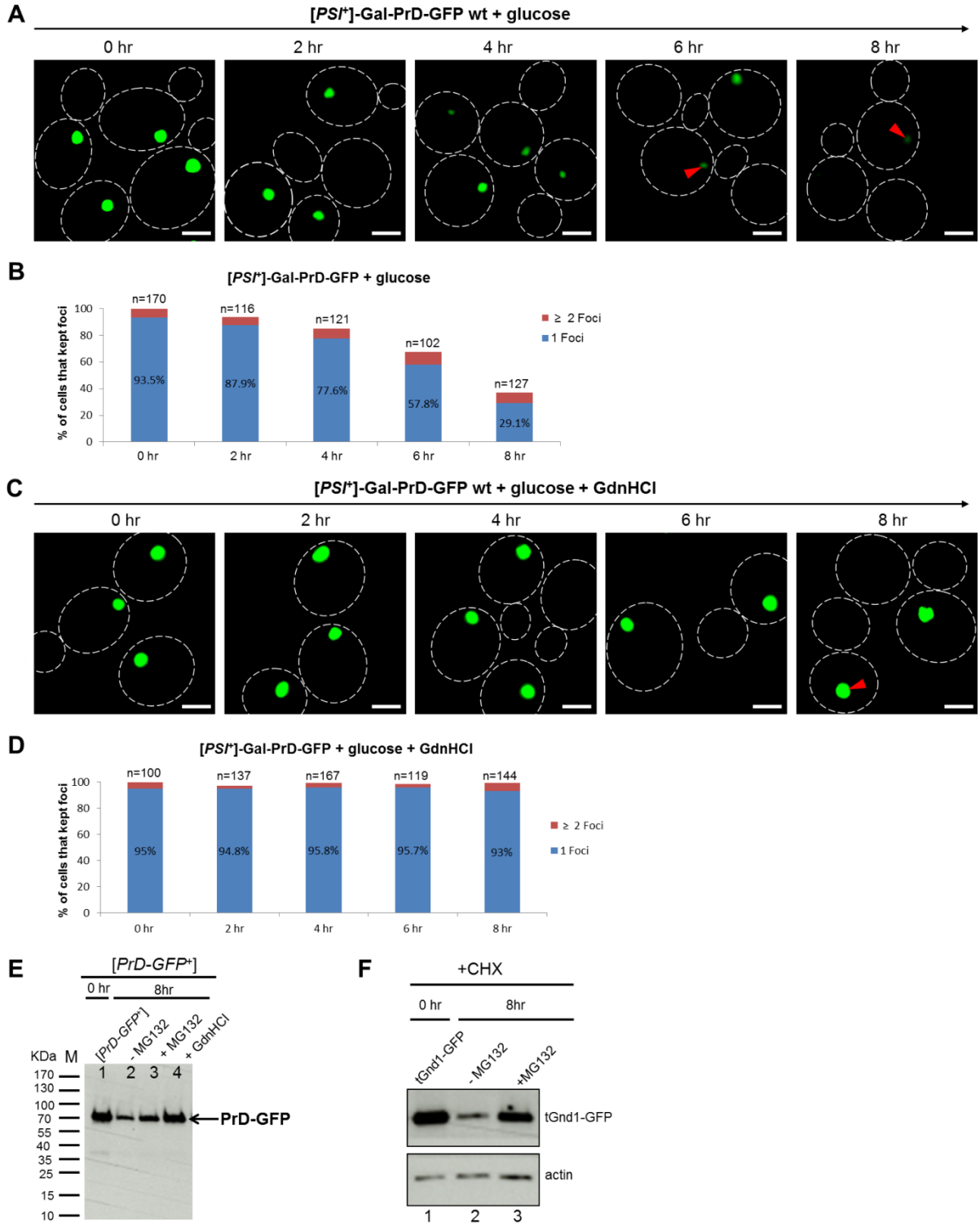

FIGURE 29: PrD-GFP is slowly extracted from the IPOD by Hsp104 and progressively decays over time – (**A**) PrD-GFP was induced with galactose for 6 hours in a [*PSI*$^+$] strain to allow for deposition of PrD-GFP at the IPOD, pelleted and resuspended in YPD for further incubation. At indicated times, aliquots were withdrawn, the OD_{600} was determined prior to fixation and fluorescence microscopy. **(B)** IPOD decay was determined for the aliquots withdrawn in (A) by plotting of the number of cells with aggregates as % of cells with aggregates originally present in the culture at the shift to YPD (compare methods for details). **(C, D)** Same experiment as in (A, B), but after PrD-GFP

induction, the cells were resuspended in YPD + 5 mM of GdnHCl (Hsp104 inhibition). **(E)** PrD-GFP IPOD was induced with galactose for 6 hours in a [*PSI*$^{+}$] Δpdr5 background strain. Subsequently, the PrD-GFP IPOD was chased with glucose for 8 h. At the indicated times, the same volume of culture was withdrawn (compare methods in section 5.4.5. for details) and analyzed by Western Blotting with an antibody against GFP. PrD-GFP levels after the glucose chase in the absence of the proteasomal inhibitor MG132 (- MG132) and in the presence of MG132 (+MG132) or GdnHCl (+ GdnHCl) were compared to those before the glucose chase at "time 0h". MG132 was refreshed/replenished every 2 hours. **(F)** A strain expressing tGnd1-GFP [103] as a substrate for proteasomal degradation (positive control for successful inhibition of the proteasome) was grown to mid-log phase and 100 µg/ml of cycloheximide (CHX) was added. At "time 0h", an aliquot for determination of the tGnd1-GFP levels by Western Blotting was withdrawn. Subsequently, the culture was split into two aliquots and was incubated further for 8 h without MG132 (- MG132) or with MG132 (+ MG132). Aliquots were withdrawn and analyzed by Western Blotting with an antibody against GFP. An anti-actin antibody served as loading control. Scale bar, 2 µm.

4

Discussion and Outlook

4.1 The involvement of vesicular transport in recruitment of amyloid aggregates to the IPOD

In this thesis, I observed that cells employ a vesicular transport system to guide aggregates to their respective deposition sites. This is novel concept because it has never been reported that aggregates can associate with transport vesicles that are moved along actin cables to get to their destination sites.

PrD-GFP amyloid aggregates and the CVT substrate preApe1 are recruited via a similar vesicular transport machinery to the adjacent sites IPOD and PAS, respectively

In this dissertation, I explored a novel cellular recruitment machinery that is involved in the recruitment of different amyloid substrates to the IPOD (*i*nsoluble *pro*tein *d*eposit) deposition site in *S. cerevisiae*. This machinery is disturbed upon impairment of components of the actin cable-based transport machinery such as Myo2, Cmd1 and Tpm1/2, but also upon impairment of SNARE function (see Fig 15 and 24). The IPOD is in close proximity to the PAS (Phagophore Assembly Site) [56, 65] where the cells initiate formation of autophagosomes and CVT (Cytoplasm-to-Vacuole Targeting) vesicles [113, 128]. The CVT pathway is destined to deliver precursor hydrolases to the vacuole. Remarkably, I found that amyloid aggregates use a similar recruitment machinery to the IPOD as CVT substrates (preApe1) for their recruitment to the PAS. This recruitment machinery for CVT substrates was known to consist of actin cables and transport vesicles that contain the transmembrane protein Atg9. Therefore, these vesicles were termed Atg9 vesicles [114]. At the PAS, the vacuolar precursor aminopeptidase 1 (preApe1) is enwrapped into the double-membrane CVT vesicles that subsequently fuse with the vacuolar membrane and release their content into the lumen. For its recruitment to the PAS, preApe1 first oligomerizes into multiple dodecamers (Ape1 complex) that forms the so called CVT complex with its receptor Atg19 and then binds to Atg9 vesicles via the adaptor Atg11 [112-114, 116, 127, 128]. These Atg9 vesicles, loaded with preApe1, move to the PAS along actin cables [114]. The actin-related protein 2/3 (Arp2/3) complex is also involved in the

transport of Atg9 vesicles to the PAS [206]. Therefore, impairment of actin cytoskeleton by genetic mutation, inhibition of actin polymerization or conditional depletion of the Arp2/3 complex blocks the recruitment of both Atg9 and preApe1 to the PAS [179, 206]. This suggested that both Atg9 and preApe1 move to the PAS in a coordinated fashion and was explained by two ways: (I) Atg9 vesicles loaded with the preApre1 precursor complexes move actively along actin cables or (II) these vesicles move to the PAS via a passive mechanism. In such a passive mechanism, the binding of Atg9 vesicles to the Arp2/3 complex can activate the Arp2/3 complex itself, which in turn induces the nucleation and elongation (synthesis) of new actin filaments. Such elongation of the actin filaments can physically push these vesicles to the PAS [114]. However, in those studies, it was unclear which factor links Atg9 vesicles to actin cables and mediates the transport of Atg9 and preApe1 to the PAS. My finding shows that depletion of Myo2 blocks recruitment of preApe1 to the PAS. This strongly supports the hypothesis that Myo2-based active movement is crucial for Atg9 vesicle transport along actin cables (see Fig 30). This is also consistent with the known role of Myo2 in the inheritance of different organelles such as vacuolar lobes and post-Golgi vesicles, which are bound to Myo2 by their specific receptors and adaptors (for example the Vac8/17 receptor/adaptor system during vacuole inheritance) and then transported from the mother to daughter cells along actin cables [207, 208]. In addition, my findings show that depletion of the SNARE chaperone Sec18 [209] also disturbs preApe1 recruitment to the PAS, consistent with the recent finding that impairment of SNARE proteins blocks the CVT pathway and recruitment of CVT structural components to the PAS [182].

The reversible failure of PrD-GFP aggregates to be recruited to the IPOD upon impairment of the Myo2-based transport machinery and the co-accumulation of PrD-GFP transport intermediates with the CVT substrate preApe1 under Myo2 depleting conditions led me to put forward the hypothesis that both amyloid aggregates and CVT substrates use a similar vesicular transport machinery for their deposition at the adjacent destination sites IPOD and PAS, respectively (Fig 30). From my current study, it remains unclear whether both substrates, PrD-GFP aggregates and preApe1, are loaded onto identical Atg9 transport vesicles or on different types of vesicles. Nevertheless, both types of substrates can be targeted to their destination sites independently of each other, e.g. PrD-GFP in the absence of preApe1 and vice versa, and both require the Myo2 motor protein to drive this transport process. I also observed that the additional IPOD substrates, Htt103Q-CFP, Rnq1-GFP and Ure2-YFP [56] were not targeted to the central IPOD upon Myo2 depletion, suggesting that the recruitment machinery is not limited to PrD-GFP, but that amyloids in general, use a Myo2-based vesicular transport machinery to be deposited at the IPOD.

I also observed that PrD-GFP transport intermediates co-localize not only with different CVT pathway components including preApe1, Atg9 and Atg8, but also with the Myo2 motor protein. Among these components, RFP-Atg8 and Myo2-3XmCherry showed stronger co-localization with PrD-GFP as compared to preApe1 and Atg9. This suggests that PrD-GFP and preApe1 may use similar, but not identical vesicles

for their recruitment to the respective sites, but co-accumulated at the same cellular location upon impairment of SNARE-mediated vesicular transport or actin-tropomyosin based transport (see Fig 30). However, differences in the degree of co-localization of PrD-GFP aggregates with the different components mentioned above must not necessarily mean a biological difference, but could potentially also be explained by technical reasons such as interference of the fluorescence protein tag added to these factors that may impair the functionality to a certain degree.

The role of the actin cytoskeleton in sorting of amyloid aggregates during asymmetric inheritance of aggregates

It has been reported by different groups that amyloid aggregates are associated with the actin cytoskeleton [210, 211]. Recently, Song and coworkers showed that Htt103Q aggregates partially co-localize with Myo2, Cmd1 and Sec18 during their asymmetric inheritance [139]. However, these aggregates were found as multiple punctate structures in the cytosol rather than at one central IPOD inclusion. It remained unclear whether these multiple punctate foci either represented transport intermediates of Htt103Q on transit to the IPOD, similar to those I observed here upon depletion of components of the actin cable-based transport machinery, or whether they represented IPOD-independent deposits. If the former was the case, it would need to be established why transport intermediates to the IPOD would accumulate and not reach the IPOD in the experimental conditions used in the study [139], because there were no particular proteins depleted that could explain the accumulation of transport intermediates.

A putative role of endosomal vesicular transport in asymmetric inheritance of heat-induced aggregates

Recently, heat-induced protein aggregates, visualized with Hsp104-GFP, were shown to be retained in the mother cells during asymmetric inheritance by "hitchhiking" on the route of ER-Golgi trafficking or late endocytosis that also employs Cmd1/Myo2/actin-based transport [139, 212]. However, from those studies, it remained unclear which transport vesicles are involved during asymmetric inheritance of aggregated proteins. Since Myo2 links Atg9 vesicles loaded with PrD-GFP aggreagtes to actin cables, it is also possible that Myo2 could link an unknown class of vesicles to the actin cytoskeleton during asymmetric inheritance of heat-induced protein aggregates. Thus, there might be a connection between asymmetric inheritance of damaged proteins [139, 146, 212] and sorting of prion aggregates to the IPOD site as both employ actin/Myo2-based vesicular transport.

Subsequently, it was shown that Vac17 is also involved in asymmetric retention of damaged/misfolded proteins in mother cells during ageing [212]. Vac17 is a vacuolar adaptor protein which is involved in vacuole inheritance by attaching vacuole vesicles

to actin cables through its interaction with Vac8 on the one hand and to Myo2 motor protein on the other hand [213]. In this study, heat-induced protein aggregates (Hsp104-GFP substrates) were further shown to be deposited near the IPOD in a Myo2/Vac17-dependent manner [212]. Later, Vac17 was found to bind with Hsp104-GFP *in vitro* in immunoprecipitation experiments, therefore the authors speculated that aggregates may hitchhike Vac17/Myo2 –based vesicular transport routes to the vacuole because of the normal role of Vac17 in actin cable-dependent vacuole inheritance [212]. Thus, these studies would confirm the novel concept that aggregate sorting can employ vesicular transport. Strikingly, however, the deletion of the VAC17 adaptor did not affect the inheritance of Huntingtin Htt103Q aggregates in this very recent study [212], suggesting that amyloids may not employ this Myo2–Vac17–Vac8 transport complex [193] during amyloid recruitment to the IPOD. This could mean that different aggregates may use different vesicular transport systems for their recruitment to the IPOD or IPOD adjacent sites, but these issues need to be studied in more detail to allow for conclusive statements. It would indeed be very interesting to test the effect of the proteins found in the study (Vac17, Vac8, Vps1 etc) [212] with my substrates on the one hand, and depletion of Myo2, Sec18 and Sec14 with their aggregate markers on the other hand.

SNARE proteins function is required for vesicle-based transport of PrD-GFP aggregates to the IPOD

I found evidence that PrD-GFP aggregates, during their sorting to the IPOD, are associated with Atg9-containing vesicles (see Fig23), which are also known to transport the CVT substrate, preApe1, to the PAS along actin cables [114] (see Fig7). Atg9 is a multispanning transmembrane protein which exists on small cytoplasmic vesicles termed as Atg9 vesicles [181]. Trafficking of these Atg9 vesicles from peripheral sites to the PAS requires several SNARE proteins such as Sso1/2, Sec9, Tlg2, Ykt6 and Sec22. A role for the Sec18 SNARE chaperone in Atg9 vesicular trafficking was also suggested [182]. Remarkably, I fished Sec18, a SNARE disassembly chaperone to bind with PrD fibers *in vitro* (see Fig13), which was found further to be involved in PrD-GFP recruitment to the IPOD (see Fig24C). Therefore, Atg9 and Sec18 SNARE-mediated vesicular transport machinery is crucial for sorting both substrates, PrD-GFP aggregates and preApe1to their adjacent deposition sites, IPOD and PAS, respectively. However, the mechanism by which these SNAREs are involved in the sorting of PrD-GFP aggregates to the IPOD needs to be further investigated.

Role of Sec14 and Sec21 in sorting PrD-GFP aggregates to the IPOD

Next to the likely involvement of the Atg9 vesicular trafficking machinery in the sorting of PrD-GFP to the IPOD, additional proteins involved in various steps of vesicular transport processes were identified to bind to immobilized PrD-GFP (see Fig13).

Among those, I found Sec14 and Sec21 that are involved in the formation of Golgi-derived vesicles and their further trafficking steps [214-216]. Interestingly, the depletion of Sec14 and Sec21 also interfered with PrD-GFP sorting to the IPOD similar to the depletion of Myo2 (see Fig24). Sec14 is a phosphatidylinositol/ phosphatidylcholine (PI/PC) transfer protein which associates preferentially to Golgi membranes. It transfers phosphatidylinositol (PI) lipid from the ER to the Golgi complex, where PI is phosphorylated to form phosphatidylinositol-4-phosphate (PI4P) by the PI4P kinase, Pik1 [186, 217, 218]. It has been shown that the pool of PI4P lipids generated by Pik1 regulates the formation of Golgi-derived secretory vesicles and the subsequent transport of these vesicles to their destination sites after their exit/release from the Golgi [218]. Therefore, when Sec14 or Pik1 function is abolished, the amount of PI4P is reduced. This eventually blocks *de novo* formation of Golgi-derived secretory vesicles and downstream vesicular transport pathways. Remarkably, Atg9 vesicles that have also been shown to serve as membrane supplier for the autophagosomes/CVT vesicles [219, 220] are also derived from the Golgi apparatus [219]. In line with this, it was shown that inactivation of Pik1 at the nonpermissive temperature (which reduces the level of PI4P) blocks the formation of Atg9 vesicles from the Golgi [186]. Therefore, such impairment in the Pik1 function also blocks the autophagy/CVT pathway indirectly because the generation of Golgi-derived Atg9 vesicles and their movement to the PAS is reduced [186]. Since, Sec14 functions upstream of Pik1 in the formation of PI4P lipids [217, 218], it might be possible that Sec14 function is also crucial for releasing of Atg9 vesicles from the Golgi similar to Pik1 [186]. This would plausibly explain why PrD-GFP aggregates are not recruited to the IPOD in the absence of Sec14.

Besides the role of PI4P lipids on the formation of Golgi-derived Atg9 transport vesicles [186], PI4P also serves as a substrate for the PIP5-kinase Mss4 to generate $PI(4,5)P_2$ lipids, which are required for the proper organization of the actin cytoskeleton [221]. In agreement with, it was shown that impaired production of PI4P in pik1-101 mutant cells at the permissive temperature results in less $PI(4,5)P_2$ generation, which causes the disruption (depolarization) of actin cables [222]. Therefore, upon Sec14 depletion, PI is not transported properly to Pik1 kinase for the generation of PI4P which then eventually reduces the levels of $PI(4,5)P_2$ lipids and could affect the organization of the actin cytoskeleton. This could also account for the effect of Sec14 depletion on the recruitment of PrD-GFP to the IPOD. Taken together, since PrD-GFP aggregates are recruited to the PAS via Atg9 transport vesicles along actin cables, impaired function of Sec14 would disturb the sorting of PrD-GFP aggregates to the IPOD by two different mechanisms, both of which would fit in my proposed model (see Fig 30). Future studies are required to further confirm the possible involvement of these two mechanisms that are linked to a Sec14-mediated recruitment of prion aggregates to the IOPD.

Sec21, a COPI coatomer protein was found to associate with Vid (vacuole import and degradation) vesicles to deliver inactive fructose-1,6-bisphosphatase (FBPase) into the vacuole for its degradation by autophagy [188]. Depletion of Sec21 also gave a

multiple PrD-GFP foci phenotype compared to Sec18 or Myo2 depletion, highlighting again that vesicular trafficking is crucial for amyloid recruitment to the IPOD. However, it needs to be further determined whether this effect of depletion of Sec21 on PrD-GFP delivery to the IPOD is a direct effect or a more indirect consequence of impairment of upstream vesicular transport processes.

4.2. Tethering of prion aggregates to the CVT vesicular transport machinery

My study shed light onto a novel cellular mechanism that is involved in the recruitment of prion aggregates to the IPOD along actin cables. However, there are still key questions remaining, for example how prion aggregates are attached to the Atg9 transport vesicles e.g. what the linking factor is (receptor/adaptor)? Deletion of receptor for preApe1, Atg19 [127, 128], did not affect the targeting of PrD-GFP to the central IPOD, suggesting PrD-GFP is not recognized by the same receptor as preApe1, but may require other receptor(s) for its binding to Atg9 vesicles (Fig 30).
In summary, however, this study nicely confirms the novel principle I discovered here, which is that protein aggregates can employ a vesicular transport machinery to be recruited to distinct deposition sites.

Tethering of prion aggregates to Atg9 vesicles

The short-lived and stress-induced protein Lsb2 was shown previously to associate with prion aggregates and to link them to the actin cytoskeleton during prion induction [211]. Lsb2 is a low abundant protein whose levels are increased in response to environmental stress such as heat shock, and such increased levels of Lsb2 facilitate *de novo* induction of the [*PSI*$^+$] and [*PIN*$^+$]/[*RNQ*$^+$] prions[211]. After heat shock, overproduced Lsb2 binds to soluble Sup35 protein and triggers [*PSI*$^+$] prion induction (Sup35 prion fibrillization) and subsequent association of corresponding prion aggregates at the cortical actin cytoskeleton. Therefore, Lsb2 seems to have a tethering function during *de novo* formation of [*PSI*$^+$] by linking misfolded Sup35 molecules to the actin cytoskeleton [211]. Although I cannot exclude a possible involvement of Lsb2 in tethering of PrD-GFP aggregates to the Atg9 vesicle based transport machinery and/or actin cables, I consider this to be less likely because my experiments were performed under non-stress conditions where Lsb2 levels should be low. In line with this, deletion of Lsb2 did not cause any effect on the IPOD formation (unpublished results from the Tyedmers Lab), also arguing against an essential role of Lsb2 in tethering of PrD-GFP aggregates to the Atg9 vesicles.

Hsp104, an aggregate-remodeling and prion maintenance factor was shown to bind to heat-induced aggregates and to link these aggregates to actin cables during

asymmetric inheritance [141]. Hsp104 was also shown to associate with different amyloids/prions such as Sup35p PrD, Mot3 and Lsm4 [65, 203]. If Hsp104 was crucial for tethering the PrD-GFP transport intermediates to the actin cytoskeleton on transit to the IPOD, then inhibition of Hsp104 in cells harboring prion aggregates should impair proper sorting of prion aggregates to the IPOD. However, it was found that the IPOD was even increased in size upon inhibition of Hsp104 [203] rather than leading to multiple foci formation as I observed it here when the recruitment machinery was impaired. This suggests that Hsp104 is not crucial for tethering prion aggregates to the actin cytoskeleton during proper sorting of prion amyloids to the IPOD via the novel recruitment machinery discovered here. Thus the sorting of prion aggregates to the IPOD observed here, and the retention of aggregated proteins in mother cells during asymmetric inheritance, may employ different tethering mechanisms.

An alternative mechanism of prion tethering could be mediated by direct binding of prions to the components of the Atg9-based vesicular transport machinery. Such direct binding of prion aggregates to components of the vesicular recruitment machinery discovered here seems possible when I consider that components of the endocytosis machinery (e.g. Sla1, Sla2, Pan1, Las17, Apl1, Apl3, Hof1 etc) are also involved in initiation of polyQ aggregation [223]. Furthermore, two endocytic components, Sla1 and Sla2 were shown previously to be involved in organizing and handling of [*PSI*$^{+}$] aggregates [168, 169]. Sla1 and Sla2 are actin-binding proteins that act as adaptors and link endocytic vesicles to the cortical actin cytoskeleton during endocytosis [224, 225]. Interestingly, I also found Sla2 to bind with PrD fibers on the column during my fishing approach (see Fig13). Therefore, the role of Sla1/2 and their interactions with amyloids needs to be studied in more detail to reveal whether they might be involved in sorting prion aggregates to the IPOD.

Lastly, mature amyloids and prefibrillar oligomers have an intrinsic affinity for direct binding to lipid membranes [226]. This provides another alternative possibility for direct tethering of PrD-GFP aggregates to lipids present in the Atg9 transport vesicles. However, in such a case, it would need to be established how specificity to Atg9 vesicles, but not other types of membranes, is established.

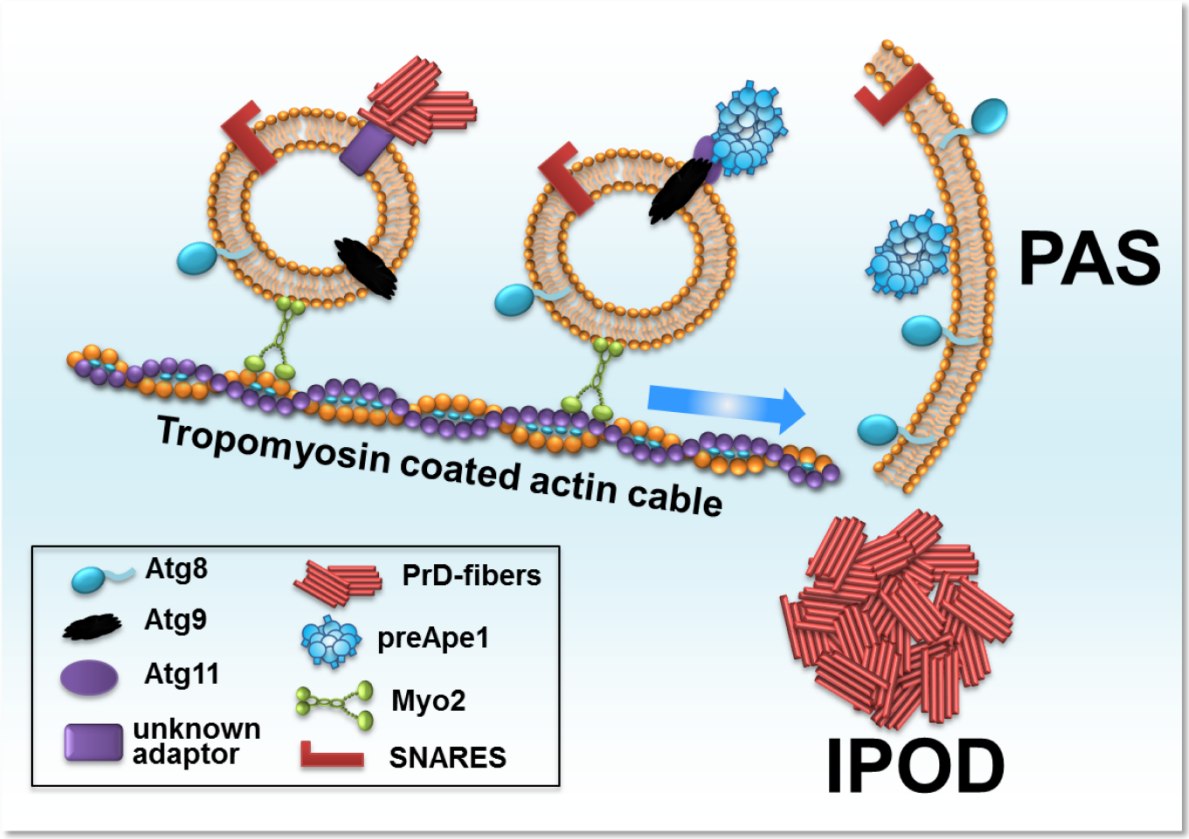

FIGURE 30: A model for the recruitment of PrD-GFP prion aggregates to the IPOD amyloid deposition site in yeast – PrD-GFP prion aggregates are recruited via an unknown receptor/adaptor to Atg9 transport vesicles which also target the CVT complex consisting of preApe1 and its receptor Atg19 via its adaptor Atg11 to the Phagophore Assembly Site (PAS). PrD-GFP and preApe1 as cargo molecules are loaded on Atg9 vesicles and then transported via Myo2 and tropomyosin-coated actin cable-based transport to their adjacent destination sites, IPOD and PAS respectively. Moy2 links these Atg9 vesicles to the actin cytoskeleton.

4.3. PrD-GFP is turned over after extraction from the IPOD by the Hsp104 based disaggregation machinery

I observed that PrD-GFP and CVT substrate preApe1 both use a similar vesicular transport machinery for their recruitment to the respective adjacent destination sites IPOD and PAS, respectively. At the PAS, the preApe1 substrate is enwrapped by double-membrane vesicle to form CVT vesicles which subsequently transport preApe1 into the vacuolar lumen for its maturation [127]. This raised the question if PrD-GFP is also deposited for the same purpose i.e. the packaging into double-

membrane autophagosomes for their autophagic degradation. This would parallel the autophagic turnover of aggresomes observed in mammalian cells where aggresomes are enwrapped into autophagosomes and fuse with lysosomes for their proteolytic degradation [122]. Remarkably, I did not find any positive evidence for bulk turnover by autophagy when PrD-GFP was overexpressed under control of the rather strong GPD or Gal promoters under normal, non-starvation conditions. This is consistent with previous electron microscopy studies where [*PSI*$^{+}$] aggregates at the IPOD were never found associated with any (autophagosomal) membrane [65, 167, 227], suggesting that PrD-GFP aggregates are not packaged into autophagosomes at the PAS adjacent IPOD for their possible turnover by autophagy under these conditions, at least not to a significant extend that would become visible in electron microscopic images [65, 167, 227] or changes in PrD-GFP protein levels.

If the accumulation of PrD-GFP at the IPOD did not primarily serve the purpose of subjecting the aggregates to autophagic turnover, then another reason for PrD-GFP accumulation at the IPOD could be temporary storage of excess PrD-GFP when the capacity of downstream proteolytic machineries (UPS, autophagy, others?) involved in PrD-GFP degradation is not sufficient (Fig 31). This allows amyloid aggregates to be sequestered temporally at the IPOD to avoid possible harmful effects in the cytosol [228] until the Hsp104 disaggregase and downstream degradation machineries are available. This is consistent with a recent finding showing that the IPOD serves as an intermediate compartment where large molecular weight molecules such as inactive proteasomes [155] are deposited temporally before they are finally processed. After accumulation at the IPOD, amyloid aggregates can be extracted slowly by the Hsp104 disaggregation machinery and might afterwards be subjected to proteolysis by either the proteasome [71], autophagy [205] or other unknown degradation pathways. Therefore, revealing the fate of different amyloid substrates at the IPOD and the possible involvement of unknown degradation pathway (s) in this process could explain their deposition purpose at the IPOD site. Besides this, deposition of amyloid aggregates at the IPOD was also suggested to facilitate asymmetric aggregate inheritance [56, 65, 145, 146, 211].

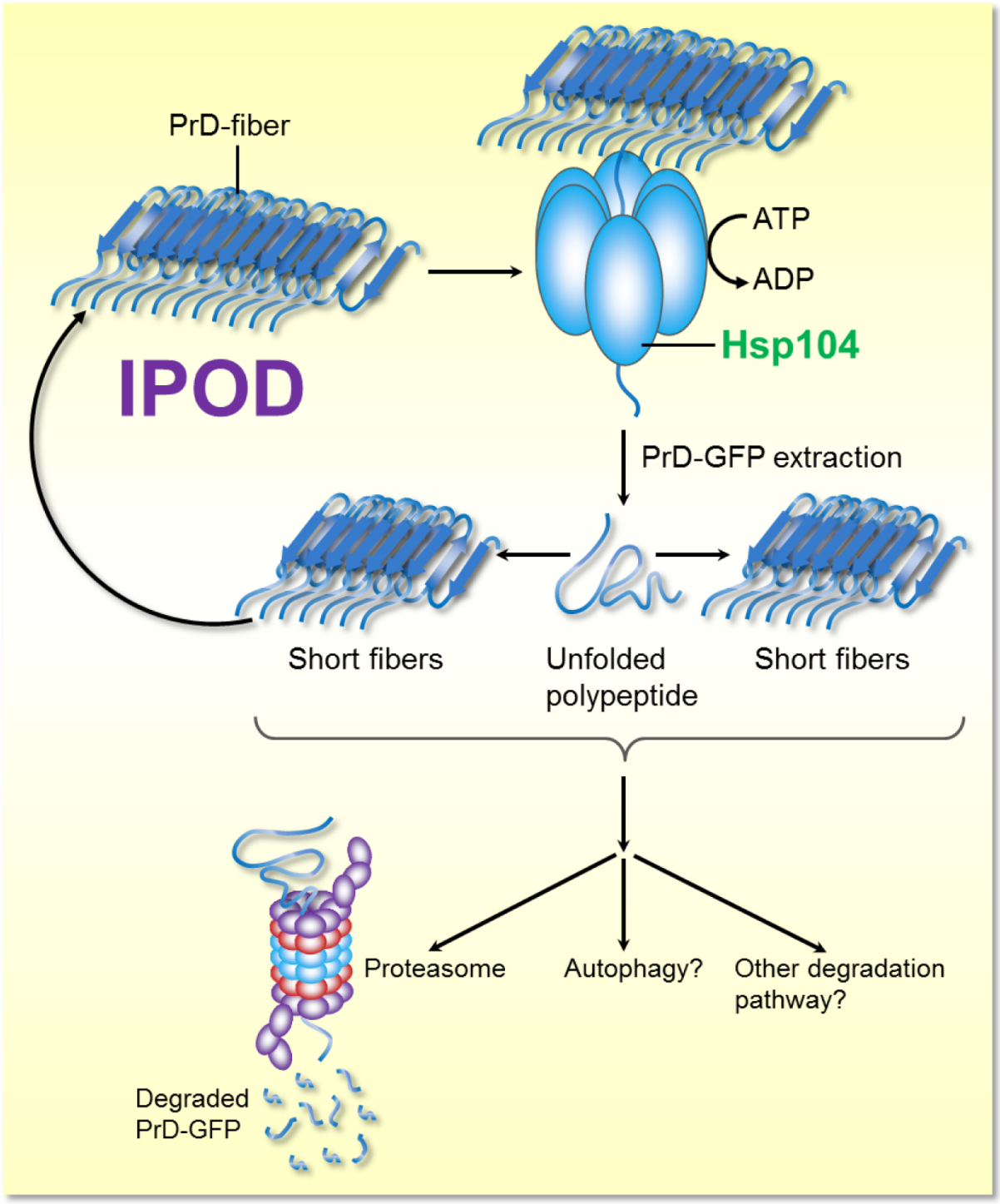

FIGURE 31: A model for the possible fate of PrD-GFP amyloids deposited at the IPOD deposition site in yeast – PrD-GFP fibers after accumulation at the IPOD are extracted slowly by Hsp104 threading activity. This extraction leads to prion fragmentation and results in small pieces of PrD fibers or single unfolded PrD-GFP molecules, which are subsequently subjected to proteolysis by either the proteasome [71] or autophagy and/or other cellular degradation pathways. Short PrD-GFP fiber fragments can also act as seeds and grow to longer PrD-GFP fibers by addition of soluble PrD-GFP molecules to their ends.

Outlook

In summary, I showed that prion aggregates are targeted to the IPOD via Atg9 vesicles along tropomyosin-coated actin cables and the Myo2 motor protein. I could further reveal that this is also true for preApe1 sorting to the PAS. However, it is not completely clear how PrD-GFP and other bona fide IPOD substrates are associated with such vesicles. Do these prions directly bind to Atg9 vesicles or do they require a specific receptor/adaptor system? Therefore, revealing a linking factor between Atg9 transport vesicles and different IPOD substrates will shed light on this recruitment machinery and will help to answer the question whether it is driven directly or indirectly. Moreover, direct visualization of PrD-GFP foci with Atg9 vesicles in Myo2/Sec18 depleting conditions with Correlative Light and Electron Microscopy (CLEM) will support the current model. To identify an unknown linking factor (s), any suitable approach can be applied, such as: (I) Testing deletion of known vesicle/PAS components on co-localization of PrD-GFP with PAS marker or (II) Pull-down/Co-immunoprecipitation of both structures (HA-tagged Atg9 and PrD-GFP) in Myo2/Sec18 depleting conditions and finally perform a Mass Spectrometry Analysis. Subsequently, depletion of the identified putative linking factor (s) has to reveal if this disturbs the association of PrD-GFP with a PAS marker or Atg9 *in vivo* using fluorescence microscopy and/or CLEM.

Sec18 SNARE chaperone -mediated vesicular transport and fusion is also required for PrD-GFP sorting to the IPOD (compare section 3.2.10). In the future, the detailed molecular composition of the transport vesicles and the identity of the involved SNARE proteins (chaperoned by Sec18) have to be revealed. Such study could explain why the endocytosis machinery of ER-to-Golgi trafficking can participate in the recruitment of amyloids to the IPOD similar to their role in autophagy [182].

The IPOD is directly adjacent to the PAS where the cells initiate formation of CVT vesicles and autophagosomes [56, 65]. This raised a question if the presence of the PrD-GFP amyloids at IPOD interfere the autophagy or CVT pathway? Since amyloids are large complex structures, they could potentially inhibit many different autophagic processes due to its adjacent localization to the PAS. Therefore, future studies could to reveal the impact of an IPOD on autophagic flux or the turnover of different autophagic substrates such as defect mitochondria, peroxidomes, bulk cytoplasm, amongst others. This can be achieved by (I) looking whether mCherry-Atg8 (or mCherry-tagged autophagic substrates) still enter into the vacuole for autophagic turnover upon autophagy induction by starvation/spermidine to the same degree when a PrD-GFP IPOD is present in the cells or not, or (II) monitoring HA/MYC-Atg8 processing in cells with or without a PrD-GFP IPOD upon autophagy induction. An Ape1 processing assay can be monitored with similar conditions to see if the presence of an IPOD affects the CVT pathway. In addition, the biological significance of the PAS on the formation and fate of the IPOD is also not known. Therefore, if it is possible, the impact of abolishing PAS formation on IPOD formation should be studied.

5

Material and Methods

5.1. Materials

5.1.1. Software and Equipment

Computer Software

Image J	National Institutes of Health
Office 2010	Microsoft Corp.
SnapGene	GSL Biotech
Inkscape	Scalable Vector Graphics (SVG)
Excellence	Olympus Soft Imaging Solutions
Adobe Acrobat	Adobe Systems Inc.
Excel	Adobe Systems Inc.

Equipment

Agarose gel chambers and trays	University Hospital workshop
Balances	Mettler
Gel documentation system	Biometra GmbH
Centrifuges	Heraeus
Glass ware	Schott
Incubators	Forma Thermo Scientific
Water bath MaxQ 7000	Dinkelberg analytics
Power supply	Perkin-Elmer?, University Hospital workshop
SDS gel chambers	Biorad
Vortex mixer	Heidolph
Western blot chambers, semi-dry	Biorad
Magnetic stirrer MR 3001 K	Heidolph
pH meter	Werner Hassa GmbH
Spectrophotometer	Eppendorf
T-Gradient Thermocycler	Biometra GmbH

Mixer mill MM 400	Retsch
French press	Sim-Aminco/Bukau lab

Microscopes

Olympus CellR-PointFRAP IX81	ZMBH Imaging Facility
Olympus CellR-PointFRAP IX81	Bukau lab

Olympus xcellence PointFRAP IX81 microscope

Microscope stand	Olympus IX81, inverted microscope, motorized stage
Objectives	PlanC N 10x/0.25 UPlanSApo 20x/0.75 UPlanSApo 40x/0.95 UPlanFL N 60x/0.90 Apo N 60x/1.49 Oil UApo N 100x/1.49 Oil
Fluorescence Lamp	MT 20 illumination system with 150 W Xe or 150 W Hg/Xe arc burner
Excitation Filters	387nm/11 , 427nm/10, 470nm/40, 485nm/20, 504nm/12, 560nm/25, 572nm/35, 650nm/13
Emission Filters	Dualband CFP/YFP sbx HC filter set, Dualband GFP/mCherry sbx ET filter set, Quadband DAPI/FITC/Cy3/Cy5 sbx HC filter set
Camera	EM-CCD C9100-02 (Hamamatsu)
Software	xcellence (Olympus)
Temperature control	Incubation Chamber (ZMBH Wor kshop) tempcontrol 37-2 digital and heating unit (Pecon)
Custom made heat shock stage (Olympus)	Peltier element (BelektroniG) combined with water cooling device (innovatek), Control Unit: HAT-control B-20 and Software (BelektroniG)

5.1.2. Expendable items

Cover slides	Thermo Scientific Inc.
Cover slips, 20 x 20 mm	Menzel-Gläser (Thermo Scientific Inc.)
Cuvettes	Sarstedt AG & Co.
Falcon tubes 15, 50 ml	Greiner
Petri dishes	Greiner
Microcentrifuge tubes, 1.5 ml, 2 ml	Sarstedt AG & Co.
Low protein binding microcentrifuge tubes, 1.5 ml	Eppendorf
PCR tubes, 200 µl	Kisker Biotech GmbH & Co.
PVDF membrane	Millipore
Sterile filters, 0.2 µM	GE Healthcare
Whatman paper, 3 mm	Schleicher & Schuell
Amicon Concentrators	Millipore
Costar 96-well plate	Greiner
100 Mesh copper grids (formvar/carbon coated)	Electron Microscopy Sciences

5.1.3. Chemicals

If not mentioned differently, all chemicals were purchased from Roth, Sigma-Aldrich, Invitrogen, AppliChem or Merck.

Enzymes and protease inhibitors

Aprotinin	AppliChem
DNase I	AppliChem
Pepstatin A	Pepta Nova GmbH
Leupeptin	Peptide Institute, Inc.
Phenylmethylsulfonyl Fluoride (PMSF)	Sigma-Aldrich Co.
MyFi OptiTaq DNA Polymerase	Bioline
My Taq Red DNA polymerase	Bioline
Restr iction Enzymes	NEB, Thermo Scientific Inc., Promega
Zymolyase 100T	Amsbio

Standards and Kits

Bio-Rad Protein Assay Dye Reagent Concentrate (5 x Bradford reagent)	Bio-Rad Laboratories, Inc.
peqGOLD Plasmid Miniprep Kit	PEQLAB
QIAquick Gel Extraction Kit	QIAGEN GmbH
GeneRuler 1 kb DNA Ladder (#SM1163)	Thermo Scientific Inc.
PageRuler Prestained Protein Ladder (# 26616)	Thermo Scientific Inc

Components for Media

Bacto™Agar	Becton, Dickinson and Company
Bacto™Peptone	Becton, Dickinson and Company
Bacto™Tryptone	Becton, Dickinson and Company
Bacto™Yeast extract	Becton, Dickinson and Company
Difco™Yeast Nitrogen Base w/o amino acids and ammonium sulfate	Becton, Dickinson and Company
Complete Supplement Mixture (CSM) (- amino acids for drop out media)	MP Biomedicals, LLC

Antibiotics

All listed concentrations are the final concentrations. Stock solutions were filter sterilized.

Ampicillin (Amp)	100 µg/ml	Sigma-Aldrich Co.
Chloramphenicol	25 µg/ml	Sigma-Aldrich Co.

Cycloheximide (CHX)	100 µg/ml	Serva Electrophoresis GmbH
Hygromycin B (Hyg)	250 µg/ml	InvivoGen
Geneticin (G418)	200 µg/ml	Sigma-Aldr ich Co.
Nourseothr icin (clonNAT)	200 µg/ml	Werner BioAgents

Other Chemicals and Reagents

Bromphenol Blue	Sigma-Aldrich Co.
ECF Substrate	GE Healthcare Life Sciences
MG132 (Z-Leu-Leu-Leu-al)	Peptide Institute, Inc
Yeastmaker™ Carrier DNA	Clonetech Laboratories, Inc.
Guanidine hydrochloride	Sigma-Aldrich Co.
Spermidine	Sigma-Aldrich Co.
Indole-3-acetic acid sodium salt (auxin)	Sigma-Aldrich Co.
Paraformaldehyde (PFA)	Sigma-Aldrich Co.
Agarose	Sigma-Aldrich Co.
D (+)-Biotin	Roth
IPTG	Thermo Scientific Inc.
Ni-NTA His-Bind Resin (# 70666)	Millipore
hyBeads Streptavidin Beads (#311092)	Hyglos GmbH

5.1.4. Media and Buffers

All media were sterilized by filtration or autoclaving prior to usage. For the preparation of solid agar plates, 2% (w/v) autoclaved agar was added to the medium prior to pouring plates.

LB (Luria-Bertani) medium

10g/l tryptone

5 g/l yeast extract

10 g/l NaCl

TB (Terrific Broth) medium

12g/l tryptone

24 g/l yeast extract

16.4g/l potassium phosphate, dibasic

2.3g/l potassium phosphate, monobasic

4ml/l glycerol

YPD/YPG	20 g/l peptone 10 g/l yeast extract 20 g/l D-Glucose/Galactose
SD (Synthetic Dropout) medium	1.7 g/l Yeast Nitrogen Base w/o amino acids and ammonium sulfate 0.7 g/l CSM mix (according to desired dropout) 5 g/l ammonium sulfate or 1 g/l glutamate 2% (v/v) desired sugar, added post sterilization
PBS and PBST	137 mM NaCl 2.7 mM KCl 10 mM Na_2HPO4 2 mM NaH_2PO4 pH was adjusted to 7.4 with HCl for PBST, 0.25% (v/v) Tween-20 was added

5.1.5. Plasmids, Strains, Primers and Antibodies

TABLE 1.: Plasmids used in this study

Name	Characteristic Features	Source/Reference
pH10-Sumo-PrD-TEV-Avi	AmpR	This study/Tyedmers lab
pHis-Sumo-PrD-STOP	AmpR	This study/Tyedmers lab
pRS413-mCherry-Atg8	AmpR; HIS3	Nava Segev lab
pRS414-RFP-Atg8	AmpR; TRP1	Daniel Klionsky lab
pRS303-Ape1-mCherry	AmpR; HIS3	Yoshinori Ohsumi lab
pRS416-GFP-Atg8	AmpR; URA3	Daniel Klionsky lab
pBS35	AmpR; hphNT1	The Yeast Resource Center
pFA6a-kanMX4	AmpR; kanMX4	[229]
pFA6a-hphNT1	AmpR; hphNT1	Michael Knop lab [230]
pFA6a-natNT2	AmpR; natNT2	Michael Knop lab [230]
pYM-N17	AmpR; hphNT1	Michael Knop lab [230]
pNHK53	AmpR; URA3	[172]

pMK43_HA	AmpR; kanMX4	[172]
pMaM144 (3 x mCherry)	AmpR; hphNT1	Micheal Knop lab
pRS305 Gal RNQ1-GFP::LEU2	AmpR; LEU2	Bernd Bukau lab
pRS305 Gal URE2-YFP::LEU2	AmpR; LEU2	Bernd Bukau lab
pRS304 Gal 103Q-CFP::TRP1	AmpR; TRP1	Bernd Bukau lab
pYM25	AmpR; yeGFP; hphNT1	Michael Knop lab [230]

Yeast strains

All strains used in this study are derivatives of 74D-694 (MAT**a** ade1-14 his3 leu2 trp1 ura3 [*PSI*$^{+}$] or [psi^{-}]) [198] that express integrated PrD-GFP under a galactose-inducible promoter [49] (termed 74D [*PSI*$^{+}$]-Gal-PrD-GFP) or under a constitutive GPD promoter with a deletion of endogenous SUP35-PrD locus [65] (termed 74D-GPD-PrD-GFP). Yeast strains with additional genetics manipulations are shown in Table 2.

TABLE 2.: Strains used in this study

Name	Genotype	Source/Reference
RK1	74D-694-[*PSI*$^{+}$]-Gal-PrD-GFP::LEU2	[65]
RK1a	RK1 tpm1Δ::natNT2	This study
RK1b	RK1a-OsTIR1::URA3	This study
RK1c	RK1b-TPM2-AID ::*kanMX4*	This study
RK1d	RK1-OsTIR1::URA3	This study
RK1e	RK1d-MYO2-AID::kanMX4	This study
RK1f	RK1d-CMD1-AID::kanMX4	This study
RK1g	RK1d-SEC18-AID::kanMX4	This study
RK1 atg9Δ	RK1 atg9::hphNT1	This study
RK1 atg11Δ	RK1 atg11::natNT2	This study
RK1 atg19Δ	RK1 atg19:natNT2	This study
RK1 ape1Δ	RK1 ape1::kanMX4	This study
RK1 ams1Δ	RK1 ams1::kanMX4	This study
RK1e + pRFP-ATG8	RK1e + pRS414 RFP-ATG8	This study
RK1e APE1-mCh	RK1e-303 APE1-mCh::HIS3	This study
RK1e ATG9-3xmCh	RK1e-ATG9-3xmCh::hph NT1	This study
RK1g + pmCh-ATG8	RK1g + pRS413 mCh-ATG8	This study
RK1g MYO2-3xmCh	RK1g-MYO2-3xmCh::hph NT1	This study
RK2	74D-694-[*psi*$^{-}$]-Gal-PrD-GFP::LEU2	[65]
RK2a	RK2-OsTIR1::URA3	This study
RK1b	RK2a-MYO2-AID::kanMX4	This study

RK1c	RK2a-CMD1-AID::kanMX4	This study
RK3	74D-694-ΔPrD (SUP35) [*PrD-GFP*$^{+}$]::TRP1	[65]
RK3 TPM1-mCh	RK3-TPM1-mCh::hphNT1	This study
RK3 TPM2-mCh	RK3-TPM2-mCh::hphNT1	This study
RK3 SSA1-mCh	RK3- SSA1-mCh::hphNT1	This study
RK3 PUB1-mCh	RK3-PUB1-mCh::hphNT1	This study
RK3 PAB1-mCh	RK3-PAB1-mCh::hphNT1	This study
RK3 atg1Δ	RK3 atg1Δ::natNT2	This study
RK3 atg6Δ	RK3 atg6Δ::natNT2	This study
RK3 atg7Δ	RK3 atg7Δ::natNT2	This study
RK3 atg8Δ	RK3 atg8Δ::natNT2	This study
RK3 atg14Δ	RK3 atg14Δ::natNT2	This study
RK3 atg16Δ	RK3 atg16Δ::natNT2	This study
RK3 pep4Δ	RK3 pep4Δ::natNT2	This study
RK4	74D-694-ΔPrD (SUP35) [*prd-gfp*$^{-}$]::TRP1	[65]
RK4 pep4Δ	RK4 pep4Δ::natNT2	This study
74D	74D-694-[*PSI*$^{+}$]	[198]
RK5a	74D-OsTIR1::URA3	This study
RK5b	RK5a-MYO2-AID::kanMX4	This study
RK5c	RK5b-GFP-preApe1::natNT2	This study
RK5d	RK5b-GFP-ATG8::natNT2	This study
RK5e	RK5a-SEC18-AID::kanMX4	This study
RK5f	RK5e-GFP-ATG8::natNT2	This study
RK5b Rnq1-GFP	RK5b-305 Gal RNQ1-GFP::LEU2	This study
RK5b Ure2-YFP	RK5b-305 Gal URE2-YFP::LEU2	This study
RK5b 103Q-CFP	RK5b-304 Gal 103Q-CFP::TRP1	This study
RK6	74D-305 Gal RNQ1-GFP::LEU2	This study
RK7	74D-305 Gal URE2-YFP::LEU2	This study
RK8	74D-304 Gal 103Q-CFP::TRP1	This study
RK1h	RK1d-SEC14-AID::kanMX4	This study
RK1i	RK1d-SEC21-AID::kanMX4	This study
RK1j	RK1d-SEC53-AID::kanMX4	This study
tGnd1-GFP	BY4741-tGnd1-GFP:: natNT2 Δprd5 ::kanMX4	[103]
RK1 Δprd5	74D-694-[*PSI*$^{+}$]-Gal-PrD-GFP::LEU2 Δprd5::hph NT1	This study
RK9	RK5b-304 Gal 103Q-CFP::TRP1-305 Gal URE2-YFP::LEU2	This study

TABLE 3.: Primers used in this study

Name	Sequence	Source
pH10-Sumo_P1	GTGAGCGGATAACAATTCCCCTC	J. Tyedmers
pH10-Sumo_P2	CCTTGGTTTGAATCCGACATaccaccaatctgttctctgtgagcctcaataatatcg	J. Tyedmers
PrD-GFP_P3	gaggctcacagagaacagattggtggtATGTCGGATTCAAACCAAGGCAACAATC	J. Tyedmers
PrD-GFP_P4	ggtacccgGGATCCATCGTTAACAACTTCGTCATCC	J. Tyedmers
F_Ssa1_mCherry	CCTCCAGCTCCAGAGGCTGAAGGTCCAACCGTTGAAGAAGTTGATggtcgacggatccccgg	
R_Ssa1_mCherry	CATTAAAAGACATTTTCGTTATTATCAATTGCCGCACCAATTGGCatcgatgaattcgagctcg	
Ssa1_Check_ORF	CGATGTCGACTCTAACGG	
F_Tpm1_mCherry	GCAAAGAAGGAACTGGACGAAATTGCTGCATCTCTGGAAAACTTGggtcgacggatccccgg	
R_Tpm1_mCherry	CAGCGTGTTGGGGAAAAGAAAAAGAAAACAAAAAACAAAAGTAGAatcgatgaattcgagctcg	
Tpm1_Check_ORF	GCAATTGTCCGAGGACTCTC	
F_Tpm2_mCherry	GCTCAAAAAGAATTGGACGAAATTGCTAATTCATTGGAAAATTTAggtcgacggatccccggg	
R_Tpm2_mCherry	GTTTGTCGTTTGTATCTTCCGTAATTTTAGTCTTATCAATGGGAAatcgatgaattcgagctcg	
Tpm2_Check_ORF	CTCGACAGTGAAGTGGAGAAG	
F_Pub1_mCherry	ATGTCTGAGCAACAACAGCAACAGCAGCAACAGCAGCAACAACAAggtcgacggatccccgg	
R_Pub1_mCherry	TCTTTATTCTTTCTTTTTGTTTCATTCCACTTTTCTTCATAATATatcgatgaattcgagctcg	
Pub1_Check_ORF	CCGCACTTTGCCACTGAAGC	
F_Pab1_mCherry	TATGAGTCTTTCAAAAAGGAGCAAGAACAACAAACTGAGCAAGCTGGTCGACGGATCCCCGGG	
R_Pab1_mCherry	GATGATAAGTTTGTTGAGTAGGGAAGTAGGTGATTACATAGAGCAATCGATGAATTCGAGCTCG	
Pab1_Check_ORF	CGGCATGCCACCTCAATTTAG	
Tpm1_F_upstr	CATTGCTGTCATTCACTAATG	
Tpm1_R_downstr	CAGGCACAAGTGTGAGTCC	
F_Tpm2_aid_Fusion	GCTCAAAAAGAATTGGACGAAATTGCTAATTCATTGGAAAATTTAcgtacgctgcaggtcgac	
R_Tpm2_aid_Fusion	GTTTGTCGTTTGTATCTTCCGTAATTTTAGTCTTATCAATGGGAA	
F_Cmd1_aid_Fusion	TCAGGCGAGATCAACATTCAACAATTCGCTGCTTTGTTATCTAAAcgtacgctgcaggtcgac	
R_Cmd1_aid_Fusion	ATGGTAAGGGTAAGATAGCGGGAGCAAAAAATCACAAGGATGCACatcgatgaattcgagctcg	
Cmd1_Check_ORF	GGCTCTGATGTCTCGTCAAC	
F_Myo2_aid_Fusion	AGAATAGTTGACCTTGTTGCCCAACAAGTCGTTCAAGACGGCCACcgtacgctgcaggtcgac	
R_Myo2_aid_Fusion	TTTTTTTAGCATTCATGTACAATTTTGTTTCTCGCGCCATCAGTTatcgatgaattcgagctcg	
Myo2_Check_ORF	GGCCATCAATGCTGTGGTC	
F_Myo2_3xmCh_Fusn	AGAATAGTTGACCTTGTTGCCCAACAAGTCGTTCAAGACGGCCACcgtacgctgcaggtcgac	
R_Myo2_3xmCh_Fusn	TTTTTTTAGCATTCATGTACAATTTTGTTTCTCGCGCCATCAGTTgcataggccactagtggatctg	
F_Atg9_3xmCh_Fusn	TTAGGACTTGTTAAAGAGTATTACAAGAAGTCTGACGTCGGAAGAcgtacgctgcaggtcgac	
R_Atg9_3xmCh_Fusn	TTATATATATAGTTATATTGGATGATGTACACGACACAGTCTGCCgcataggccactagtggatctg	
Atg9_Check_ORF	GGCCCTGGCCATAATATTTC	
F_Sec18_aid_Fusion	GAAGATCCCGTGAACGAGCTTGTTGAGTTGATGACCCAATCCGCAcgtacgctgcaggtcgac	
R_Sec18_aid_Fusion	AGGGATAAAGAATAAAAATACAAGGACATGAAAAATTTGAAATAAatcgatgaattcgagctcg	
Sec18_Check_ORF	CGACAATGAGATAGCAGTTCC	
F_Sec14_aid_Fusion	TATATTGGACCGGAAGGTGAAGCTCCGGAAGCCTTTTCGATGAAAcgtacgctgcaggtcgac	
R_Sec14_aid_Fusion	ACTCCTCTTTTCTCTCTCGAAAAAAAAATGTCTTTAAAAATAATAATCGATGAATTCGAGCTCG	

Sec14_Check_ORF	CATATGTTAGGGAAGCCTCC	
For_GFP-Atg8_N-tagging	TTGTAAAGTTGAGAAAATCATAATAAAATAATTACTAGAGACATGCGTACGCTGCAGGTCGAC	
Rev_GFP-Atg8_N-tagging	CGCCTTCCTTTTTTCAAATGGATATTCAGACTTAAATGTAGACTTCATCGATGAATTCTCTGTCG	
R_Atg8_ N´ tag_Chk_ORF	CCTACGGTAAGGTCAGCAG	
For_GFP-Ape1_N-tagging	ATTGTAGAAACCTGCACAACCAACAAAATTAAGAAAAAAAGAATGCGTACGCTGCAGGTCGAC	
Rev_GFP-Ape1_N-tagging	CTGCAGAGTTTTCTTCAATTGTTCCAGTATTTCACGTTGTTCCTCCATCGATGAATTCTCTGTCG	
R_Ape1_ N´ tag_Chk_ORF	GCGTCCACATGAGATCCAATG	
Ape1_F_upstr	CAACTAGGGGTGATGCTG	
Ape1_R_downstr	CAAGGCCCACATTGGTGTTC	
ForApe1_KO	ATTGTAGAAACCTGCACAACCAACAAAATTAAGAAAAAAAGAATGCAGCTGAAGCTTCGTACGC	
R_Ape1_mCherry	GATAAAGAAACAGAAATCAAAAGAAATAAAAAGAGTGTGGCAAAAATCGATGAATTCGAGCTCG	
Atg8_F_upstr	GACAGACCCAATTGGTGATG	
Atg8_R_downstr	GCATTGAACAGATCGTAATCTG	
ForPEP4	GTATTTAATCCAAATAAAATTCAAACAAAAACCAAAACTAACATGCAGCTGAAGCTTCGTACGC	J. Tyedmers
RevPEP4	ATGGCAGAAAAGGATAGGGCGGAGAAGTAAGAAAAGTTTAGCTCAGCATAGGCCACTAGTGGATCTG	J. Tyedmers
ForATG1	TTTTCAAATCTCTTTTACAACACCAGACGAGAAATTAAGAAAATGCAGCTGAAGCTTCGTACGC	J. Tyedmers
RevATG1	CAGGTCATTTGTACTTAATAAGAAAACCATATTATGCATCACTTAGCATAGGCCACTAGTGGATCTG	J. Tyedmers
ForVPS30	CAGTCACTGTTTTCGCAAAGACTCCCAGACACGGGCATTAAAATGCAGCTGAAGCTTCGTACGC	J. Tyedmers
RevVPS30	CCCTTTATCACATTTATGAAAAAATGCATTTATATGAACTACTTAGCATAGGCCACTAGTGGATCTG	J. Tyedmers
ForATG7	AGTTCATTATATTTCAACAAATATAAGATAATCAAGAATAAAATGCAGCTGAAGCTTCGTACGC	J. Tyedmers
RevATG7	AGTGGCACCACAATATGTACCAATGCTATTATATGCAAAATATTAGCATAGGCCACTAGTGGATCTG	J. Tyedmers
ForATG8	TGTAAAGTTGAGAAAATCATAATAAAAATAATTACTAGAGACATGCAGCTGAAGCTTCGTACGC	J. Tyedmers
RevATG8	CGATTTTAGATGTTAACGCTTCATTTCTTTTCATATAAAAGACTAGCATAGGCCACTAGTGGATCTG	J. Tyedmers
ForATG9	TAAGAACAGCCTGAAATATCAAAATCACGGAATTATTAGGTTATGCAGCTGAAGCTTCGTACGC	J. Tyedmers
RevATG9	TATATATAGTTATATTGGATGATGTACACGACACAGTCTGCCTTAGCATAGGCCACTAGTGGATCTG	J. Tyedmers
ForATG11	TTGTTGTTCGGAAAGTACTTCTTTTATTTTCTTTTATACATCATGCAGCTGAAGCTTCGTACGC	J. Tyedmers
RevATG11	ATAATTAAAATCTTGTCATTTGTGACAAACGTTTAGCACTGTTCAGCATAGGCCACTAGTGGATCTG	J. Tyedmers
ForATG14	AAAAAGGGAAGTAAAAGTTAAAAACTAGAATCCTAGTATGACATGCAGCTGAAGCTTCGTACGC	J. Tyedmers
RevATG14	ACATGCAACTTTATACACACGGCAGGAAAAAAAGTGCGCACTCTAGCATAGGCCACTAGTGGATCTG	J. Tyedmers
ForATG19	GCGGCACTTGCTTCAGTAACGCCCAAAGGAGAGTTCTGGTAAATGCAGCTGAAGCTTCGTACGC	J. Tyedmers
RevATG19	ATGTGAAAAGGTACTCATTGCTGTATAAAAATAGAGTTTGACCTAGCATAGGCCACTAGTGGATCTG	J. Tyedmers
ForATG16_KO	TGTTATTAACCTGCGCGAATCTGTATTAAGGGCGCATATTCCATGCAGCTGAAGCTTCGTACGC	
RevATG16_KO	TTTCTTTTGTATGCATTTTGTGACGATTTGACAACTGATGCATCAGCATAGGCCACTAGTGGATCTG	
ForAms1_KO	ATAGAGATTAAGGCTGCAAAAGAGTTTCAAAAATAATTAATTATGCAGCTGAAGCTTCGTACGC	
RevAms1_KO	TTTGGGAGTGAGTGAATGTAAAAAACAGTGAGGGAGACAAACTCAGCATAGGCCACTAGTGGATCTG	
ForPDR5_KO	TTAAGTTTTCGTATCCGCTCGTTCGAAAGACTTTAGACAAAAATGCAGCTGAAGCTTC	

	GTACGC
RevPDR5_KO	CATCTTGGTAAGTTTCTTTTCTTAACCAAATTCAAAATTCTATTAGCATAGGCCACTAG TGGATCTG
Kan B	CAATTCAACGCGTCTGTGAG
GFP_Check_Fowd	CCAATTGGTGATGGTCCAGTC
Rev_mCherry	Cttcaagtagtcggggatgtc
Rev_GFP	CATAACCTTCTGGCATGGC
Pep4_R_upstr	CCTGCTTGATGTGGTACAAC
Up ATG1	GGCCGAGGTTAATTCTAG
UpVPS30/ATG6	CGCAATTTCCTTCTGGTTCGTAGGC
UPATG7	CGAGAACACACCCGTTGAATC
Upstr_ATG9	CGCACTCGCATCTGTCGAG
Upstr_ATG19	GCACGCTGAGAGTATCATC
UpATG11	CAAGTAGTAGCGGAACATCCG
UpATG14	CTAGCAGCAAGCATTCTTGCAG
UpATG16	CATCGTCGGCAGTGGAATTC
Ams1_F_upstr	CAAATGGGCGACCCTATTGTC
Ams1_R_downstr	CTTCCAAGGCGCAACAACTCAG
Up_PDR5	CTACGCCGTGGTACGATATC
5' upURA	GAAGGTTAATGTGGCTGTGG
5' inURA	GTCATGCAAGGGCTCCCTATC
REVCompTIR1	GACTTGAACGGATCCACTAGC

TABLE 4.: Antibodies used in this study

Antibody	Dilution	Source/Company
anti-GFP (mouse)	1:1000	Roche
anti-actin (mouse)	1: 5000	Millipore
Anti-HA (mouse)	1: 4000	Sigma-Aldrich Co.
HRP-linked Antibody (mouse)	1: 5000	Cell Signaling

5.2. Molecular Biology Methods

5.2.1. Agarose gel electrophoresis

1 % agarose was prepared by boiling the agarose in 0.5X TBE until completely melted. Ethidium bromide (10 µl of 1 % (w/v) stock solution per 100 ml) was added to the molten agarose and directly poured into a flat-bed tray with combs. After solidifying the agarose, it was transferred to the electrophoresis chamber filled with 0.5X TBE buffer. Samples were loaded with loading dye and electrophoresis was carried out at 130-170 volt until the dye reached the bottom part of the gel. The gel was visualized under a UV transilluminator at 265 nm. If required, gel excision was performed at 365 nm to avoid any DNA damage.

5X TBE	54g/l Tris 27.5g/l Boric acid 20ml/l 0.5M EDTA (pH 8.0)
6x DNA loading dye	30 % (v/v) Glycerol 0.25 % (w/v) Bromophenol blue

5.2.2. Restriction digestion of DNA

Restriction digestions were performed to linearize the plasmids for genomic integration. About 1 U of restriction enzyme/µg of DNA was used to digest the plasmid in a total 50 µl reaction volume. The reaction was carried out according to the manufacturers' instruction.

5.2.3. Purification of DNA fragments

If required, the linearized DNA or PCR product was separated by agarose gel electrophoresis and excised from the gel using a sharp scalpel. The DNA was then extracted using QIAquick Gel Extraction Kit (Qiagen) according to the manufacturers' instruction.

5.2.4. Polymerase Chain Reaction (PCR)

PCR was used to amplify a fusion cassette for yeast genomic integration or checking the correct genomic insertion/integration or deletion. The PCR reaction was performed in 50-100 µl total volume containing 0.4 µM of each primer, template DNA (plasmids: 25–200 ng, genomic DNA: 0.5–1 µg) and 1X My Taq Red buffer (1 mM dNTPs and 3 mM $MgCl_2$). To amplify the PCR cassette for genomic integration, MyFi Mix was used that contained high fidelity Taq polymerase. Correct genomic integration and deletions were verified by a colony PCR using normal Taq polymerase.

TABLE 5.: PCR protocol

Step	Temp.	Time	Cycles
Initial denaturation	95 °C	1 min	
Denaturation	95 °C	15 s	
Annealing	50 °C	15 s	X 33
Extension	72 °C	30 s/kb	
Final extension	72 °C	10 min	
	4 °C	∞	

Bacterial Methods

5.2.5. Construction of pHis10-Sumo-PrD-TEV-Avi and pHis10-Sumo-PrD-STOP (Done by J. Tyedmers)

The pHis10-Sumo-PrD-TEV-Avi construct was generated by a fusion PCR from "pHis10-Sumo" [231] using pH10-Sumo_P1 and pH10-Sumo_P2 primers for the amplification of the N-terminal His-Sumo-tag and PrD-GFP_P3 and PrD-GFP_P4 primes for the amplification of PrD-GFP [49]. This amplification product was afterwards cloned into an Avi-tag (Avidity Avitag™) vector [232] to make pHis10-Sumo-PrD-TEV-Avi construct. The pHis10-Sumo-PrD-STOP was generated from this pHis10sumo-PrD-TEV-Avi construct by introducing a STOP codon with a QuikChange PCR.

5.2.6. Transformation of *E. coli*

An aliquot of competent *E. coli* cells was thawed on ice, and 1 µl (~100 ng) DNA was added. The mixture was incubated on ice for 10 min. A heat shock was given at 42°C for 1 min and immediately incubated on ice for 5 min. 1 ml of LB was added to this mix and allowed for the recovery by incubating at 37 °C for 1 h at 150 rpm prior to plating on antibiotic containing LB plates. Plates were incubated overnight at 37°C.

5.2.7. Plasmid isolation

Plasmids were isolated from *E. coli* using standard peqGOLD Plasmid Miniprep Kit (PEQLAB) according to the manufacturers' instruction.

5.2.8. Purification of 10xHis-Sumo-PrD-AviTag and 10xHis-Sumo-PrD-STOP

The two constructs 10xHis-Sumo-PrD-AviTag and 10xHis-Sumo-PrD-STOP were freshly transformed into *E. coli* BL21 (DE3) harboring a biotin ligase from an IPTG-inducible pBirAcm plasmid (chloramphenicol resistance). BirA biotin ligase catalyzes the biotinylation (covalent attachment of a biotin/Avi-tag) of recombinant PrD proteins from AviTag™ vector once the free biotin is supplied in the media. A pre-culture was grown over night at 37°C. Next morning, 2% of the pre-culture was diluted into freshly prepared Terrific Broth (TB) containing ampicillin and chloramphenicol and grown until OD_{600} reached 0.7-0.8. During the dilution, 20mg/lit of free biotin (prepared into 50 % ethanol) was added in the culture harboring 10xHis-Sumo-PrD-AviTag. 1 mM IPTG was added for 4 h to induce the expression. Cells were harvested by centrifugation (6000 rpm, 15 min, 4°C), resuspended in 20 ml of LWB buffer and disrupted by French Press (Bukau Lab). After centrifugation (12000 rpm, 45 min, 4°C), the cleared supernatant was mixed with equilibrated 1.5 ml of Ni-NTA beads (Millipore) and rotated gently for 2 h at 4°C. The beads were washed 3 times with LWB buffer and brought to a column, and proteins were afterwards eluted with 250 mM imidazole in 10-15 fractions. Major eluted fractions were pooled and partially denatured with 2 M urea. Ulp1 protease (at 4 µg/µl) was added to remove the 10xHis-Sumo tag and dialyzed in 3 lit of LWB buffer + 2 M urea buffer without any imidazole. To get rid of cleaved His-sumo tag, digested protein was again incubated with Ni-NTA for 1 h at 4°C and flow-through was collected. Purified PrD-AviTag and PrD-STOP were then concentrated with 30 kDa MWCO Amicon concentrators to get about 6 mg/ml of protein concentration. The concentrated proteins were brought to 8M urea and then methanol precipitated to further concentrate by a factor of 10 and the pellet was resuspended in 6 M of GdnHCl prior to store at –80°C.

Lysis and washing buffer (LWB)	40 mM HEPES-KOH (pH 7.4)
	150 mM KCl
	5 mM $MgCl_2$
	5 % Glycerol
	10 mM imidazole
	2 mM β-mercaptoethanol
	1 mM PMSF
	Protease inhibitors

Yeast Methods

5.2.9. Transformation of yeast

Yeast transformation was performed using a standard lithium acetate (LiAc)/single-stranded carrier DNA/ PEG method [233, 234]. For one transformation, 10 ml of logarithmic growth phase culture (OD_{600} of 0.3-0.7) in YPD was pellet by centrifugation (3000 rpm, RT, 5 min), washed once with sterile H_2O and finally resuspended in 60 µl 0.1 M LiAc prior to incubation at 30°C for 15 min. This cell/ LiAc mix was then transferred to an eppendorf tube containing 100 µg salmon sperm ss DNA and 0.2-0.5 µg DNA to be transformed (plasmid, linearized plasmid or PCR product). 300 µl of PEG mix were added to the tube, and the transformation mixture was subsequently incubated at 30°C for 25-30 min on a heating block. Cells were heat shocked for 42°C for 20-25 min, followed by a centrifugation step at 3,000 rpm for 5 min. In the case of transformation was with an antibiotic resistance cassette, cells were resuspended in 1.5 ml of YPD and incubated for overnight at RT on a roller wheel prior to plating on the respective antibiotic plate. In a case of auxotrophic markers, transformed cells were resuspended in sterile H_2O and directly plated on particular drop out plate. Positive clone were confirmed by colony PCR, microscopy and /or Western Blot after 2-3 days of incubation at 30°C.

PEG mix	0.1 M LiAc
	50% (w/v) PEG 4000

5.2.10. Genetic manipulation in yeast

In yeast, genetic manipulation can be easily achieved due to homologous recombination. PCR cassettes with a desired tag can be created with primers flanking homologous sequences of gene of interest from the yeast genome. Gene deletions and genomic N/C-terminal tagging were performed as described before [230]. Alternatively, desired gene deletion cassettes were amplified by PCR using a genomic DNA as a template from the yeast deletion library of Tyedmers lab. C-terminal tagging of essential genes with “aid” degron was performed as the genomic integration of mCherry.

5.2.11. Spotting assay

Serial dilution spotting assay was performed to check the cell viability after auxin-induced depletion of essential proteins. Conditional “aid” mutants were grown to mid-log phase in the absence and presence of 20mM auxin, and OD_{600} was adjusted to 0.5. These cells were further 5-fold serial diluted and spotted onto YPD plates. Plates were incubated 30°C for 2-3 days and imaged. For Colony-forming units (CFU) assay, 100 µl from 10^{-4} and 10^{-5} serial dilution was spread onto YPD plates in triplicates and incubated at 30°C. CFUs were counted after 2 days.

5.2.12. Preparation of yeast cell lysate for Western Blotting

Yeast cells were grown to mid-log phase. The culture with equivalent to OD_{600} 1.0 was centrifuged, resuspended in 500 µl of 0.2 M NaOH and incubated on ice for 15 min. Cells were again centrifuged, and the pellet was resuspended in 100 µl of 2x SDS sample buffe. Samples were boiled at 95°C for 5-10 min. For analysis by SDS-PAGE and Western Blot, generally, 10 µl protein extract was loaded.

5 x SDS sample buffer	300 mM Tris/HCl (pH 6.8)
	10 % (w/v) SDS
	50 % Glycerol
	25 % (w/v) β-mercaptoethanol
	0.1 % (w/v) Bromophenol blue

5.2.13. Preparation of yeast cell lysate in a mixer mill for fishing approach

50 ml of a yeast culture in logarithmic growth phase at an OD_{600} ~ 0.4–0.6 were harvested, and the pellet was transferred to 1.5 ml eppendorf tubes, resuspended in 100 µl of fiber attachment buffer and dripped in liquid nitrogen present in a 2-ml round bottom eppendorf tube that contained a 7 mm stainless steel ball. After boiling out of the liquid nitrogen, the tubes were closed and placed in an adaptor for 2 ml tubes into a Retsch Mixer Mill MM 400 (Bukau Lab) and agitated twice for 2 min at 30 Hz. The sample was cooled in liquid nitrogen in between the two rounds of agitation. The resulting powder of lysed cells was transferred into a 1.5 ml tube and resuspended in 500 µl of FAB buffer, spun at 2300 rpm for 2 min at 4°C to remove the cell debris. The resulting supernatant was spun down again at 14000 rpm for 30 min to separate insoluble fraction from the soluble fraction. The soluble fraction was used for the fishing experiment.

Fiber attachment buffer (FAB)	25 mM Tris/HCl (pH 7.4) 150 mM KAc 5 mM MgAc 5% Glycerol 1 mM DTT 1 mM PMSF Protease inhibitors

5.3. Biochemical Methods

5.3.1. Bradford assay

Standard Bradford assay was used to determine the protein concentration. The Bradford reagent (Bio-Rad Laboratories, Inc.) was diluted 1:5 with H_2O and mixed with protein sample. The absorption was measured at the wavelength of λ = 595 nm and concentration was calculated based on BSA calibration curve.

5.3.2. SDS-polyacrylamide gel electrophoresis (SDS-PAGE)

Proteins with different sizes were separated by denaturing SDS polyacrylamide gel electrophoresis (SDS-PAGE). If not mentioned, protein samples were mixed with sample buffer and boiled at 95°C for 5 min prior to loading onto the gel. Samples were run at 150-200 volt till the blue dye reached the bottom part of the gel to guarantee for optimal separation.

SDS Running Buffer	193 mM Gycine 25 mM Tris 0.1 % (w/v) SDS

5.3.3. Western Blot

Specific proteins in cell lysates were identified by Western Blot using specific antibodies. Protein mixture was separated by SDS-PAGE and transferred onto a PVDF membrane using semidry transfer method. The semidry transfer was performed using Trans-Blot®Turbo™system (Bio-Rad Laboratories, Inc). Before the transfer, the PVDF membrane was activated in methanol and equilibrated in Semidry Transfer Buffer. Transfer sandwich was assembled onto transfer cassette with the following order: 3 Whatman papers, PVDF membrane, gel and 3 Whatman papers followed by careful removal of air bubbles with a plastic roller. The transfer was performed at 25 volts for 30 min. After the transfer, the membrane was blocked in 5 % milk powder in 1X PBST at RT for 1 hr. The membrane was incubated with primary antibody in 1 % milk powder in 1X PBST for overnight at 4°C. The blot was rinsed once with 1X PBST for 10 min. The blot was incubated with HRP-conjugated secondary antibody in 1 % milk powder in 1X PBST at RT for 1-2 hr. The blot was rinsed 3 times with 1X PBST for 10 min and incubated with an enhanced chemiluminescent (ECL) HRP substrate for 1 min prior to developing at AGFA Curix 60 Film Processor (AGFA HealthCare).

Semidry transfer buffer	14.4 g/l Glycine
	3.03 g/l Tris
	200 ml/l MeOH

5.3.4. *In vitro* formation of PrD-fibers

Purified PrD-AviTag was mixed to PrD-STOP at 1:50 Molar ratio (in GdnHCl) and mixture was then diluted 100-fold in fiber formation buffer and rotated at 8 rpm over night at RT. Formed fibers were fragmented by sonication for 5 min a water bath sonicator (Bukau Lab). These fibers were washed twice in FAB buffer and equilibrated for their immobilization on streptavidin magnetic beads in my fishing approach.

Fiber formation buffer	5 mM Potassium phosphate buffer (pH 7.4) 150 mM NaCl

5.3.5. Fishing approach for the identification of amyloid binding proteins

A 50 µl of streptavidin magnetic beads was blocked with 5 mg/ml of BSA in PBS at 4°C over night. Subsequently, the beads were incubated with 500 µl of 5 mg/ml BSA in FAB buffer for 1 hour and equilibrated by washing 3 times with FAB buffer. 375 µl of equilibrated biotinylated PrD fibers (concentration 15 µM) were added to the beads and incubated for ~ 1-2 h at 4°C. Beads were gently washed 3 times with FAB buffer to remove unbound fibers and then incubated with 500 µl of yeast cell lysate (~2 mg/ml protein concentration) in low binding eppendorf tubes at 4°C over night under gentle agitation (17 rpm) in an overhead incubator. Subsequently, the beads were washed 4 times with 200 µl fiber attachment buffer and proteins bound to PrD-GFP were eluted by boiling the beads at 95°C in 2X SDS-PAGE sample buffer (Laemmli buffer) for 10 min. Eluted samples were separated by SDS-PAGE and subjected for mass spectrometry analysis at the Core Facility to Mass Spectrometry & Proteomics/ZMBH, Heidelberg.

5.4. Microscopy

5.4.1. Fixation of yeast cells for standard microscopy

For image acquisition by fluorescence microscopy, 10 ml of culture was harvested by centrifugation (3500 rpm, RT, 5 min). 5 ml of the supernatant was removed, and the pellet was resuspended in remaining 5 ml of media. This culture then mixed with 5 ml of 8% PFA (paraformaldehyde) and incubated immediately for 10 min at RT. Cells were pelleted by centrifugation (3500 rpm, RT, 5 min) and washed once with 5 ml of 0.1M potassium phosphate buffer (pH 6.5). Cells were pelleted by centrifugation (3500 rpm, RT, 5 min) and resuspended in 1ml PBS and then transferred into an Eppendorf tube. After one centrifugation at max speed for 1 min, cells were resuspended in 15-20 µl of PBS and subjected to fluorescence microscopy.

5.4.2. Microscopy image acquisition, processing, and data interpretation

The fixed cells were used for acquiring the images under the microscope. Unless specified differently, optical sections of 0.2 µm were acquired to image the whole cell volume using a widefield system (xcellence IX81Olympus, ZMBH Imaging Facility/Bukau Lab) and a Plan-Apochromat 100x /NA 1.45 oil immersion objective.

All images were acquired with a Hamamatsu ORCA-R2 camera. Acquired z-stacks were deconvolved with xcellence (Olympus) software using the Wiener Filter. Further digital image processing was performed with ImageJ by a linear adjustment of brightness and contrast.

5.4.3. Time-lapse microscopy

Time-lapse microscopy was performed on agarose pads of 20 x 20 x 1 mm. These pads were prepared by pouring ultrapure agarose (1% w/v) in SD or YPD media directly onto a microscope slide. After addition of the cells onto the pad, it was covered with a cover slide and sealed with melted VLAP wax (1:1:1 Vaseline:lanolin:paraffin). I acquired a stack of ~15 optical sections spaced 0.2 – 0.3 µm apart in every 2-5 min.

5.4.4. Quantification of amyloid aggregates and PAS substrates

In general, numbers of PrD-GFP aggregates and PAS substrates within/among the cells were analyzed manually. Around 100 cells were taken into account for the quantification. For determination of the phenotype of multiple dispersed PrD-GFP or PAS substrates, cells with single or multiple PrD-GFP/PAS markers were counted and plotted as “percentage”. The degree of co-localization of PrD-GFP aggregates with other proteins including preApe1, Atg8, Atg9 or Myo2 was determined by counting clear and distinguishable PrD-GFP fluorescent foci within the cells and was taken into account that how many of those distinct PrD-GFP foci co-localized at least partially with the corresponding other protein.

5.4.5. PrD-GFP decay experiments

To monitor the decay of pre-existing PrD-GFP single foci (IPODs), I used cells where the PrD-GFP IPOD was pre-formed for 6 hours by galactose induction. The cells were then shifted and diluted with OD_{600} of 0.3 (“time point 0”) in glucose-based media to stop the ongoing synthesis of PrD-GFP and further incubated for up to 8 hours at 30°C where they grew more. I withdrew samples at the indicated time points, measured the OD_{600} to monitor how often the cells had divided in the glucose-based media, fixed the cells and counted the number of total cells as well as the number of cells that still had visible PrD-GFP aggregates.

This was done for roughly hundred cells per 0.3 OD_{600} units. Finally, based upon the measured OD_{600} for the time point of interest, I calculated the number of the newly born cells since the beginning of glucose chase (OD at “time point 0” was 0.3) and

subtracted this number from the total number of cells determined. Finally, I determined how many of those cells present since the beginning of the decay experiment still had a PrD-GFP aggregate (in %). This method is based on the observation that the IPOD is retained in the mother cells during cell divisions [65, 146].
When the amount of PrD-GFP was determined after such a decay experiment in glucose by Western Blotting (e.g. Fig 29E), I did not use the same number of cells for Western Blotting, but the same volume of culture, because the cells sometimes grew at different rates.
Since new synthesis of PrD-GFP from the Gal promoter was ceased by glucose, the same volume of culture should contain the same amount of original PrD-GFP that may have been partitioned between a mother and multiple progeny or stayed in fewer cells when cells divided slower. For these reasons, no classical loading control could be included for this Western Blot.

5.4.6. Electron microscopy

The biotin-labeled PrD amyloid fibers were confirmed by Electron Microscopy (EM) at BioQuant/Electron Microscopy Core Facility (EMCF), Heidelberg. A 10 µl of PrD fibers with 2-5 µM concentration was adsorbed onto 100-mesh activated formvar/carbon-coated copper grids for 2–10 min until air dry. Grids were washed 3 times with H_2O, and air dried and negatively stained with freshly prepared 2% uranyl acetate. Grids were again air dried for 10 min and subjected to electron microscopy for imaging at 50000X magnification.

List of Abbreviations

ATP . . . . . adenosine triphosphate

BSA . . . . . bovine serum albumin

CHX . . . . . cycloheximide

CVT ..... Cytosol to vacuole targeting

CytoQ . . . . . cytosolic protein quality control compartment

DNA . . . . . deoxyribonucleic acid

dNTP . . . . . deoxynucleoside triphosphate

DTT . . . . . L,D-dithiotreitol

DUB ..... Deubiquitylating enzyme

E. coli . . . . . *Escherichia coli*

EM . . . . . electron microscopy

Fig ..... Figure

Gal . . . . . galactose

GdnHCl . . . . . guanidine hydrochloride

GFP . . . . . green fluorescent protein

Glu . . . . . glucose

Hsp . . . . . heat shock protein

HSR . . . . . heat shock response

INQ .....*i*ntra*n*uclear *q*uality control compartment

IPOD .....*i*nsoluble *p*ro*t*ein *d*eposit

JUNQ .....*ju*xta*n*uclear *q*uality control compartment

kDa . . . . . kilo Dalton

LB . . . . .Luria Bertani

LiAc . . . . lithium acetate

MTOC . . . . microtubule organizing center

OD . . . . opitcal densitiy

PAGE . . . . . polyacrylamide gel electrophoresis

PBS . . . . phosphate buffered saline

PEG . . . . . ., polyethylene glycol

PFA . . . . . p-formaldehyde

PMSF . . . . . .phenylmethylsulphonyl fluoride

polyQ . . . . . polyglutamine

PrP . . . . . Prion Protein

rpm . . . . . revolutions per minute

RT . . . . . room temperature

S. cerevisiae . . . . *Saccharomyces cerevisiae*

SD . . . . . synthetic dropout

SDS . . . . . sodium dodecylsulfate

sHsp . . . . . small heat shock protein

SPB . . . . . spindle pole body

TBS . . . . . Tris buffered saline

Tris . . . . . tris(hydroxymethyl)aminomethane

UPS . . . . . ubiquitin-proteasome system

VHL . . . . . von Hippel-Lindau disease tumor suppressor

WT ..... Wild-type

Bibliography

1. Zhou HX: **Influence of crowded cellular environments on protein folding, binding, and oligomerization: biological consequences and potentials of atomistic modeling**. *FEBS letters* 2013, **587**(8):1053-1061.
2. Powers ET, Morimoto RI, Dillin A, Kelly JW, Balch WE: **Biological and chemical approaches to diseases of proteostasis deficiency**. *Annual review of biochemistry* 2009, **78**:959-991.
3. Dinner AR, Sali A, Smith LJ, Dobson CM, Karplus M: **Understanding protein folding via free-energy surfaces from theory and experiment**. *Trends in biochemical sciences* 2000, **25**(7):331-339.
4. Vabulas RM, Raychaudhuri S, Hayer-Hartl M, Hartl FU: **Protein folding in the cytoplasm and the heat shock response**. *Cold Spring Harbor perspectives in biology* 2010, **2**(12):a004390.
5. Hoffmann A, Bukau B, Kramer G: **Structure and function of the molecular chaperone Trigger Factor**. *Biochimica et biophysica acta* 2010, **1803**(6):650-661.
6. Chiti F, Dobson CM: **Protein misfolding, functional amyloid, and human disease**. *Annual review of biochemistry* 2006, **75**:333-366.
7. Hartl FU, Bracher A, Hayer-Hartl M: **Molecular chaperones in protein folding and proteostasis**. *Nature* 2011, **475**(7356):324-332.
8. Diaz-Villanueva JF, Diaz-Molina R, Garcia-Gonzalez V: **Protein Folding and Mechanisms of Proteostasis**. *International journal of molecular sciences* 2015, **16**(8):17193-17230.
9. van Oosten-Hawle P, Porter RS, Morimoto RI: **Regulation of organismal proteostasis by transcellular chaperone signaling**. *Cell* 2013, **153**(6):1366-1378.
10. Wu C, Lei H, Duan Y: **Formation of partially ordered oligomers of amyloidogenic hexapeptide (NFGAIL) in aqueous solution observed in molecular dynamics simulations**. *Biophysical journal* 2004, **87**(5):3000-3009.
11. Khurana R, Gillespie JR, Talapatra A, Minert LJ, Ionescu-Zanetti C, Millett I, Fink AL: **Partially folded intermediates as critical precursors of light chain amyloid fibrils and amorphous aggregates**. *Biochemistry* 2001, **40**(12):3525-3535.
12. Fink AL: **Protein aggregation: folding aggregates, inclusion bodies and amyloid**. *Folding & design* 1998, **3**(1):R9-23.
13. Gidalevitz T, Ben-Zvi A, Ho KH, Brignull HR, Morimoto RI: **Progressive disruption of cellular protein folding in models of polyglutamine diseases**. *Science* 2006, **311**(5766):1471-1474.
14. Petruska J, Hartenstine MJ, Goodman MF: **Analysis of strand slippage in DNA polymerase expansions of CAG/CTG triplet repeats associated with neurodegenerative disease**. *The Journal of biological chemistry* 1998, **273**(9):5204-5210.
15. Budworth H, McMurray CT: **A brief history of triplet repeat diseases**. *Methods in molecular biology* 2013, **1010**:3-17.
16. Chen S, Berthelier V, Yang W, Wetzel R: **Polyglutamine aggregation behavior in vitro supports a recruitment mechanism of cytotoxicity**. *Journal of molecular biology* 2001, **311**(1):173-182.

17. Aziz NA, Roos RA, Gusella JF, Lee JM, Macdonald ME: **CAG repeat expansion in Huntington disease determines age at onset in a fully dominant fashion**. *Neurology* 2012, **79**(9):952; author reply 952-953.
18. Furukawa Y, Fu R, Deng HX, Siddique T, O'Halloran TV: **Disulfide cross-linked protein represents a significant fraction of ALS-associated Cu, Zn-superoxide dismutase aggregates in spinal cords of model mice**. *Proceedings of the National Academy of Sciences of the United States of America* 2006, **103**(18):7148-7153.
19. Andley UP: **Crystallins and hereditary cataracts: molecular mechanisms and potential for therapy**. *Expert reviews in molecular medicine* 2006, **8**(25):1-19.
20. Fiesel FC, Caulfield TR, Moussaud-Lamodiere EL, Ogaki K, Dourado DF, Flores SC, Ross OA, Springer W: **Structural and Functional Impact of Parkinson Disease-Associated Mutations in the E3 Ubiquitin Ligase Parkin**. *Human mutation* 2015, **36**(8):774-786.
21. Drummond DA, Wilke CO: **The evolutionary consequences of erroneous protein synthesis**. *Nature reviews Genetics* 2009, **10**(10):715-724.
22. Willmund F, del Alamo M, Pechmann S, Chen T, Albanese V, Dammer EB, Peng J, Frydman J: **The cotranslational function of ribosome-associated Hsp70 in eukaryotic protein homeostasis**. *Cell* 2013, **152**(1-2):196-209.
23. Chu J, Hong NA, Masuda CA, Jenkins BV, Nelms KA, Goodnow CC, Glynne RJ, Wu H, Masliah E, Joazeiro CA *et al*: **A mouse forward genetics screen identifies LISTERIN as an E3 ubiquitin ligase involved in neurodegeneration**. *Proceedings of the National Academy of Sciences of the United States of America* 2009, **106**(7):2097-2103.
24. Wolff S, Weissman JS, Dillin A: **Differential scales of protein quality control**. *Cell* 2014, **157**(1):52-64.
25. Kramer G, Boehringer D, Ban N, Bukau B: **The ribosome as a platform for co-translational processing, folding and targeting of newly synthesized proteins**. *Nature structural & molecular biology* 2009, **16**(6):589-597.
26. del Alamo M, Hogan DJ, Pechmann S, Albanese V, Brown PO, Frydman J: **Defining the specificity of cotranslationally acting chaperones by systematic analysis of mRNAs associated with ribosome-nascent chain complexes**. *PLoS biology* 2011, **9**(7):e1001100.
27. Wang F, Durfee LA, Huibregtse JM: **A cotranslational ubiquitination pathway for quality control of misfolded proteins**. *Molecular cell* 2013, **50**(3):368-378.
28. Duttler S, Pechmann S, Frydman J: **Principles of cotranslational ubiquitination and quality control at the ribosome**. *Molecular cell* 2013, **50**(3):379-393.
29. Parsell DA, Kowal AS, Singer MA, Lindquist S: **Protein disaggregation mediated by heat-shock protein Hsp104**. *Nature* 1994, **372**(6505):475-478.
30. Stadtman ER, Levine RL: **Protein oxidation**. *Annals of the New York Academy of Sciences* 2000, **899**:191-208.
31. Nystrom T: **Role of oxidative carbonylation in protein quality control and senescence**. *The EMBO journal* 2005, **24**(7):1311-1317.
32. Suzuki YJ, Carini M, Butterfield DA: **Protein carbonylation**. *Antioxidants & redox signaling* 2010, **12**(3):323-325.
33. Wang J, Farr GW, Zeiss CJ, Rodriguez-Gil DJ, Wilson JH, Furtak K, Rutkowski DT, Kaufman RJ, Ruse CI, Yates JR, 3rd *et al*: **Progressive aggregation despite chaperone associations of a mutant SOD1-YFP in transgenic mice that develop ALS**. *Proceedings of the National Academy of Sciences of the United States of America* 2009, **106**(5):1392-1397.
34. Morley JF, Brignull HR, Weyers JJ, Morimoto RI: **The threshold for polyglutamine-expansion protein aggregation and cellular toxicity is dynamic and influenced by aging in Caenorhabditis elegans**. *Proceedings of the National Academy of Sciences of the United States of America* 2002, **99**(16):10417-10422.
35. Erjavec N, Larsson L, Grantham J, Nystrom T: **Accelerated aging and failure to segregate damaged proteins in Sir2 mutants can be suppressed by overproducing the protein aggregation-remodeling factor Hsp104p**. *Genes & development* 2007, **21**(19):2410-2421.

36. Kikis EA, Gidalevitz T, Morimoto RI: **Protein homeostasis in models of aging and age-related conformational disease**. *Advances in experimental medicine and biology* 2010, **694**:138-159.
37. Taylor RC, Dillin A: **Aging as an event of proteostasis collapse**. *Cold Spring Harbor perspectives in biology* 2011, **3**(5).
38. Morell M, Bravo R, Espargaro A, Sisquella X, Aviles FX, Fernandez-Busquets X, Ventura S: **Inclusion bodies: specificity in their aggregation process and amyloid-like structure**. *Biochimica et biophysica acta* 2008, **1783**(10):1815-1825.
39. de Groot NS, Sabate R, Ventura S: **Amyloids in bacterial inclusion bodies**. *Trends in biochemical sciences* 2009, **34**(8):408-416.
40. Sunde M, Serpell LC, Bartlam M, Fraser PE, Pepys MB, Blake CC: **Common core structure of amyloid fibrils by synchrotron X-ray diffraction**. *Journal of molecular biology* 1997, **273**(3):729-739.
41. Papsdorf K, Kaiser CJ, Drazic A, Grotzinger SW, Haessner C, Eisenreich W, Richter K: **Polyglutamine toxicity in yeast induces metabolic alterations and mitochondrial defects**. *BMC genomics* 2015, **16**:662.
42. Prusiner SB, McKinley MP, Bowman KA, Bolton DC, Bendheim PE, Groth DF, Glenner GG: **Scrapie prions aggregate to form amyloid-like birefringent rods**. *Cell* 1983, **35**(2 Pt 1):349-358.
43. Prusiner SB: **Novel proteinaceous infectious particles cause scrapie**. *Science* 1982, **216**(4542):136-144.
44. Scheibel T, Bloom J, Lindquist SL: **The elongation of yeast prion fibers involves separable steps of association and conversion**. *Proceedings of the National Academy of Sciences of the United States of America* 2004, **101**(8):2287-2292.
45. Colby DW, Prusiner SB: **Prions**. *Cold Spring Harbor perspectives in biology* 2011, **3**(1):a006833.
46. Alberti S, Halfmann R, Lindquist S: **Biochemical, cell biological, and genetic assays to analyze amyloid and prion aggregation in yeast**. *Methods in enzymology* 2010, **470**:709-734.
47. Crow ET, Li L: **Newly identified prions in budding yeast, and their possible functions**. *Seminars in cell & developmental biology* 2011, **22**(5):452-459.
48. True HL, Lindquist SL: **A yeast prion provides a mechanism for genetic variation and phenotypic diversity**. *Nature* 2000, **407**(6803):477-483.
49. Tyedmers J, Madariaga ML, Lindquist S: **Prion switching in response to environmental stress**. *PLoS biology* 2008, **6**(11):e294.
50. Cascarina SM, Ross ED: **Yeast prions and human prion-like proteins: sequence features and prediction methods**. *Cellular and molecular life sciences : CMLS* 2014, **71**(11):2047-2063.
51. Liebman SW, Chernoff YO: **Prions in yeast**. *Genetics* 2012, **191**(4):1041-1072.
52. Sondheimer N, Lindquist S: **Rnq1: an epigenetic modifier of protein function in yeast**. *Molecular cell* 2000, **5**(1):163-172.
53. Schwimmer C, Masison DC: **Antagonistic interactions between yeast [PSI(+)] and [URE3] prions and curing of [URE3] by Hsp70 protein chaperone Ssa1p but not by Ssa2p**. *Molecular and cellular biology* 2002, **22**(11):3590-3598.
54. Nakayashiki T, Kurtzman CP, Edskes HK, Wickner RB: **Yeast prions [URE3] and [PSI+] are diseases**. *Proceedings of the National Academy of Sciences of the United States of America* 2005, **102**(30):10575-10580.
55. Tyedmers J, Mogk A, Bukau B: **Cellular strategies for controlling protein aggregation**. *Nature reviews Molecular cell biology* 2010, **11**(11):777-788.
56. Kaganovich D, Kopito R, Frydman J: **Misfolded proteins partition between two distinct quality control compartments**. *Nature* 2008, **454**(7208):1088-1095.
57. Heinrich SU, Lindquist S: **Protein-only mechanism induces self-perpetuating changes in the activity of neuronal Aplysia cytoplasmic polyadenylation element binding protein (CPEB)**. *Proceedings of the National Academy of Sciences of the United States of America* 2011, **108**(7):2999-3004.

58. Cox BS: **A recessive lethal super-suppressor mutation in yeast and other psi phenomena**. *Heredity* 1971, **26**(2):211-232.
59. Michelitsch MD, Weissman JS: **A census of glutamine/asparagine-rich regions: implications for their conserved function and the prediction of novel prions**. *Proceedings of the National Academy of Sciences of the United States of America* 2000, **97**(22):11910-11915.
60. Wickner RB, Edskes HK, Bateman DA, Kelly AC, Gorkovskiy A, Dayani Y, Zhou A: **Amyloids and yeast prion biology**. *Biochemistry* 2013, **52**(9):1514-1527.
61. Tuite MF, Cox BS: **Propagation of yeast prions**. *Nature reviews Molecular cell biology* 2003, **4**(11):878-890.
62. Choe YJ, Ryu Y, Kim HJ, Seok YJ: **Increased [PSI+] appearance by fusion of Rnq1 with the prion domain of Sup35 in Saccharomyces cerevisiae**. *Eukaryotic cell* 2009, **8**(7):968-976.
63. Arslan F, Hong JY, Kanneganti V, Park SK, Liebman SW: **Heterologous aggregates promote de novo prion appearance via more than one mechanism**. *PLoS genetics* 2015, **11**(1):e1004814.
64. Dulle JE, True HL: **Low activity of select Hsp104 mutants is sufficient to propagate unstable prion variants**. *Prion* 2013, **7**(5):394-403.
65. Tyedmers J, Treusch S, Dong J, McCaffery JM, Bevis B, Lindquist S: **Prion induction involves an ancient system for the sequestration of aggregated proteins and heritable changes in prion fragmentation**. *Proceedings of the National Academy of Sciences of the United States of America* 2010, **107**(19):8633-8638.
66. Ferreira PC, Ness F, Edwards SR, Cox BS, Tuite MF: **The elimination of the yeast [PSI+] prion by guanidine hydrochloride is the result of Hsp104 inactivation**. *Molecular microbiology* 2001, **40**(6):1357-1369.
67. Mogk A, Kummer E, Bukau B: **Cooperation of Hsp70 and Hsp100 chaperone machines in protein disaggregation**. *Frontiers in molecular biosciences* 2015, **2**:22.
68. Wickner RB, Shewmaker FP, Bateman DA, Edskes HK, Gorkovskiy A, Dayani Y, Bezsonov EE: **Yeast prions: structure, biology, and prion-handling systems**. *Microbiology and molecular biology reviews : MMBR* 2015, **79**(1):1-17.
69. Frederick KK, Debelouchina GT, Kayatekin C, Dorminy T, Jacavone AC, Griffin RG, Lindquist S: **Distinct prion strains are defined by amyloid core structure and chaperone binding site dynamics**. *Chemistry & biology* 2014, **21**(2):295-305.
70. Liu JJ, Lindquist S: **Oligopeptide-repeat expansions modulate 'protein-only' inheritance in yeast**. *Nature* 1999, **400**(6744):573-576.
71. Chernova TA, Wilkinson KD, Chernoff YO: **Physiological and environmental control of yeast prions**. *FEMS microbiology reviews* 2014, **38**(2):326-344.
72. Paushkin SV, Kushnirov VV, Smirnov VN, Ter-Avanesyan MD: **Interaction between yeast Sup45p (eRF1) and Sup35p (eRF3) polypeptide chain release factors: implications for prion-dependent regulation**. *Molecular and cellular biology* 1997, **17**(5):2798-2805.
73. Tyedmers J: **Patterns of [PSI (+)] aggregation allow insights into cellular organization of yeast prion aggregates**. *Prion* 2012, **6**(3):191-200.
74. Chen B, Retzlaff M, Roos T, Frydman J: **Cellular strategies of protein quality control**. *Cold Spring Harbor perspectives in biology* 2011, **3**(8):a004374.
75. Dobson CM: **Protein folding and misfolding**. *Nature* 2003, **426**(6968):884-890.
76. Brehme M, Voisine C: **Model systems of protein-misfolding diseases reveal chaperone modifiers of proteotoxicity**. *Disease models & mechanisms* 2016, **9**(8):823-838.
77. Doyle SM, Genest O, Wickner S: **Protein rescue from aggregates by powerful molecular chaperone machines**. *Nature reviews Molecular cell biology* 2013, **14**(10):617-629.
78. Saibil H: **Chaperone machines for protein folding, unfolding and disaggregation**. *Nature reviews Molecular cell biology* 2013, **14**(10):630-642.
79. Winkler J, Tyedmers J, Bukau B, Mogk A: **Chaperone networks in protein disaggregation and prion propagation**. *Journal of structural biology* 2012, **179**(2):152-160.
80. Kim YE, Hipp MS, Bracher A, Hayer-Hartl M, Hartl FU: **Molecular chaperone functions in protein folding and proteostasis**. *Annual review of biochemistry* 2013, **82**:323-355.

81. Neckers L, Tsutsumi S, Mollapour M: **Visualizing the twists and turns of a molecular chaperone**. *Nature structural & molecular biology* 2009, **16**(3):235-236.
82. Kampinga HH, Craig EA: **The HSP70 chaperone machinery: J proteins as drivers of functional specificity**. *Nature reviews Molecular cell biology* 2010, **11**(8):579-592.
83. Mogk A, Tomoyasu T, Goloubinoff P, Rudiger S, Roder D, Langen H, Bukau B: **Identification of thermolabile Escherichia coli proteins: prevention and reversion of aggregation by DnaK and ClpB**. *The EMBO journal* 1999, **18**(24):6934-6949.
84. De Los Rios P, Ben-Zvi A, Slutsky O, Azem A, Goloubinoff P: **Hsp70 chaperones accelerate protein translocation and the unfolding of stable protein aggregates by entropic pulling**. *Proceedings of the National Academy of Sciences of the United States of America* 2006, **103**(16):6166-6171.
85. Mayer MP, Bukau B: **Hsp70 chaperones: cellular functions and molecular mechanism**. *Cellular and molecular life sciences : CMLS* 2005, **62**(6):670-684.
86. Mogk A, Bukau B: **Molecular chaperones: structure of a protein disaggregase**. *Current biology : CB* 2004, **14**(2):R78-80.
87. Sanchez Y, Lindquist SL: **HSP104 required for induced thermotolerance**. *Science* 1990, **248**(4959):1112-1115.
88. Liberek K, Lewandowska A, Zietkiewicz S: **Chaperones in control of protein disaggregation**. *The EMBO journal* 2008, **27**(2):328-335.
89. Glover JR, Lindquist S: **Hsp104, Hsp70, and Hsp40: a novel chaperone system that rescues previously aggregated proteins**. *Cell* 1998, **94**(1):73-82.
90. Haslberger T, Weibezahn J, Zahn R, Lee S, Tsai FT, Bukau B, Mogk A: **M domains couple the ClpB threading motor with the DnaK chaperone activity**. *Molecular cell* 2007, **25**(2):247-260.
91. Haslbeck M, Franzmann T, Weinfurtner D, Buchner J: **Some like it hot: the structure and function of small heat-shock proteins**. *Nature structural & molecular biology* 2005, **12**(10):842-846.
92. Vilchez D, Saez I, Dillin A: **The role of protein clearance mechanisms in organismal ageing and age-related diseases**. *Nature communications* 2014, **5**:5659.
93. Hershko A, Heller H, Elias S, Ciechanover A: **Components of ubiquitin-protein ligase system. Resolution, affinity purification, and role in protein breakdown**. *The Journal of biological chemistry* 1983, **258**(13):8206-8214.
94. Wilk S, Orlowski M: **Evidence that pituitary cation-sensitive neutral endopeptidase is a multicatalytic protease complex**. *Journal of neurochemistry* 1983, **40**(3):842-849.
95. Lu S, Wang J: **The resistance mechanisms of proteasome inhibitor bortezomib**. *Biomarker research* 2013, **1**(1):13.
96. Verma R, Aravind L, Oania R, McDonald WH, Yates JR, 3rd, Koonin EV, Deshaies RJ: **Role of Rpn11 metalloprotease in deubiquitination and degradation by the 26S proteasome**. *Science* 2002, **298**(5593):611-615.
97. Voges D, Zwickl P, Baumeister W: **The 26S proteasome: a molecular machine designed for controlled proteolysis**. *Annual review of biochemistry* 1999, **68**:1015-1068.
98. Jariel-Encontre I, Bossis G, Piechaczyk M: **Ubiquitin-independent degradation of proteins by the proteasome**. *Biochimica et biophysica acta* 2008, **1786**(2):153-177.
99. Eisele F, Wolf DH: **Degradation of misfolded protein in the cytoplasm is mediated by the ubiquitin ligase Ubr1**. *FEBS letters* 2008, **582**(30):4143-4146.
100. Nillegoda NB, Theodoraki MA, Mandal AK, Mayo KJ, Ren HY, Sultana R, Wu K, Johnson J, Cyr DM, Caplan AJ: **Ubr1 and Ubr2 function in a quality control pathway for degradation of unfolded cytosolic proteins**. *Molecular biology of the cell* 2010, **21**(13):2102-2116.
101. Gardner RG, Nelson ZW, Gottschling DE: **Degradation-mediated protein quality control in the nucleus**. *Cell* 2005, **120**(6):803-815.
102. Heck JW, Cheung SK, Hampton RY: **Cytoplasmic protein quality control degradation mediated by parallel actions of the E3 ubiquitin ligases Ubr1 and San1**. *Proceedings of the National Academy of Sciences of the United States of America* 2010, **107**(3):1106-1111.

103. Miller SB, Ho CT, Winkler J, Khokhrina M, Neuner A, Mohamed MY, Guilbride DL, Richter K, Lisby M, Schiebel E *et al*: **Compartment-specific aggregases direct distinct nuclear and cytoplasmic aggregate deposition**. *The EMBO journal* 2015, **34**(6):778-797.
104. Seufert W, Jentsch S: **Ubiquitin-conjugating enzymes UBC4 and UBC5 mediate selective degradation of short-lived and abnormal proteins**. *The EMBO journal* 1990, **9**(2):543-550.
105. Mony VK, Benjamin S, O'Rourke EJ: **A lysosome-centered view of nutrient homeostasis**. *Autophagy* 2016, **12**(4):619-631.
106. Glick D, Barth S, Macleod KF: **Autophagy: cellular and molecular mechanisms**. *The Journal of pathology* 2010, **221**(1):3-12.
107. Lamark T, Johansen T: **Aggrephagy: selective disposal of protein aggregates by macroautophagy**. *International journal of cell biology* 2012, **2012**:736905.
108. Yang Z, Klionsky DJ: **An overview of the molecular mechanism of autophagy**. *Current topics in microbiology and immunology* 2009, **335**:1-32.
109. Yorimitsu T, Klionsky DJ: **Autophagy: molecular machinery for self-eating**. *Cell death and differentiation* 2005, **12 Suppl 2**:1542-1552.
110. Das G, Shravage BV, Baehrecke EH: **Regulation and function of autophagy during cell survival and cell death**. *Cold Spring Harbor perspectives in biology* 2012, **4**(6).
111. Nair U, Klionsky DJ: **Molecular mechanisms and regulation of specific and nonspecific autophagy pathways in yeast**. *The Journal of biological chemistry* 2005, **280**(51):41785-41788.
112. Nakatogawa H, Suzuki K, Kamada Y, Ohsumi Y: **Dynamics and diversity in autophagy mechanisms: lessons from yeast**. *Nature reviews Molecular cell biology* 2009, **10**(7):458-467.
113. Reggiori F, Klionsky DJ: **Autophagic processes in yeast: mechanism, machinery and regulation**. *Genetics* 2013, **194**(2):341-361.
114. Monastyrska I, Rieter E, Klionsky DJ, Reggiori F: **Multiple roles of the cytoskeleton in autophagy**. *Biological reviews of the Cambridge Philosophical Society* 2009, **84**(3):431-448.
115. Klionsky DJ: **The molecular machinery of autophagy: unanswered questions**. *Journal of cell science* 2005, **118**(Pt 1):7-18.
116. Farre JC, Subramani S: **Mechanistic insights into selective autophagy pathways: lessons from yeast**. *Nature reviews Molecular cell biology* 2016.
117. Suzuki K, Kondo C, Morimoto M, Ohsumi Y: **Selective transport of alpha-mannosidase by autophagic pathways: identification of a novel receptor, Atg34p**. *The Journal of biological chemistry* 2010, **285**(39):30019-30025.
118. Svenning S, Johansen T: **Selective autophagy**. *Essays in biochemistry* 2013, **55**:79-92.
119. Schuck S, Gallagher CM, Walter P: **ER-phagy mediates selective degradation of endoplasmic reticulum independently of the core autophagy machinery**. *Journal of cell science* 2014, **127**(Pt 18):4078-4088.
120. Mochida K, Oikawa Y, Kimura Y, Kirisako H, Hirano H, Ohsumi Y, Nakatogawa H: **Receptor-mediated selective autophagy degrades the endoplasmic reticulum and the nucleus**. *Nature* 2015, **522**(7556):359-362.
121. Johansen T, Lamark T: **Selective autophagy mediated by autophagic adapter proteins**. *Autophagy* 2011, **7**(3):279-296.
122. Hyttinen JM, Amadio M, Viiri J, Pascale A, Salminen A, Kaarniranta K: **Clearance of misfolded and aggregated proteins by aggrephagy and implications for aggregation diseases**. *Ageing research reviews* 2014, **18**:16-28.
123. Pankiv S, Clausen TH, Lamark T, Brech A, Bruun JA, Outzen H, Overvatn A, Bjorkoy G, Johansen T: **p62/SQSTM1 binds directly to Atg8/LC3 to facilitate degradation of ubiquitinated protein aggregates by autophagy**. *The Journal of biological chemistry* 2007, **282**(33):24131-24145.
124. Kirkin V, Lamark T, Sou YS, Bjorkoy G, Nunn JL, Bruun JA, Shvets E, McEwan DG, Clausen TH, Wild P *et al*: **A role for NBR1 in autophagosomal degradation of ubiquitinated substrates**. *Molecular cell* 2009, **33**(4):505-516.

125. Petroi D, Popova B, Taheri-Talesh N, Irniger S, Shahpasandzadeh H, Zweckstetter M, Outeiro TF, Braus GH: **Aggregate clearance of alpha-synuclein in Saccharomyces cerevisiae depends more on autophagosome and vacuole function than on the proteasome**. *The Journal of biological chemistry* 2012, **287**(33):27567-27579.
126. Lu K, Psakhye I, Jentsch S: **Autophagic clearance of polyQ proteins mediated by ubiquitin-Atg8 adaptors of the conserved CUET protein family**. *Cell* 2014, **158**(3):549-563.
127. Lynch-Day MA, Klionsky DJ: **The Cvt pathway as a model for selective autophagy**. *FEBS letters* 2010, **584**(7):1359-1366.
128. Suzuki K, Ohsumi Y: **Current knowledge of the pre-autophagosomal structure (PAS)**. *FEBS letters* 2010, **584**(7):1280-1286.
129. Zaffagnini G, Martens S: **Mechanisms of Selective Autophagy**. *Journal of molecular biology* 2016, **428**(9 Pt A):1714-1724.
130. Bednarska NG, Schymkowitz J, Rousseau F, Van Eldere J: **Protein aggregation in bacteria: the thin boundary between functionality and toxicity**. *Microbiology* 2013, **159**(Pt 9):1795-1806.
131. Lindner AB, Madden R, Demarez A, Stewart EJ, Taddei F: **Asymmetric segregation of protein aggregates is associated with cellular aging and rejuvenation**. *Proceedings of the National Academy of Sciences of the United States of America* 2008, **105**(8):3076-3081.
132. Winkler J, Seybert A, Konig L, Pruggnaller S, Haselmann U, Sourjik V, Weiss M, Frangakis AS, Mogk A, Bukau B: **Quantitative and spatio-temporal features of protein aggregation in Escherichia coli and consequences on protein quality control and cellular ageing**. *The EMBO journal* 2010, **29**(5):910-923.
133. Johnston JA, Ward CL, Kopito RR: **Aggresomes: a cellular response to misfolded proteins**. *The Journal of cell biology* 1998, **143**(7):1883-1898.
134. Kawaguchi Y, Kovacs JJ, McLaurin A, Vance JM, Ito A, Yao TP: **The deacetylase HDAC6 regulates aggresome formation and cell viability in response to misfolded protein stress**. *Cell* 2003, **115**(6):727-738.
135. Olzmann JA, Chin LS: **Parkin-mediated K63-linked polyubiquitination: a signal for targeting misfolded proteins to the aggresome-autophagy pathway**. *Autophagy* 2008, **4**(1):85-87.
136. Wang G, Gao Y, Li L, Jin G, Cai Z, Chao JI, Lin HK: **K63-linked ubiquitination in kinase activation and cancer**. *Front Oncol* 2012, **2**:5.
137. Garcia-Mata R, Gao YS, Sztul E: **Hassles with taking out the garbage: aggravating aggresomes**. *Traffic* 2002, **3**(6):388-396.
138. Bjorkoy G, Lamark T, Brech A, Outzen H, Perander M, Overvatn A, Stenmark H, Johansen T: **p62/SQSTM1 forms protein aggregates degraded by autophagy and has a protective effect on huntingtin-induced cell death**. *The Journal of cell biology* 2005, **171**(4):603-614.
139. Song J, Yang Q, Yang J, Larsson L, Hao X, Zhu X, Malmgren-Hill S, Cvijovic M, Fernandez-Rodriguez J, Grantham J *et al*: **Essential genetic interactors of SIR2 required for spatial sequestration and asymmetrical inheritance of protein aggregates**. *PLoS genetics* 2014, **10**(7):e1004539.
140. Tessarz P, Schwarz M, Mogk A, Bukau B: **The yeast AAA+ chaperone Hsp104 is part of a network that links the actin cytoskeleton with the inheritance of damaged proteins**. *Molecular and cellular biology* 2009, **29**(13):3738-3745.
141. Liu B, Larsson L, Caballero A, Hao X, Oling D, Grantham J, Nystrom T: **The polarisome is required for segregation and retrograde transport of protein aggregates**. *Cell* 2010, **140**(2):257-267.
142. Erjavec N, Cvijovic M, Klipp E, Nystrom T: **Selective benefits of damage partitioning in unicellular systems and its effects on aging**. *Proceedings of the National Academy of Sciences of the United States of America* 2008, **105**(48):18764-18769.
143. Zhou C, Slaughter BD, Unruh JR, Eldakak A, Rubinstein B, Li R: **Motility and segregation of Hsp104-associated protein aggregates in budding yeast**. *Cell* 2011, **147**(5):1186-1196.
144. Coelho M, Lade SJ, Alberti S, Gross T, Tolic IM: **Fusion of protein aggregates facilitates asymmetric damage segregation**. *PLoS biology* 2014, **12**(6):e1001886.

145. Zhou C, Slaughter BD, Unruh JR, Guo F, Yu Z, Mickey K, Narkar A, Ross RT, McClain M, Li R: **Organelle-based aggregation and retention of damaged proteins in asymmetrically dividing cells**. *Cell* 2014, **159**(3):530-542.
146. Spokoini R, Moldavski O, Nahmias Y, England JL, Schuldiner M, Kaganovich D: **Confinement to organelle-associated inclusion structures mediates asymmetric inheritance of aggregated protein in budding yeast**. *Cell reports* 2012, **2**(4):738-747.
147. Rujano MA, Bosveld F, Salomons FA, Dijk F, van Waarde MA, van der Want JJ, de Vos RA, Brunt ER, Sibon OC, Kampinga HH: **Polarised asymmetric inheritance of accumulated protein damage in higher eukaryotes**. *PLoS biology* 2006, **4**(12):e417.
148. Ogrodnik M, Salmonowicz H, Brown R, Turkowska J, Sredniawa W, Pattabiraman S, Amen T, Abraham AC, Eichler N, Lyakhovetsky R *et al*: **Dynamic JUNQ inclusion bodies are asymmetrically inherited in mammalian cell lines through the asymmetric partitioning of vimentin**. *Proceedings of the National Academy of Sciences of the United States of America* 2014, **111**(22):8049-8054.
149. Malinovska L, Kroschwald S, Munder MC, Richter D, Alberti S: **Molecular chaperones and stress-inducible protein-sorting factors coordinate the spatiotemporal distribution of protein aggregates**. *Molecular biology of the cell* 2012, **23**(16):3041-3056.
150. Gallina I, Colding C, Henriksen P, Beli P, Nakamura K, Offman J, Mathiasen DP, Silva S, Hoffmann E, Groth A *et al*: **Cmr1/WDR76 defines a nuclear genotoxic stress body linking genome integrity and protein quality control**. *Nature communications* 2015, **6**:6533.
151. Roth DM, Balch WE: **Q-bodies monitor the quinary state of the protein fold**. *Nat Cell Biol* 2013, **15**(10):1137-1139.
152. Escusa-Toret S, Vonk WI, Frydman J: **Spatial sequestration of misfolded proteins by a dynamic chaperone pathway enhances cellular fitness during stress**. *Nature cell biology* 2013, **15**(10):1231-1243.
153. Specht S, Miller SB, Mogk A, Bukau B: **Hsp42 is required for sequestration of protein aggregates into deposition sites in Saccharomyces cerevisiae**. *The Journal of cell biology* 2011, **195**(4):617-629.
154. Miller SB, Mogk A, Bukau B: **Spatially organized aggregation of misfolded proteins as cellular stress defense strategy**. *Journal of molecular biology* 2015, **427**(7):1564-1574.
155. Marshall RS, McLoughlin F, Vierstra RD: **Autophagic Turnover of Inactive 26S Proteasomes in Yeast Is Directed by the Ubiquitin Receptor Cue5 and the Hsp42 Chaperone**. *Cell reports* 2016, **16**(6):1717-1732.
156. Tongaonkar P, Beck K, Shinde UP, Madura K: **Characterization of a temperature-sensitive mutant of a ubiquitin-conjugating enzyme and its use as a heat-inducible degradation signal**. *Analytical biochemistry* 1999, **272**(2):263-269.
157. McClellan AJ, Scott MD, Frydman J: **Folding and quality control of the VHL tumor suppressor proceed through distinct chaperone pathways**. *Cell* 2005, **121**(5):739-748.
158. Derkatch IL, Bradley ME, Hong JY, Liebman SW: **Prions affect the appearance of other prions: the story of [PIN(+)]**. *Cell* 2001, **106**(2):171-182.
159. Kama R, Robinson M, Gerst JE: **Btn2, a Hook1 ortholog and potential Batten disease-related protein, mediates late endosome-Golgi protein sorting in yeast**. *Molecular and cellular biology* 2007, **27**(2):605-621.
160. Glover JR, Kowal AS, Schirmer EC, Patino MM, Liu JJ, Lindquist S: **Self-seeded fibers formed by Sup35, the protein determinant of [PSI+], a heritable prion-like factor of S. cerevisiae**. *Cell* 1997, **89**(5):811-819.
161. Paushkin SV, Kushnirov VV, Smirnov VN, Ter-Avanesyan MD: **In vitro propagation of the prion-like state of yeast Sup35 protein**. *Science* 1997, **277**(5324):381-383.
162. Serio TR, Cashikar AG, Kowal AS, Sawicki GJ, Moslehi JJ, Serpell L, Arnsdorf MF, Lindquist SL: **Nucleated conformational conversion and the replication of conformational information by a prion determinant**. *Science* 2000, **289**(5483):1317-1321.

163. Barenz F, Inoue D, Yokoyama H, Tegha-Dunghu J, Freiss S, Draeger S, Mayilo D, Cado I, Merker S, Klinger M *et al*: **The centriolar satellite protein SSX2IP promotes centrosome maturation**. *The Journal of cell biology* 2013, **202**(1):81-95.
164. Cosson B, Couturier A, Chabelskaya S, Kiktev D, Inge-Vechtomov S, Philippe M, Zhouravleva G: **Poly(A)-binding protein acts in translation termination via eukaryotic release factor 3 interaction and does not influence [PSI(+)] propagation**. *Molecular and cellular biology* 2002, **22**(10):3301-3315.
165. Kiktev DA, Patterson JC, Muller S, Bariar B, Pan T, Chernoff YO: **Regulation of chaperone effects on a yeast prion by cochaperone Sgt2**. *Mol Cell Biol* 2012, **32**(24):4960-4970.
166. Li X, Rayman JB, Kandel ER, Derkatch IL: **Functional role of Tia1/Pub1 and Sup35 prion domains: directing protein synthesis machinery to the tubulin cytoskeleton**. *Molecular cell* 2014, **55**(2):305-318.
167. Saibil HR, Seybert A, Habermann A, Winkler J, Eltsov M, Perkovic M, Castano-Diez D, Scheffer MP, Haselmann U, Chlanda P *et al*: **Heritable yeast prions have a highly organized three-dimensional architecture with interfiber structures**. *Proceedings of the National Academy of Sciences of the United States of America* 2012, **109**(37):14906-14911.
168. Bagriantsev SN, Gracheva EO, Richmond JE, Liebman SW: **Variant-specific [PSI+] infection is transmitted by Sup35 polymers within [PSI+] aggregates with heterogeneous protein composition**. *Molecular biology of the cell* 2008, **19**(6):2433-2443.
169. Ganusova EE, Ozolins LN, Bhagat S, Newnam GP, Wegrzyn RD, Sherman MY, Chernoff YO: **Modulation of prion formation, aggregation, and toxicity by the actin cytoskeleton in yeast**. *Mol Cell Biol* 2006, **26**(2):617-629.
170. Gunning PW, Hardeman EC, Lappalainen P, Mulvihill DP: **Tropomyosin - master regulator of actin filament function in the cytoskeleton**. *Journal of cell science* 2015, **128**(16):2965-2974.
171. Drees B, Brown C, Barrell BG, Bretscher A: **Tropomyosin is essential in yeast, yet the TPM1 and TPM2 products perform distinct functions**. *The Journal of cell biology* 1995, **128**(3):383-392.
172. Nishimura K, Fukagawa T, Takisawa H, Kakimoto T, Kanemaki M: **An auxin-based degron system for the rapid depletion of proteins in nonplant cells**. *Nature methods* 2009, **6**(12):917-922.
173. Clayton JE, Pollard LW, Sckolnick M, Bookwalter CS, Hodges AR, Trybus KM, Lord M: **Fission yeast tropomyosin specifies directed transport of myosin-V along actin cables**. *Molecular biology of the cell* 2014, **25**(1):66-75.
174. Hodges AR, Krementsova EB, Bookwalter CS, Fagnant PM, Sladewski TE, Trybus KM: **Tropomyosin is essential for processive movement of a class V myosin from budding yeast**. *Current biology : CB* 2012, **22**(15):1410-1416.
175. Brockerhoff SE, Stevens RC, Davis TN: **The unconventional myosin, Myo2p, is a calmodulin target at sites of cell growth in Saccharomyces cerevisiae**. *The Journal of cell biology* 1994, **124**(3):315-323.
176. Liu B, Larsson L, Franssens V, Hao X, Hill SM, Andersson V, Hoglund D, Song J, Yang X, Oling D *et al*: **Segregation of protein aggregates involves actin and the polarity machinery**. *Cell* 2011, **147**(5):959-961.
177. Zhou P, Derkatch IL, Liebman SW: **The relationship between visible intracellular aggregates that appear after overexpression of Sup35 and the yeast prion-like elements [PSI(+)] and [PIN(+)]**. *Molecular microbiology* 2001, **39**(1):37-46.
178. Rock RS: **Molecular motors: a finicky myosin V chooses its own path**. *Current biology : CB* 2012, **22**(15):R606-608.
179. Reggiori F, Monastyrska I, Shintani T, Klionsky DJ: **The actin cytoskeleton is required for selective types of autophagy, but not nonspecific autophagy, in the yeast Saccharomyces cerevisiae**. *Molecular biology of the cell* 2005, **16**(12):5843-5856.
180. Olzscha H, Schermann SM, Woerner AC, Pinkert S, Hecht MH, Tartaglia GG, Vendruscolo M, Hayer-Hartl M, Hartl FU, Vabulas RM: **Amyloid-like aggregates sequester numerous metastable proteins with essential cellular functions**. *Cell* 2011, **144**(1):67-78.

181. Kakuta S, Yamamoto H, Negishi L, Kondo-Kakuta C, Hayashi N, Ohsumi Y: **Atg9 vesicles recruit vesicle-tethering proteins Trs85 and Ypt1 to the autophagosome formation site**. *The Journal of biological chemistry* 2012, **287**(53):44261-44269.
182. Nair U, Jotwani A, Geng J, Gammoh N, Richerson D, Yen WL, Griffith J, Nag S, Wang K, Moss T *et al*: **SNARE proteins are required for macroautophagy**. *Cell* 2011, **146**(2):290-302.
183. Mari M, Griffith J, Rieter E, Krishnappa L, Klionsky DJ, Reggiori F: **An Atg9-containing compartment that functions in the early steps of autophagosome biogenesis**. *The Journal of cell biology* 2010, **190**(6):1005-1022.
184. Bi E, Park HO: **Cell polarization and cytokinesis in budding yeast**. *Genetics* 2012, **191**(2):347-387.
185. Geng J, Nair U, Yasumura-Yorimitsu K, Klionsky DJ: **Post-Golgi Sec proteins are required for autophagy in Saccharomyces cerevisiae**. *Molecular biology of the cell* 2010, **21**(13):2257-2269.
186. Wang K, Yang Z, Liu X, Mao K, Nair U, Klionsky DJ: **Phosphatidylinositol 4-kinases are required for autophagic membrane trafficking**. *The Journal of biological chemistry* 2012, **287**(45):37964-37972.
187. Wickner W: **Yeast vacuoles and membrane fusion pathways**. *The EMBO journal* 2002, **21**(6):1241-1247.
188. Brown CR, Wolfe AB, Cui D, Chiang HL: **The vacuolar import and degradation pathway merges with the endocytic pathway to deliver fructose-1,6-bisphosphatase to the vacuole for degradation**. *The Journal of biological chemistry* 2008, **283**(38):26116-26127.
189. Pollard LW, Lord M: **Getting myosin-V on the right track: tropomyosin sorts transport in yeast**. *Bioarchitecture* 2014, **4**(1):35-38.
190. Avaro S, Belgareh-Touze N, Sibella-Arguelles C, Volland C, Haguenauer-Tsapis R: **Mutants defective in secretory/vacuolar pathways in the EUROFAN collection of yeast disruptants**. *Yeast* 2002, **19**(4):351-371.
191. Prescianotto-Baschong C, Riezman H: **Morphology of the yeast endocytic pathway**. *Molecular biology of the cell* 1998, **9**(1):173-189.
192. Ostrowicz CW, Meiringer CT, Ungermann C: **Yeast vacuole fusion: a model system for eukaryotic endomembrane dynamics**. *Autophagy* 2008, **4**(1):5-19.
193. Hammer JA, 3rd, Sellers JR: **Walking to work: roles for class V myosins as cargo transporters**. *Nature reviews Molecular cell biology* 2012, **13**(1):13-26.
194. Cebollero E, Reggiori F: **Regulation of autophagy in yeast Saccharomyces cerevisiae**. *Biochimica et biophysica acta* 2009, **1793**(9):1413-1421.
195. Klionsky DJ: **For the last time, it is GFP-Atg8, not Atg8-GFP (and the same goes for LC3)**. *Autophagy* 2011, **7**(10):1093-1094.
196. Guimaraes RS, Delorme-Axford E, Klionsky DJ, Reggiori F: **Assays for the biochemical and ultrastructural measurement of selective and nonselective types of autophagy in the yeast Saccharomyces cerevisiae**. *Methods* 2015, **75**:141-150.
197. Morselli E, Marino G, Bennetzen MV, Eisenberg T, Megalou E, Schroeder S, Cabrera S, Benit P, Rustin P, Criollo A *et al*: **Spermidine and resveratrol induce autophagy by distinct pathways converging on the acetylproteome**. *The Journal of cell biology* 2011, **192**(4):615-629.
198. Chernoff YO, Lindquist SL, Ono B, Inge-Vechtomov SG, Liebman SW: **Role of the chaperone protein Hsp104 in propagation of the yeast prion-like factor [psi+]**. *Science* 1995, **268**(5212):880-884.
199. Satpute-Krishnan P, Langseth SX, Serio TR: **Hsp104-dependent remodeling of prion complexes mediates protein-only inheritance**. *PLoS biology* 2007, **5**(2):e24.
200. Kryndushkin DS, Alexandrov IM, Ter-Avanesyan MD, Kushnirov VV: **Yeast [PSI+] prion aggregates are formed by small Sup35 polymers fragmented by Hsp104**. *The Journal of biological chemistry* 2003, **278**(49):49636-49643.
201. Satpute-Krishnan P, Serio TR: **Prion protein remodelling confers an immediate phenotypic switch**. *Nature* 2005, **437**(7056):262-265.

202. Romanova NV, Chernoff YO: **Hsp104 and prion propagation**. *Protein and peptide letters* 2009, **16**(6):598-605.
203. Winkler J, Tyedmers J, Bukau B, Mogk A: **Hsp70 targets Hsp100 chaperones to substrates for protein disaggregation and prion fragmentation**. *The Journal of cell biology* 2012, **198**(3):387-404.
204. Kummer E, Oguchi Y, Seyffer F, Bukau B, Mogk A: **Mechanism of Hsp104/ClpB inhibition by prion curing Guanidinium hydrochloride**. *FEBS letters* 2013, **587**(6):810-817.
205. Speldewinde SH, Doronina VA, Grant CM: **Autophagy protects against de novo formation of the [PSI+] prion in yeast**. *Molecular biology of the cell* 2015, **26**(25):4541-4551.
206. Monastyrska I, He C, Geng J, Hoppe AD, Li Z, Klionsky DJ: **Arp2 links autophagic machinery with the actin cytoskeleton**. *Molecular biology of the cell* 2008, **19**(5):1962-1975.
207. Bretscher A: **Polarized growth and organelle segregation in yeast: the tracks, motors, and receptors**. *The Journal of cell biology* 2003, **160**(6):811-816.
208. Pruyne D, Legesse-Miller A, Gao L, Dong Y, Bretscher A: **Mechanisms of polarized growth and organelle segregation in yeast**. *Annual review of cell and developmental biology* 2004, **20**:559-591.
209. Ungermann C, Nichols BJ, Pelham HR, Wickner W: **A vacuolar v-t-SNARE complex, the predominant form in vivo and on isolated vacuoles, is disassembled and activated for docking and fusion**. *The Journal of cell biology* 1998, **140**(1):61-69.
210. Ali M, Chernova TA, Newnam GP, Yin L, Shanks J, Karpova TS, Lee A, Laur O, Subramanian S, Kim D *et al*: **Stress-dependent proteolytic processing of the actin assembly protein Lsb1 modulates a yeast prion**. *The Journal of biological chemistry* 2014, **289**(40):27625-27639.
211. Chernova TA, Romanyuk AV, Karpova TS, Shanks JR, Ali M, Moffatt N, Howie RL, O'Dell A, McNally JG, Liebman SW *et al*: **Prion induction by the short-lived, stress-induced protein Lsb2 is regulated by ubiquitination and association with the actin cytoskeleton**. *Molecular cell* 2011, **43**(2):242-252.
212. Hill SM, Hao X, Gronvall J, Spikings-Nordby S, Widlund PO, Amen T, Jorhov A, Josefson R, Kaganovich D, Liu B *et al*: **Asymmetric Inheritance of Aggregated Proteins and Age Reset in Yeast Are Regulated by Vac17-Dependent Vacuolar Functions**. *Cell reports* 2016, **16**(3):826-838.
213. Weisman LS: **Organelles on the move: insights from yeast vacuole inheritance**. *Nature reviews Molecular cell biology* 2006, **7**(4):243-252.
214. Gaynor EC, Graham TR, Emr SD: **COPI in ER/Golgi and intra-Golgi transport: do yeast COPI mutants point the way?** *Biochimica et biophysica acta* 1998, **1404**(1-2):33-51.
215. Lefebvre F, Prouzet-Mauleon V, Hugues M, Crouzet M, Vieillemard A, McCusker D, Thoraval D, Doignon F: **Secretory pathway-dependent localization of the Saccharomyces cerevisiae Rho GTPase-activating protein Rgd1p at growth sites**. *Eukaryotic cell* 2012, **11**(5):590-600.
216. Bankaitis VA, Aitken JR, Cleves AE, Dowhan W: **An essential role for a phospholipid transfer protein in yeast Golgi function**. *Nature* 1990, **347**(6293):561-562.
217. de Saint-Jean M, Delfosse V, Douguet D, Chicanne G, Payrastre B, Bourguet W, Antonny B, Drin G: **Osh4p exchanges sterols for phosphatidylinositol 4-phosphate between lipid bilayers**. *The Journal of cell biology* 2011, **195**(6):965-978.
218. Hama H, Schnieders EA, Thorner J, Takemoto JY, DeWald DB: **Direct involvement of phosphatidylinositol 4-phosphate in secretion in the yeast Saccharomyces cerevisiae**. *The Journal of biological chemistry* 1999, **274**(48):34294-34300.
219. Yamamoto H, Kakuta S, Watanabe TM, Kitamura A, Sekito T, Kondo-Kakuta C, Ichikawa R, Kinjo M, Ohsumi Y: **Atg9 vesicles are an important membrane source during early steps of autophagosome formation**. *The Journal of cell biology* 2012, **198**(2):219-233.
220. Noda T, Kim J, Huang WP, Baba M, Tokunaga C, Ohsumi Y, Klionsky DJ: **Apg9p/Cvt7p is an integral membrane protein required for transport vesicle formation in the Cvt and autophagy pathways**. *The Journal of cell biology* 2000, **148**(3):465-480.

221. Desrivieres S, Cooke FT, Parker PJ, Hall MN: **MSS4, a phosphatidylinositol-4-phosphate 5-kinase required for organization of the actin cytoskeleton in Saccharomyces cerevisiae**. *The Journal of biological chemistry* 1998, **273**(25):15787-15793.
222. Walch-Solimena C, Novick P: **The yeast phosphatidylinositol-4-OH kinase pik1 regulates secretion at the Golgi**. *Nature cell biology* 1999, **1**(8):523-525.
223. Meriin AB, Zhang X, Alexandrov IM, Salnikova AB, Ter-Avanesian MD, Chernoff YO, Sherman MY: **Endocytosis machinery is involved in aggregation of proteins with expanded polyglutamine domains**. *FASEB journal : official publication of the Federation of American Societies for Experimental Biology* 2007, **21**(8):1915-1925.
224. Warren DT, Andrews PD, Gourlay CW, Ayscough KR: **Sla1p couples the yeast endocytic machinery to proteins regulating actin dynamics**. *Journal of cell science* 2002, **115**(Pt 8):1703-1715.
225. Wesp A, Hicke L, Palecek J, Lombardi R, Aust T, Munn AL, Riezman H: **End4p/Sla2p interacts with actin-associated proteins for endocytosis in Saccharomyces cerevisiae**. *Molecular biology of the cell* 1997, **8**(11):2291-2306.
226. Andreasen M, Lorenzen N, Otzen D: **Interactions between misfolded protein oligomers and membranes: A central topic in neurodegenerative diseases?** *Biochimica et biophysica acta* 2015, **1848**(9):1897-1907.
227. Kawai-Noma S, Pack CG, Kojidani T, Asakawa H, Hiraoka Y, Kinjo M, Haraguchi T, Taguchi H, Hirata A: **In vivo evidence for the fibrillar structures of Sup35 prions in yeast cells**. *The Journal of cell biology* 2010, **190**(2):223-231.
228. Park SH, Kukushkin Y, Gupta R, Chen T, Konagai A, Hipp MS, Hayer-Hartl M, Hartl FU: **PolyQ proteins interfere with nuclear degradation of cytosolic proteins by sequestering the Sis1p chaperone**. *Cell* 2013, **154**(1):134-145.
229. Wach A, Brachat A, Pohlmann R, Philippsen P: **New heterologous modules for classical or PCR-based gene disruptions in Saccharomyces cerevisiae**. *Yeast* 1994, **10**(13):1793-1808.
230. Janke C, Magiera MM, Rathfelder N, Taxis C, Reber S, Maekawa H, Moreno-Borchart A, Doenges G, Schwob E, Schiebel E *et al*: **A versatile toolbox for PCR-based tagging of yeast genes: new fluorescent proteins, more markers and promoter substitution cassettes**. *Yeast* 2004, **21**(11):947-962.
231. Andreasson C, Fiaux J, Rampelt H, Mayer MP, Bukau B: **Hsp110 is a nucleotide-activated exchange factor for Hsp70**. *The Journal of biological chemistry* 2008, **283**(14):8877-8884.
232. Oh E, Becker AH, Sandikci A, Huber D, Chaba R, Gloge F, Nichols RJ, Typas A, Gross CA, Kramer G *et al*: **Selective ribosome profiling reveals the cotranslational chaperone action of trigger factor in vivo**. *Cell* 2011, **147**(6):1295-1308.
233. Gietz RD, Schiestl RH: **Applications of high efficiency lithium acetate transformation of intact yeast cells using single-stranded nucleic acids as carrier**. *Yeast* 1991, **7**(3):253-263.
234. Gietz RD, Schiestl RH: **High-efficiency yeast transformation using the LiAc/SS carrier DNA/PEG method**. *Nature protocols* 2007, **2**(1):31-34.

A

Appendix

A1. Factors identified to bind to PrD (SUP35) fibers *in vitro*

Appendix Table 1.: **List of genes identified to bind to PrD (SUP35) fibers**. A systematic and standard name and gene descriptions is given. Source of description is: yeastgenome.org

Systematic Name	Standard Name	Description
YER165W	PAB1	Poly(A) binding protein; part of the 3'-end RNA-processing complex, mediates interactions between the 5' cap structure and the 3' mRNA poly(A) tail, involved in control of poly(A) tail length, interacts with translation factor eIF-4G; stimulates, but is not required for the deadenylation activity of the Pan2p-Pan3p poly(A)-ribonuclease complex
YNL016W	PUB1	Poly (A)+ RNA-binding protein; abundant mRNP-component protein that binds mRNA and is required for stability of many mRNAs; component of glucose deprivation induced stress granules, involved in P-body-dependent granule assembly; protein abundance increases in response to DNA replication stress
YFR031C-A	RPL2A	Ribosomal 60S subunit protein L2A; homologous to mammalian ribosomal protein L2 and bacterial L2; RPL2A has a paralog, RPL2B, that arose from the whole genome duplication
YNL178W	RPS3	Protein component of the small (40S) ribosomal subunit; has apurinic/apyrimidinic (AP) endonuclease activity; essential for viability; nascent Rps3p is bound by specific chaperone Yar1p during translation; homologous to mammalian ribosomal protein S3 and bacterial S3
YPL090C	RPS6A	Protein component of the small (40S) ribosomal subunit; homologous to mammalian ribosomal protein S6, no bacterial homolog; phosphorylated on S233 by Ypk3p in a TORC1-dependent manner, and on S232 in a TORC1/2-dependent manner by Ypk1/2/3p; RPS6A has a paralog, RPS6B, that arose from the whole genome duplication
YML024W	RPS17A	Ribosomal protein 51 (rp51) of the small (40s) subunit; homologous to mammalian ribosomal protein S17, no bacterial homolog; RPS17A has a paralog, RPS17B, that arose from the whole genome duplication
YOL123W	HRP1	Subunit of cleavage factor I; cleavage factor I is a five-subunit complex required for the cleavage and polyadenylation of pre-mRNA 3' ends; RRM-containing heteronuclear RNA binding protein and hnRNPA/B family member that binds to poly (A) signal sequences; required for genome stability
YJR145C	RPS4a	Protein component of the small (40S) ribosomal subunit; mutation affects 20S pre-rRNA processing; homologous to mammalian ribosomal protein S4, no bacterial homolog; RPS4A has a paralog, RPS4B, that arose from the whole genome duplication
YPL131W	RPL5	Ribosomal 60S subunit protein L5; nascent Rpl5p is bound by specific chaperone Syo1p during

		translation; homologous to mammalian ribosomal protein L5 and bacterial L18; binds 5S rRNA and is required for 60S subunit assembly
YLR448W	RPL6B	Ribosomal 60S subunit protein L6B; binds 5.8S rRNA; homologous to mammalian ribosomal protein L6, no bacterial homolog; RPL6B has a paralog, RPL6A, that arose from the whole genome duplication
YMR242C	RPL20A	Ribosomal 60S subunit protein L20A; homologous to mammalian ribosomal protein L18A, no bacterial homolog; RPL20A has a paralog, RPL20B, that arose from the whole genome duplication
YLR441C	RPS1A	Ribosomal protein 10 (rp10) of the small (40S) subunit; homologous to mammalian ribosomal protein S3A, no bacterial homolog; RPS1A has a paralog, RPS1B, that arose from the whole genome duplication
YIL094C	LYS12	Homo-isocitrate dehydrogenase; an NAD-linked mitochondrial enzyme required for the fourth step in the biosynthesis of lysine, in which homo-isocitrate is oxidatively decarboxylated to alpha-ketoadipate
YDL055C	PSA1	GDP-mannose pyrophosphorylase (mannose-1-phosphate guanyltransferase); synthesizes GDP-mannose from GTP and mannose-1-phosphate in cell wall biosynthesis; required for normal cell wall structure
YOL086C	ADH1	Alcohol dehydrogenase; fermentative isozyme active as homo- or heterotetramers; required for the reduction of acetaldehyde to ethanol, the last step in the glycolytic pathway; ADH1 has a paralog, ADH5, that arose from the whole genome duplication
YOR136W	IDH2	Subunit of mitochondrial NAD(+)-dependent isocitrate dehydrogenase; complex catalyzes the oxidation of isocitrate to alpha-ketoglutarate in the TCA cycle; phosphorylated
YNL141W	AAH1	Adenine deaminase (adenine aminohydrolase); converts adenine to hypoxanthine; involved in purine salvage; transcriptionally regulated by nutrient levels and growth phase; Aah1p degraded upon entry into quiescence via SCF and the proteasome
YHL011C	PRS3	5-phospho-ribosyl-1(alpha)-pyrophosphate synthetase; synthesizes PRPP, which is required for nucleotide, histidine, and tryptophan biosynthesis; one of five related enzymes, which are active as heteromultimeric complexes
YNL231C	PDR16	Phosphatidylinositol transfer protein (PITP); controlled by the multiple drug resistance regulator Pdr1p; localizes to lipid particles and microsomes; controls levels of various lipids, may regulate lipid synthesis; homologous to Pdr17p; protein abundance increases in response to DNA replication stress
YNL037C	IDH1	Subunit of mitochondrial NAD(+)-dependent isocitrate dehydrogenase; complex catalyzes the oxidation of isocitrate to alpha-ketoglutarate in the TCA cycle
YER023W	PRO3	Delta 1-pyrroline-5-carboxylate reductase; catalyzes the last step in proline biosynthesis
YGR159C	NSR1	Nucleolar protein that binds nuclear localization sequences; required for pre-rRNA processing and ribosome biogenesis; binds to single stranded telomeric DNA and mRNA; methylated by Hmt1p; interaction with Top1p and nucleolar localization are negatively regulated by polyphosphorylation
YDL160C	DHH1	Cytoplasmic DExD/H-box helicase, stimulates mRNA decapping; coordinates distinct steps in mRNA function and decay, interacts with both the decapping and deadenylase complexes, role in translational repression, mRNA decay, and processing body dynamics; may have a role in mRNA export; C-terminus of Dhh1p interacts with Ngr1p and promotes POR1, but not EDC1 mRNA decay; forms cytoplasmic foci upon DNA replication stress
YPR086W	SUA7	Transcription factor TFIIB; a general transcription factor required for transcription initiation and start site selection by RNA polymerase II
YEL034W	HYP2	Translation elongation factor eIF-5A; required for translation of proteins containing polyproline stretches, including Bni1p, and this leads to a requirement for mating projection formation; structural homolog of bacterial EF-P; undergoes an essential hypusination modification; HYP2 has a paralog, ANB1, that arose from the whole genome duplication; human EIF5A complements the inviability of the yeast hyp2 anb1 double null mutant
YMR116C	ASC1	G-protein beta subunit and guanine dissociation inhibitor for Gpa2p; ortholog of RACK1 that inhibits translation; core component of the small (40S) ribosomal subunit; required to prevent frameshifting at ribosomes stalled at repeated CGA codons; regulates P-body formation induced by replication stress; represses Gcn4p in the absence of amino acid starvation
YKL110C	KTI12	Protein that plays a role in modification of tRNA wobble nucleosides; protein plays role in tRNA wobble nucleoside modification with Elongator complex; involved in sensitivity to G1 arrest induced by zymocin; interacts with chromatin throughout the genome; also interacts with Cdc19p
YDR432W	NPL3	RNA-binding protein; promotes elongation, regulates termination, and carries poly(A) mRNA from nucleus to cytoplasm; represses translation initiation by binding eIF4G; required for pre-mRNA splicing; interacts with E3 ubiquitin ligase Bre1p, linking histone ubiquitination to mRNA processing; may have role in telomere maintenance; dissociation from mRNAs promoted by Mtr10p; phosphorylated by Sky1p in cytoplasm; protein abundance increases in response to DNA replication stress
YNL251C	NRD1	RNA-binding subunit of Nrd1 complex; complex interacts with exosome to mediate 3'-end

		formation of some mRNAs, snRNAs, snoRNAs, and CUTs; interacts with CTD of RNA pol II large subunit Rpo21p at phosphorylated Ser5 to direct transcription termination of non-polyadenylated transcripts; H3K4 trimethylation of transcribed regions by Set1p enhances recruitment of Nrd1p to those sites; role in regulation of mitochondrial abundance and cell size
YFL037W	TUB2	Beta-tubulin; associates with alpha-tubulin (Tub1p and Tub3p) to form tubulin dimer, which polymerizes to form microtubules; mutation in human ortholog is associated with congenital fibrosis of the extraocular muscles (CFEOM) with polymicrogyria
YLL001W	DNM1	Dynamin-related GTPase involved in mitochondrial organization; required for mitochondrial fission and morphology; assembles on the cytoplasmic face of mitochondrial tubules at sites at which division will occur; also participates in endocytosis and regulating peroxisome abundance; human homolog Drp1 plays an important role in mediating maintenance of mitochondrial function, autophagy, and mitochondrial autophagy in the heart and cardiomyocytes
YNL079C	TPM1	Major isoform of tropomyosin; binds to and stabilizes actin cables and filaments, which direct polarized cell growth and the distribution of several organelles; acetylated by the NatB complex and acetylated form binds actin most efficiently; TPM1 has a paralog, TPM2, that arose from the whole genome duplication
YIL138C	TPM2	Minor isoform of tropomyosin; binds to and stabilizes actin cables and filaments, which direct polarized cell growth and the distribution of several organelles; appears to have distinct and also overlapping functions with Tpm1p; TPM2 has a paralog, TPM1, that arose from the whole genome duplication
YNL243W	SLA2	Adaptor protein that links actin to clathrin and endocytosis; involved in membrane cytoskeleton assembly and cell polarization; present in the actin cortical patch of the emerging bud tip; dimer in vivo
YFR024C-A	LSB3	Protein containing a C-terminal SH3 domain; binds Las17p, which is a homolog of human Wiskott-Aldrich Syndrome protein involved in actin patch assembly and actin polymerization; protein abundance increases in response to DNA replication stress; LSB3 has a paralog, YSC84, that arose from the whole genome duplication
YDL226C	GCS1	ADP-ribosylation factor GTPase activating protein (ARF GAP); involved in ER-Golgi transport; required for prospore membrane formation; regulates phospholipase Spo14p; shares functional similarity with Glo3p; GCS1 has a paralog, SPS18, that arose from the whole genome duplication
YKR048C	NAP1	Histone chaperone; involved in histone exchange by removing and replacing histone H2A-H2B dimers or histone variant dimers from assembled nucleosomes; involved in the transport of H2A and H2B histones to the nucleus; required for the regulation of microtubule dynamics during mitosis; interacts with mitotic cyclin Clb2p; controls bud morphogenesis; phosphorylated by CK2; protein abundance increases in response to DNA replication stress
YNL007C	SIS1	Type II HSP40 co-chaperone that interacts with the HSP70 protein Ssa1p; shuttles between cytosol and nucleus; mediates delivery of misfolded proteins into the nucleus for degradation; involved in proteasomal degradation of misfolded cytosolic proteins; protein abundance increases in response to DNA replication stress; polyQ aggregates sequester Sis1p and interfere with clearance of misfolded proteins; similar to bacterial DnaJ proteins and mammalian DnaJB1
YAL005C	SSA1	ATPase involved in protein folding and NLS-directed nuclear transport; member of HSP70 family; required for ubiquitin-dependent degradation of short-lived proteins; forms chaperone complex with Ydj1p; localized to nucleus, cytoplasm, cell wall; 98% identical to paralog Ssa2p with different functional specificity in propagation of yeast [URE3] prions, vacuolar-mediated degradations of gluconeogenesis enzymes; general targeting factor of Hsp104p to prion fibrils
YLL024C	SSA2	HSP70 family ATP-binding protein; involved in protein folding, vacuolar import of proteins; required for ubiquitin-dependent degradation of short-lived proteins; associated with chaperonin-containing T-complex; 98% identical to paralog Ssa1p with distinct functional specificity in propagation of yeast [URE3] prions and vacuolar-mediated degradation of gluconeogenesis enzymes; binds tRNA, has role in tRNA nuclear import during starvation
YNL064C	YDJ1	Type I HSP40 co-chaperone; involved in regulation of HSP90 and HSP70 functions; acts as an adaptor that helps Rsp5p recognize cytosolic misfolded proteins for ubiquitylation after heat shock; critical for determining cell size at Start as a function of growth rate; involved in protein translocation across membranes; member of the DnaJ family; chimeric protein in which human p58IPK J domain replaces yeast Ydj1p J domain can complement yeast ydj1 mutant
YOR007C	SGT2	Glutamine-rich cytoplasmic cochaperone; serves as a scaffold bringing together Get4, Get5p, and other TRC complex members that are required to mediate posttranslational insertion of tail-anchored proteins into the ER membrane; interacts with the prion domain of Sup35p; amyloid sensor; plays a role in targeting chaperones to prion aggregates; similar to human cochaperone SGT; forms cytoplasmic foci upon DNA replication stress
YBR080C	SEC18	AAA ATPase and SNARE disassembly chaperone; required for vesicular transport between ER and Golgi, the 'priming' step in homotypic vacuole fusion, autophagy, and protein secretion; releases Sec17p from SNAP complexes; has similarity to mammalian N-ethylmaleimide-sensitive factor (NSF)

YDL100C	GET3	Guanine nucleotide exchange factor for Gpa1p; amplifies G protein signaling; functions as a chaperone under ATP-depleted oxidative stress conditions; subunit of GET complex, involved in ATP dependent Golgi to ER trafficking and insertion of tail-anchored (TA) proteins into ER membrane under non-stress conditions; binds as dimer to transmembrane domain (TMD) cargo, shielding TMDs from aqueous solvent; protein abundance increases under DNA replication stress
YKL196C	YKT6	Vesicle membrane protein (v-SNARE) with acyltransferase activity; involved in trafficking to and within the Golgi, endocytic trafficking to the vacuole, and vacuolar fusion; membrane localization due to prenylation at the carboxy-terminus; human homolog YKT6 can complement yeast ykt6 mutant
YCR009C	RVS161	Amphiphysin-like lipid raft protein; N-BAR domain protein that interacts with Rvs167p and regulates polarization of the actin cytoskeleton, endocytosis, cell polarity, cell fusion and viability following starvation or osmotic stress
YFL038C	YPT1	Rab family GTPase; involved in the ER-to-Golgi step of the secretory pathway; complex formation with the Rab escort protein Mrs6p is required for prenylation of Ypt1p by type II protein geranylgeranyltransferase (Bet2p-Bet4p); binds to unspliced HAC1 mRNA; regulates the unfolded protein response (UPR) by promoting the decay of HAC1 RNA; localizes to the early Golgi, the transitional Golgi and ER membranes, pre-autophagosomal structures, and cytoplasmic vesicles
YPL218W	SAR1	ARF family GTPase; component of the COPII vesicle coat; required for transport vesicle formation during ER to Golgi protein transport; lowers membrane rigidity aiding vesicle formation; localizes to ER-mitochondrial contact sites where it enhances membrane curvature, thereby reducing contact size via its N-terminal amphipathic helix; regulates mitochondrial fission and fusion dynamics
YFL005W	SEC4	Rab family GTPase; essential for vesicle-mediated exocytic secretion and autophagy; associates with the exocyst component Sec15p and may regulate polarized delivery of transport vesicles to the exocyst at the plasma membrane
YMR079W	SEC14	Phosphatidylinositol/phosphatidylcholine transfer protein; involved in regulating PtdIns, PtdCho, and ceramide metabolism, products of which regulate intracellular transport and UPR; has a role in localization of lipid raft proteins; functionally homologous to mammalian PITPs; SEC14 has a paralog, YKL091C, that arose from the whole genome duplication
YNL287W	SEC21	Gamma subunit of coatomer; coatomer is a heptameric protein complex that together with Arf1p forms the COPI coat; involved in ER to Golgi transport of selective cargo
YJR121W	ATP2	Beta subunit of the F1 sector of mitochondrial F1F0 ATP synthase; which is a large, evolutionarily conserved enzyme complex required for ATP synthesis; F1 translationally regulates ATP6 and ATP8 expression to achieve a balanced output of ATP synthase genes encoded in nucleus and mitochondria; phosphorylated
YCL064C	CHA1	Catabolic L-serine (L-threonine) deaminase; catalyzes the degradation of both L-serine and L-threonine; required to use serine or threonine as the sole nitrogen source, transcriptionally induced by serine and threonine
YBR127C	VMA2	Subunit B of V1 peripheral membrane domain of vacuolar H+-ATPase; electrogenic proton pump found throughout the endomembrane system; contains nucleotide binding sites; also detected in the cytoplasm; protein abundance increases in response to DNA replication stress; human homolog ATP6V1B1, implicated in autosomal-recessive distal renal tubular acidosis (RTA) with sensorineural deafness, complements yeast null mutant
YEL051W	VMA8	Subunit D of the V1 peripheral membrane domain of V-ATPase; part of the electrogenic proton pump found throughout the endomembrane system; plays a role in the coupling of proton transport and ATP hydrolysis; the V1 peripheral membrane domain of the vacuolar H+-ATPase (V-ATPase) has eight subunit
YBL016W	FUS3	Mitogen-activated serine/threonine protein kinase involved in mating; phosphoactivated by Ste7p; substrates include Ste12p, Far1p, Bni1p, Sst2p; inhibits invasive growth during mating by phosphorylating Tec1p, promoting its; inhibits recruitment of Ste5p, Cdc42p-mediated asymmetry and mating morphogenesis
YMR095C	SNO1	Protein of unconfirmed function; involved in pyridoxine metabolism; expression is induced during stationary phase; forms a putative glutamine amidotransferase complex with Snz1p, with Sno1p serving as the glutaminase
YOR185C	GSP2	GTP binding protein (mammalian Ranp homolog); involved in the maintenance of nuclear organization, RNA processing and transport; interacts with Kap121p, Kap123p and Pdr6p (karyophilin betas); not required for viability; protein abundance increases in response to DNA replication stress; GSP2 has a paralog, GSP1, that arose from the whole genome duplication
YDR441C	APT2	Potential adenine phosphoribosyltransferase; encodes a protein with similarity to adenine phosphoribosyltransferase, but artificially expressed protein exhibits no enzymatic activity; APT2 has a paralog, APT1, that arose from the whole genome duplication
YFL045C	SEC53	Phosphomannomutase; involved in synthesis of GDP-mannose and dolichol-phosphate-mannose; required for folding and glycosylation of secretory proteins in the ER lumen
YCR027C	RHB1	Putative Rheb-related GTPase; involved in regulating canavanine resistance and arginine uptake; member of the Ras superfamily of G-proteins

YPL226W	NEW1	ATP binding cassette protein; cosediments with polysomes and is required for biogenesis of the small ribosomal subunit; Asn/Gln-rich rich region supports [NU+] prion formation and susceptibility to [PSI+] prion induction
YPL020C	ULP1	Protease that specifically cleaves Smt3p protein conjugates; required for cell cycle progression; associates with nucleoporins and may interact with septin rings during telophase; sequestered to the nucleolus under stress conditions
YDR510W	SMT3	Ubiquitin-like protein of the SUMO family; conjugated to lysine residues of target proteins; associates with transcriptionally active genes; regulates chromatid cohesion, chromosome segregation, APC-mediated proteolysis, DNA replication and septin ring dynamics; human homolog SUMO1 can complement yeast null mutant

Acknowledgements

First of all, I would like to thank **Dr. Jens Tyedmers** for giving me the opportunity and means to work on this exciting topic in his lab. Thanks you for your kind supervision and support as well as constant motivation, fruitful discussions and innovative ideas to critically reflect results and putting everything into a big picture. It has been a great pleasure to work together with you.

I also especially thank **PD Dr. Axel Mogk** for allowing me to present my research data in his lab meetings on a regular basis. Thanks Axel for your time, excellent scientific discussion and inspiring ideas towards my project. It has been a pleasure to get to know all of your lab members and to share scientific opinions.

I would like thank my TAC members, **Prof. Dr. Bernd Bukau** and **Prof. Dr. Matthias Mayer** for their constructive discussions and valuable suggestions during my TAC meetings. Thanks Prof. Bukau and his lab members for allowing me to use their equipment and lab facilities during this research.

I also thank **Dr. Brian Luke**. Thanks for being present in my first TAC meeting with a critical and open mind, providing ideas and experimental advice to promote my thesis work. I would like to thank **Dr. Sebastian Schuck** for agreeing to join the examination committee.

My hearty thanks to **Ita, Johanna, Leonard, Chris** for being wonderful colleagues and great friends. I also thank **Divija, Alba, Jakob, Nathalie, Tamara, Thomas** and **Varun** for a great working experience. I had a great time working and discussing together with you and sharing the fun, ups and downs in the lab.

My thanks also go to **Holger Lorenz** of the Imaging Facility at the ZMBH for invaluable support with any microscopy problems during microscopy analysis.

I thank the **Hartmut Hoffmann-Berling International Graduate School of Molecular and Cellular Biology (HBIGS)** for financial support for visiting an international conference during the PhD period.

I thank to all my friends **Robin, Rahul, Hrishikesh, Akram, Hathi Ram, Jaspal, Bishal** and **Abhishek** for making life in Heidelberg enjoyable.

I am indebted to my beloved **brother**, **sister**, **wife** and **son** for unconditional love, care, support and encouragement.